AD-A173 977 UNSTEADY THREE-DIMENSIONAL EULER EQUATIONS SOLUTIONS ON DYNAMIC BLOCKED GRIDS(U) AIR FORCE ARMAMENT LAB EGLIN AFB FL D M BELK OCT 86 AFATL-TR-86-74 1/2

UNCLASSIFIED F/G 1/1 NL

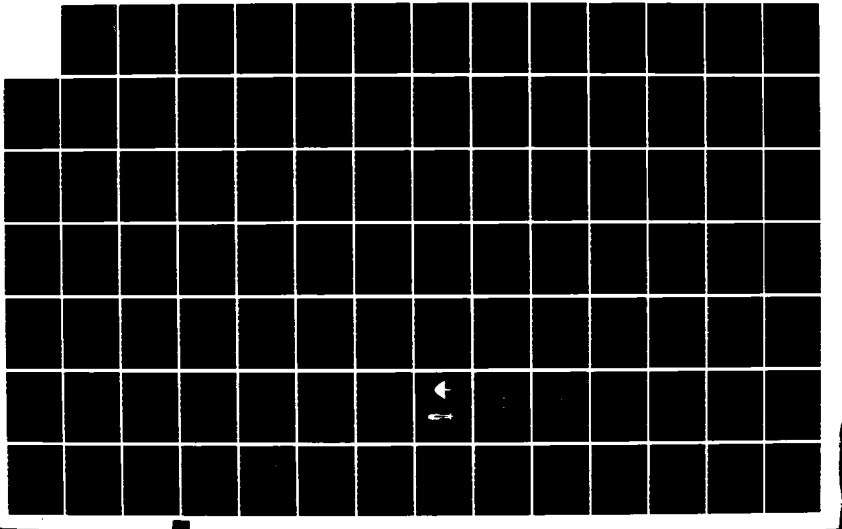

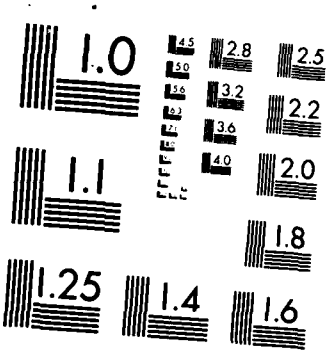

AD-A173 977

AFATL-TR-86-74

(2)

Unsteady Three-Dimensional Euler Equations Solutions on Dynamic Blocked Grids

Dave M. Belk

AIR FORCE ARMAMENT LABORATORY
AEROMECHANICS DIVISION
EGLIN AIR FORCE BASE, FLORIDA 32542-5434

OCTOBER 1986

FINAL REPORT FOR PERIOD OCTOBER 1985 - SEPTEMBER 1986

AIR FORCE ARMAMENT LABORATORY
Air Force Systems Command ▮ United States Air Force ▮ Eglin Air Force Base, Florida

NOTICE

When Government drawings, specifications, or other data are used for any purpose other than in connection with a definitely related Government procurement operation, the United States Government thereby incurs no responsibility nor any obligation whatsoever; and the fact that the Government may have formulated, furnished, or in any way supplied the said drawings, specifications, or other data, is not to be regarded by implication or otherwise as in any manner licensing the holder or any other person or corporation, or conveying any rights or permission to manufacture, use, or sell any patented invention that may in any way be related thereto.

This report has been reviewed by the Public Affairs Office (PA) and is releasable to the National Technical Information Service (NTIS). At NTIS, it will be available to the general public, including foreign nations.

This technical report has been reviewed and is approved for publication.

FOR THE COMMANDER

Donald C Daniel

DONALD C. DANIEL
Chief, Aeromechanics Division

If your address has changed, if you wish to be removed from our mailing list, or if the addressee is no longer employed by your organization, please notify AFATL/FXA , Eglin AFB FL 32542-5434.

Copies of this report should not be returned unless return is required by security considerations, contractual obligations, or notice on a specific document.

UNCLASSIFIED
SECURITY CLASSIFICATION OF THIS PAGE

AD-A173977

REPORT DOCUMENTATION PAGE

1a. REPORT SECURITY CLASSIFICATION Unclassified	1b. RESTRICTIVE MARKINGS
2a. SECURITY CLASSIFICATION AUTHORITY	3 DISTRIBUTION / AVAILABILITY OF REPORT Approved for public release; distribution unlimited.
2b. DECLASSIFICATION / DOWNGRADING SCHEDULE	
4. PERFORMING ORGANIZATION REPORT NUMBER(S)	5 MONITORING ORGANIZATION REPORT NUMBER(S) AFATL-TR-86-74
6a. NAME OF PERFORMING ORGANIZATION Air Force Armament Laboratory Aeromechanics Division 6b. OFFICE SYMBOL (If applicable) AFATL/FXA	7a NAME OF MONITORING ORGANIZATION Air Force Armament Laboratory Aeromechanics Division
6c. ADDRESS (City, State, and ZIP Code) Eglin AFB, FL 32542-5434	7b ADDRESS (City, State, and ZIP Code) Eglin AFB, FL 32542-5434
8a. NAME OF FUNDING / SPONSORING ORGANIZATION Air Force Armament Laboratory 8b. OFFICE SYMBOL (If applicable) AFATL/FXA	9 PROCUREMENT INSTRUMENT IDENTIFICATION NUMBER
8c. ADDRESS (City, State, and ZIP Code) Eglin AFB, FL 32542-5434	10 SOURCE OF FUNDING NUMBERS PROGRAM ELEMENT NO: 61102F; PROJECT NO: 2307; TASK NO: E1; WORK UNIT ACCESSION NO: 26

11. TITLE (Include Security Classification)
Unsteady Three-Dimensional Euler Equation Solutions on Dynamic Blocked Grids (U)

12. PERSONAL AUTHOR(S)
Dave M. Belk

13a. TYPE OF REPORT	13b. TIME COVERED	14 DATE OF REPORT (Year, Month, Day)	15 PAGE COUNT
Final	FROM Oct 85 TO Sep 86	October 1986	158

16. SUPPLEMENTARY NOTATION

17 COSATI CODES			18 SUBJECT TERMS (Continue on reverse if necessary and identify by block number)
FIELD	GROUP	SUB-GROUP	Computational Fluid Dynamics, Unsteady Aerodynamics, Computational Aerodynamics, Euler Equations
01	01		
20	04		

19 ABSTRACT (Continue on reverse if necessary and identify by block number)

An unsteady implicit Euler equation solution algorithm using a finite volume discretization and flux-vector splitting is presented. The effect on time-accuracy of different time step sizes, different approximate factorizations, and formal first-order versus second-order time accuracy is determined by numerical experimentation on a NACA0012 airfoil undergoing pitch oscillations in transonic flow. It is shown that time step sizes corresponding to Courant numbers of 100 or more can produce time-accurate results if flow variables are not rapidly changing. Due to better stability properties, the two-factor method gives better results than the six-factor method. Also, the second-order-time-accurate three point backward time discretization is shown to yield only slight improvement over the first-order-time-accurate backward Euler time discretization. Methods for obtaining time-accurate Euler solutions on blocked grids are analyzed and verified by comparing multi-block solutions with equivalent one-block solutions. It is shown that approximating the value of the solution vector required at block boundaries with whatever information is currently available from adjoining blocks yields unsteady results that compare well with unblocked results even for

20 DISTRIBUTION / AVAILABILITY OF ABSTRACT	21 ABSTRACT SECURITY CLASSIFICATION
☒ UNCLASSIFIED/UNLIMITED ☐ SAME AS RPT ☐ DTIC USERS	Unclassified
22a NAME OF RESPONSIBLE INDIVIDUAL Dave M. Belk	22b TELEPHONE (Include Area Code) (904) 882-5652
	22c OFFICE SYMBOL AFATL/FXA

DD FORM 1473, 84 MAR 83 APR edition may be used until exhausted
All other editions are obsolete

SECURITY CLASSIFICATION OF THIS PAGE
UNCLASSIFIED

19. ABSTRACT (CONCLUDED)

cases with a shock wave passing through the block boundary. Converged steady results with no body motion, show no error due to the block boundaries. Convergence is slowed to some extent by using blocked grids, but the use of blocked grids is economically attractive due to the greatly reduced computer memory cost. Steady and unsteady calculations of transonic flow over a rectangular planform supercritical wing using a blocked grid are compared to experimental results. The comparison is good for those cases in which viscous effects are negligible, but for higher Mach number cases the inviscid calculation places the shock downstream of the experimental location.

PREFACE

This report describes an in-house effort performed by Dave M Belk of the Aeromechanics Division (FXA), Air Force Armament Laboratory (AFATL), Eglin Air Force Base, Florida. The work reported covers the time period of October 1985 to September 1986.

ACKNOWLEDGEMENTS

The support I received from the Air Force Armament Laboratory, in time and resources, has been invaluable. I especially appreciate the encouragement and advice that Dr. Donald Daniel of the Armament Laboratory gave during all phases of this work. I thank the NASA-Ames Research Center for the use of their CRAY X-MP, on which all of these calculations were performed. Dr. Gary Chapman of NASA-Ames contributed his infectious enthusiasm along with many fresh ideas. Discussions with fellow students of Mississippi State University contributed to the blocked grid Euler code; especially helpful were chats with Abi concerning blocking techniques, and Mark Janus concerning vectorization. I thank Dr. David Whitfield, my major adviser, for the small fraction of his knowledge that I was able to pick up while working with him. Special thanks go to Susan Price for doing the most unenjoyable part, typing the manuscript, so well.

(The reverse of this page is blank)

TABLE OF CONTENTS

LIST OF FIGURES

LIST OF SYMBOLS AND ABBREVIATIONS

a_∞	freestream speed of sound
A,B,C,$\bar{K}$	Jacobians of the flux vectors
b	semi-span
c	local speed of sound, chord length of airfoil
$\vec{\xi}$	(ξ_t, η_t, ζ_t)
CFL	Courant number
C_L	lift coefficient
C_m	moment coefficient
C_p	pressure coefficient
C_p^*	critical pressure coefficient
DTMIN	time step size
e	total specific energy
E	error
f,g,h	Cartesian coordinate flux vectors
F,G,H,K	curvilinear coordinate flux vectors
I	identity operator
I	identity matrix
J	$\frac{\partial(x,y,z)}{\partial(\xi,\eta,\zeta)}$, Metric Jacobian or cell volume
J'	$\frac{\partial(x,y,z,t)}{\partial(\xi,\eta,\zeta,\tau)}$
k	general representation of a curvilinear coordinate reduced frequency
ℓ_r	reference length
L	matrix
M	Mach number
p	pressure

q	Cartesian coordinte dependent variable vector
Q	curvilinear coordinte dependent variable vector
ΔQ^n	change in dependent variable vector from time n to n+1
$\mathbf{R}$	matrix of residuals
S'	surface of moving volume in curvilinear coordinates
t	time
u,v,w	Cartesian velocity components
U,V,W,β_k	contravariant velocities
$\mathbf{U}$	matrix
V_∞	free-stream velocity
V_O	fixed volume in Cartesian coordinates
V'	moving volume in curvilinear coordinates
X	intermediate solution vector
$\mathbf{X}$	intermediate solution matrix
α	angle of attack
α_O	mean angle of attack
α_1	amplitude of unsteady angle of attack oscillation
γ	ratio of specific heats
∇	Del operator
Δ	difference operator
ε	parameter used in evaluation of flux at cell faces
δ	spatial difference operator
λ	eigenvalue
ψ	parameter in Beam-Warming formula
θ	parameter in Beam-Warming formula
θ_k	$k_x u + k_x v + k_x w$
$\bar{\jmath}_k$	$\jmath_k / \lvert\nabla k\rvert$

ρ	density
τ	transformed time variable
w	oscillatory frequency
ξ,η,ζ	curvilinear coordinates

Subscripts

i,j,k	mesh point location
ℓ	split flux number
∞	free-stream value
ξ,η,ζ,k	partial differentiation or dependence on a particular coordinate
ΔQ_I	pertaining to ΔQ_I
ΔQ_{II}	pertaining to ΔQ_{II}
r	reference value
I,II	block number

Superscripts

ℓ	eigenvalue number
L	associated with positive eigenvalues
n	time level
R	associated with negative eigenvalues
-1	inverse
$\wedge$	indicates a dimensional quantity
-	indicates division by $\lvert\nabla k\rvert$

Symbols

$\|\ \|$	absolute value
$\rightarrow$	approaches
$\times$	cross product
$\cdot$	dot product

CHAPTER I

INTRODUCTION

Accurate prediction of unsteady transonic flow about modern fighter aircraft is important due to the requirement for transonic combat and store separation, and because of the aerodynamic and aeroelastic problems encountered in this regime. Flutter, for example, is a potentially destructive coupling between flexible structural motion and the unsteady aerodynamics about that structure that is typically more critical in the transonic flight regime than in either the subsonic or supersonic. Also, the trajectory of a store separating from the parent aircraft can be greatly affected by the increased aerodynamic interference between aircraft and store that is typical of the transonic regime. Although these problems have been recognized for some time, progress in the prediction of unsteady transonic aerodynamics about complex geometries, such as a fighter aircraft with external stores, has been slow due to the inherent nonlinearity of transonic flow and the difficulties involved in obtaining solutions to the equations describing this flow.

The Navier-Stokes equations adequately describe unsteady transonic flow, including shock waves, viscous effects, and shock and boundary layer interactions. Solution of the Navier-Stokes equations about complex three-dimensional geometries on present-day computers would be very expensive. Fortunately, many flow-fields of practical interest are modeled well by the Euler equations, which may be obtained from the Navier-Stokes equations by assuming that the flow is inviscid. Numerical solution of the Euler equations, though expensive, is much less expensive than solution of the Navier-Stokes equations primarily because

of the elimination of the computational work and computer storage associated with resolving flow variations at the small length scale at which viscous effects are important. Time-accurate numerical solutions of the Euler equations about three-dimensional wings in oscillatory motion have been previously presented by Sankar, et al.,[1] and by Salmond.[2] Two-dimensional Euler or Navier-Stokes calculations about oscillating airfoils in transonic flow have been presented by Magnus and Yoshihara,[3] Steger and Bailey,[4] Chyu and Davis,[5] Janus,[6] and Smith, et al.[7] Time-accurate Euler calculations about a body of revolution moving away from a flat plate were reported in Reference 8. The explicit solution algorithms used in References 3, 6, 7, and 8 allowed only very small time steps to be taken because of stability limitations. Implicit solution algorithms, as used in References 1, 2, 4, and 5 typically allow much larger time steps to be taken while maintaining a stable solution, but the effect of such large time steps on time-accuracy is unclear. In Chapter II of this paper the Euler equations are presented and transformed from rectangular Cartesian coordinates into general time-dependent curvilinear coordinates to allow for dynamic grids that can follow the motion of the body. In Chapter III an implicit upwind finite volume scheme is presented for solving these equations, and several variations of the scheme are applied to an airfoil oscillating in pitch in transonic flow to study the effects of different time step sizes, different approximate factorizations, and first-order time-accuracy versus second-order time-accuracy on the results.

A pacing factor for the ability to obtain steady or unsteady numerical solutions of the Euler equations about complex geometries is the generation of a mesh of points, or grid, around these geometries.

The blocked grid approach described in Chapter IV allows much greater flexibility in grid generation by allowing different curvilinear coordinate transformations to be used for different parts of the grid, with only the requirement that all grid lines be continuous from one block to the next across the block-to-block boundaries. A scheme for solving the unsteady Euler equations on blocked grids by advancing the solution one time step in each block sequentially is presented in Chapter IV. Techniques for transfer of information across block boundaries are discussed along with analyses of error associated with the various techniques. Steady and unsteady calculations on blocked grids around an airfoil are compared with calculations on equivalent unblocked grids to verify the analyses and to investigate the effect of block boundaries on moving shock waves.

Three-dimensional calculations on a rectangular planform supercritical wing of aspect ratio two are presented in Chapter V for both steady flow and oscillatory pitching of the wing, and the computed results are compared with the experiment.

CHAPTER II

THE EULER EQUATIONS

The three-dimensional, time dependent Euler equations written in strong conservation law form are

$$\frac{\partial \hat{q}}{\partial \hat{t}} + \frac{\partial \hat{f}}{\partial \hat{x}} + \frac{\partial \hat{g}}{\partial \hat{y}} + \frac{\partial \hat{h}}{\partial \hat{z}} = 0 \qquad (2\text{-}1)$$

where

$$\hat{q} = \begin{bmatrix} \hat{\rho} \\ \hat{\rho}\hat{u} \\ \hat{\rho}\hat{v} \\ \hat{\rho}\hat{w} \\ \hat{e} \end{bmatrix}, \quad \hat{f} = \begin{bmatrix} \hat{\rho}\hat{u} \\ \hat{\rho}\hat{u}^2+\hat{p} \\ \hat{\rho}\hat{u}\hat{v} \\ \hat{\rho}\hat{u}\hat{w} \\ \hat{u}(\hat{e}+\hat{p}) \end{bmatrix}, \quad \hat{g} = \begin{bmatrix} \hat{\rho}\hat{v} \\ \hat{\rho}\hat{u}\hat{v} \\ \hat{\rho}\hat{v}^2+\hat{p} \\ \hat{\rho}\hat{v}\hat{w} \\ \hat{v}(\hat{e}+\hat{p}) \end{bmatrix}, \quad \hat{h} = \begin{bmatrix} \hat{\rho}\hat{w} \\ \hat{\rho}\hat{u}\hat{w} \\ \hat{\rho}\hat{v}\hat{w} \\ \hat{\rho}\hat{w}^2+\hat{p} \\ \hat{w}(\hat{e}+\hat{p}) \end{bmatrix}$$

and

$$\hat{e} = \frac{\hat{p}}{\gamma-1} + \frac{1}{2}\hat{\rho}\,(\hat{u}^2 + \hat{v}^2 + \hat{w}^2)$$

Here $\hat{\rho}$ is the mass density of the compressible fluid, $\hat{u}$, $\hat{v}$, and $\hat{w}$ are the velocity components in the $\hat{x}$,$\hat{y}$, and $\hat{z}$ Cartesian coordinate directions, respectively, $\hat{p}$ is the pressure, and $\hat{e}$ the total specific energy of the fluid. The relationship between $\hat{e}$ and $\hat{p}$ is the result of making the perfect gas assumption, and γ is the ratio of specific heats. Carets on the quantities in Equation (2-1) are used to indicate that dimensional quantities are being used. One way to non-dimensionalize Equation (2-1) is to define the following non-dimensional quantities:

$$x = \frac{\hat{x}}{\hat{\ell}_r}, \quad y = \frac{\hat{y}}{\hat{\ell}_r}, \quad z = \frac{\hat{z}}{\hat{\ell}_r}, \quad t = \frac{\hat{a}_\infty \hat{t}}{\hat{\ell}_r}$$

$$u = \frac{\hat{u}}{\hat{a}_\infty}, \quad v = \frac{\hat{v}}{\hat{a}_\infty}, \quad w = \frac{\hat{w}}{\hat{a}_\infty} \tag{2-2}$$

$$\rho = \frac{\hat{\rho}}{\hat{\rho}_\infty}, \quad e = \frac{\hat{e}}{\hat{\rho}_\infty \hat{a}_\infty^2}, \quad p = \frac{\hat{p}}{\hat{\rho}_\infty \hat{a}_\infty^2}$$

where $\hat{\ell}_r$ is any convenient reference length, $\hat{a}_\infty = (\gamma \hat{p}_\infty / \hat{\rho}_\infty)^{1/2}$, the speed of sound in undisturbed gas, and $\hat{\rho}_\infty$ is the density of undisturbed gas. After some manipulation, the non-dimensional Euler equations may be written in exactly the same form as Equation (2-1) with all carets dropped.

To simplify numerical treatment of boundary conditions around general geometries the Euler equations are recast in terms of general boundary conforming curvilinear coordinates. The curvilinear coordinates are defined as

$$\begin{aligned} \xi &= \xi(x,y,z,t) \\ \eta &= \eta(x,y,z,t) \\ \zeta &= \zeta(x,y,z,t) \\ \tau &= \tau(t) \end{aligned} \tag{2-3}$$

Note that the curvilinear coordinates are time dependent thus allowing constant coordinate surfaces to follow the unsteady motion of the boundary. Also note that the time coordinate is not dependent on spatial location.

Applying the transformation (2-3) to the non-dimensional Euler equations (Equation (2-1) with all carets dropped) gives

$$\frac{\partial Q}{\partial \tau} + \frac{\partial F}{\partial \xi} + \frac{\partial G}{\partial \eta} + \frac{\partial H}{\partial \zeta} = 0 \qquad (2\text{-}4)$$

where

$$Q = J \begin{bmatrix} \rho \\ \rho u \\ \rho v \\ \rho w \\ e \end{bmatrix}$$

$$F = t_\tau J \begin{bmatrix} \rho U \\ \rho uU + \xi_x p \\ \rho vU + \xi_y p \\ \rho wU + \xi_z p \\ U(e+p) - \xi_t p \end{bmatrix} \quad \text{and } U = \xi_x u + \xi_y v + \xi_z w + \xi_t,$$

$$G = t_\tau J \begin{bmatrix} \rho V \\ \rho uV + \eta_x p \\ \rho vV + \eta_y p \\ \rho wV + \eta_z p \\ V(e+p) - \eta_t p \end{bmatrix} \quad \text{and } V = \eta_x u + \eta_y v + \eta_z w + \eta_t,$$

$$H = t_\tau J \begin{bmatrix} \rho W \\ \rho uW + \zeta_x p \\ \rho vW + \zeta_y p \\ \rho wW + \zeta_z p \\ W(e+p) - \zeta_t p \end{bmatrix} \quad \text{and } W = \zeta_x u + \zeta_y v + \zeta_z w + \zeta_t.$$

In the above equation, J is the Jacobian of the inverse transformation, i.e. $\partial(x,y,z)/\partial(\xi,\eta,\zeta)$, and is given by

$$J = x_\xi(y_\eta z_\zeta - z_\eta y_\zeta) - y_\xi(x_\eta z_\zeta - z_\eta x_\zeta) + z_\xi(x_\eta y_\zeta - y_\eta x_\zeta).$$

The metric quantities are given by

$$\xi_x = J^{-1}(y_\eta z_\zeta - z_\eta y_\zeta) \qquad \eta_x = J^{-1}(z_\xi y_\zeta - y_\xi z_\zeta)$$

$$\xi_y = J^{-1}(z_\eta x_\zeta - x_\eta z_\zeta) \qquad \eta_y = J^{-1}(x_\xi z_\zeta - z_\xi x_\zeta)$$

$$\xi_z = J^{-1}(x_\eta y_\zeta - y_\eta x_\zeta) \qquad \eta_z = J^{-1}(x_\zeta y_\xi - y_\zeta x_\xi)$$

$$\xi_t = (-x_\tau \xi_x - y_\tau \xi_y - z_\tau \xi_z)\tau_t \qquad \eta_t = (-x_\tau \eta_x - y_\tau \eta_y - z_\tau \eta_z)\tau_t$$

$$\zeta_x = J^{-1}(y_\xi z_\eta - z_\xi y_\eta)$$

$$\zeta_y = J^{-1}(x_\eta z_\xi - z_\eta x_\xi)$$

$$\zeta_z = J^{-1}(x_\xi y_\eta - y_\xi x_\eta)$$

$$\zeta_t = (-x_\tau \zeta_x - y_\tau \zeta_y - z_\tau \zeta_z)\tau_t$$

The details of this transformation are given in Appendix A.

CHAPTER III

IMPLICIT SOLUTION ALGORITHM

3.1 FLUX SPLITTING

Hyperbolic partial differential equations, such as the Euler equations, are characterized by the existence of a limited domain of dependence. The solution at a point does not depend on every other point in the field; this means that information travels only in certain characteristic directions. Numerical schemes intended to solve hyperbolic equations are usually enhanced by insuring that the numerical method propagates information in the direction specified by the partial differential equation. This can be done by using an upwind method, or one in which the difference operator is taken in the direction from which the information should come. Stability properties are often improved by upwinding, and it is usually unnecessary to add smoothing terms or artificial viscosity to an upwind method.

The three-dimensional Euler equations, Equation (2-4), are a hyperbolic system of five equations and hence have five characteristic velocities in each of the three spatial directions. These characteristic velocities are determined from the quasilinear form of Equation (2-4),

$$\frac{\partial Q}{\partial \tau} + A\frac{\partial Q}{\partial \xi} + B\frac{\partial Q}{\partial \eta} + C\frac{\partial Q}{\partial \zeta} = 0 \qquad (3\text{-}1)$$

where the matrices A, B, and C are given by

$$A = \frac{\partial F}{\partial Q}, \quad B = \frac{\partial G}{\partial Q}, \quad C = \frac{\partial H}{\partial Q} \qquad (3\text{-}2)$$

The eigenvalues of A are the characteristic velocities in the ξ direction; the eigenvalues of B are the characteristic velocities in the η direction; and similarly the eigenvalues of C are the characteristic velocities in the ζ direction.

Since F, G, and H are identical except that where ξ appears in F, η will appear in G and ζ will appear in H, extra writing can be avoided by letting K represent either F, G, or H, when k represent either ξ, η, or ζ, respectively. Then define

$$\bar{K} = \frac{\partial K}{\partial Q} \tag{3-3}$$

which corresponds to A, B, or C depending on the meaning of K. The general flux Jacobian matrix $\bar{K}$ and its eigenvalues are derived in Reference 6. The eigenvalues of the matrix $\bar{K}$ are

$$\begin{aligned}
\lambda_k^1 &= \lambda_k^2 = \lambda_k^3 = (k_x u + k_y v + k_z w + k_t)t_\tau = \beta_k t_\tau \\
\lambda_k^4 &= (\beta_k + c|\nabla k|)t_\tau = (\beta_k + c(k_x^2 + k_y^2 + k_z^2)^{1/2})t_\tau \\
\lambda_k^5 &= (\beta_k - c|\nabla k|)t_\tau
\end{aligned} \tag{3-4}$$

where c is the speed of sound.

It is possible to split the flux vector K into three parts, one corresponding to each of the distinct eigenvalues of $\bar{K}$ given above. (For the details of this splitting, see Reference 6.) The flux vector K is then written as

$$K = \lambda_k^1 K_1 + \lambda_k^4 K_4 + \lambda_k^5 K_5 \tag{3-5}$$

where

$$K_1 = J\frac{\gamma-1}{\gamma}\begin{bmatrix}\rho\\ \rho u\\ \rho v\\ \rho w\\ \frac{\rho}{2}(u^2+v^2+w^2)\end{bmatrix} \qquad K_4 = \frac{J}{2\gamma}\begin{bmatrix}\rho\\ \rho u+\rho c\bar{k}_x\\ \rho v+\rho c\bar{k}_y\\ \rho w+\rho c\bar{k}_z\\ e+p+\rho c\bar{\theta}_k\end{bmatrix}$$

$$K_5 = \frac{J}{2\gamma}\begin{bmatrix}\rho\\ \rho u-\rho c\bar{k}_x\\ \rho v-\rho c\bar{k}_y\\ \rho w-\rho c\bar{k}_z\\ e+p-\rho c\bar{\theta}_k\end{bmatrix} \qquad (3\text{-}6)$$

and

$$\bar{k}_x = \frac{k_x}{|\nabla k|} = \frac{k_x}{(k_x^2+k_y^2+k_z^2)^{1/2}}$$

$$\bar{k}_y = \frac{k_y}{|\nabla k|}$$

$$\bar{k}_z = \frac{k_z}{|\nabla k|}$$

$$\bar{\theta}_k = \bar{k}_x u + \bar{k}_y v + \bar{k}_z w.$$

The sign of λ_k^{ℓ} in Equation (3-4) determines from which direction information should be used to determine the corresponding portion of flux, K_ℓ, for ℓ=1, 4, and 5.

The discussion above provides a rationale for writing the flux vector K as the sum of two vectors, K^L and K^R,

$$K = K^L + K^R. \tag{3-7}$$

K^L is associated with the eigenvalues that have positive signs, and K^R is associated with the eigenvalues that have negative signs. The specific method used to calculate K^L and K^R will be discussed in the next section.

3.2 Discretization

A finite volume discretization of Equation (3-1) balances the increase of the conserved quantity in a computational cell, or volume, with the flux of the quantity through the surface of the cell. Figure (3-1) depicts a portion of the computational domain with a typical cell labeled. Assuming the dependent variables are constant in the interior of cell (i, j, k), and that the flux vectors F, G, and H are constant over the constant ξ, constant η, and constant ζ surfaces of the cell, respectively, an implicit discretization of Equation (2-4) is (Reference 9)

$$(Q^{n+1}_{i,j,k} - Q^{n}_{i,j,k})\Delta\xi\Delta\eta\Delta\zeta + (F^{n+1}_{i+\frac{1}{2},j,k} - F^{n+1}_{i-\frac{1}{2},j,k})\Delta\eta\Delta\zeta\Delta\tau \tag{3-8}$$

$$+ (G^{n+1}_{i,j+\frac{1}{2},k} - G^{n+1}_{i,j-\frac{1}{2},k})\Delta\xi\Delta\zeta\Delta\tau + (H^{n+1}_{i,j,k+\frac{1}{2}} - H^{n+1}_{i,j,k-\frac{1}{2}})\Delta\xi\Delta\eta\Delta\tau = 0$$

This can be written as

$$\Delta Q^n + \Delta\tau(\delta_\xi F^{n+1} + \delta_\eta G^{n+1} + \delta_\zeta H^{n+1}) = 0 \qquad (3\text{-}9)$$

where δ_ξ, for example, is defined by

$$\delta_\xi F_{i,j,k} = \frac{1}{\Delta\xi}(F_{i+\frac{1}{2},j,k} - F_{i-\frac{1}{2},j,k}),$$

and δ_η and δ_ζ are defined analogously. Letting F^L, F^R, G^L, G^R, H^L, and H^R be the split flux vectors for F, G, and H as given by Equation (3-7), an implicit split flux discretization is given by

$$\Delta Q^n + \Delta\tau[\delta_\xi(F^L + F^R)^{n+1} + \delta_\eta(G^L + G^R)^{n+1} + \delta_\zeta(H^L + H^R)^{n+1}] = 0 \qquad (3\text{-}10)$$

The fluxes are nonlinear functions of the dependent variables, and must be linearized to obtain a system of equations that can easily be solved for ΔQ^n. Beam and Warming[10] and Briley and McDonald[11] have used the linearization

$$K^{n+1} = K^n + \bar{K}^n\Delta Q^n + O(\Delta\tau^2), \qquad (3\text{-}11)$$

where $\bar{K}^n = (\partial K/\partial Q)^n$ for a typical flux term K. The flux Jacobian matrices required to linearize Equation (3-10) are

$$A^L = \left(\frac{\partial F^L}{\partial Q}\right)^n, \qquad A^R = \left(\frac{\partial F^R}{\partial Q}\right)^n,$$

$$B^L = \left(\frac{\partial G^L}{\partial Q}\right)^n, \qquad B^R = \left(\frac{\partial G^R}{\partial Q}\right)^n, \qquad (3\text{-}12)$$

$$C^L = \left(\frac{\partial H^L}{\partial Q}\right)^n, \qquad C^R = \left(\frac{\partial H^R}{\partial Q}\right)^n,$$

and are derived in Appendix B. Using this linearization, Equation (3-10) becomes

$$[I + \Delta\tau(\delta_\xi^i A_\bullet^L + \delta_\xi^i A_\bullet^R + \delta_\eta^i B_\bullet^L + \delta_\eta^i B_\bullet^R + \delta_\zeta^i C_\bullet^L + \delta_\zeta^i C_\bullet^R)]\Delta Q^n$$

$$= -\Delta\tau(\delta_\xi^e F^n + \delta_\eta^e G^n + \delta_\zeta^e H^n), \tag{3-13}$$

where a distinction has been made between the implicit spatial difference operators and the explicit spatial difference operators by using superscripts i and e respectively. The dots are used to indicate that the difference operators apply to the product of the Jacobian matrices with ΔQ^n. If δ_ξ^e, δ_η^e, and δ_ζ^e are chosen such that

$$\delta_\xi^e = \frac{\partial}{\partial\xi} + O(\Delta\xi^2),$$

$$\delta_\eta^e = \frac{\partial}{\partial\eta} + O(\Delta\eta^2), \tag{3-14}$$

$$\delta_\zeta^e = \frac{\partial}{\partial\zeta} + O(\Delta\zeta^2),$$

and δ_ξ^i, δ_η^i, and δ_ζ^i are chosen such that

$$\delta_\xi^i = \frac{\partial}{\partial\xi} + O(\Delta\xi),$$

$$\delta_\eta^i = \frac{\partial}{\partial\eta} + O(\Delta\eta), \tag{3-15}$$

$$\delta_\zeta^i = \frac{\partial}{\partial\zeta} + O(\Delta\zeta),$$

then substitution into Equation (3-13) yields

$$\{I + \Delta\tau[\frac{\partial}{\partial\xi}(A^L_\bullet + A^R_\bullet) + \frac{\partial}{\partial\eta}(B^L_\bullet + B^R_\bullet) + \frac{\partial}{\partial\zeta}(C^L_\bullet + C^R_\bullet) + O(\Delta\xi,\Delta\eta,\Delta\zeta)]\}$$

$$(\frac{\partial Q}{\partial\tau} + O(\Delta\tau)) = -[\frac{\partial F}{\partial\xi} + \frac{\partial G}{\partial\eta} + \frac{\partial H}{\partial\zeta} + O(\Delta\xi^2,\Delta\eta^2,\Delta\zeta^2)], \qquad (3\text{-}16)$$

after dividing through by $\Delta\tau$ and using the fact that

$$\Delta Q^n = Q^{n+1} - Q^n = \Delta\tau\,\frac{\partial Q}{\partial\tau} + O(\Delta\tau^2). \qquad (3\text{-}17)$$

Using Equation (3-11) in (3-16) results in

$$\frac{\partial Q}{\partial\tau} + \frac{\partial F}{\partial\xi} + \frac{\partial G}{\partial\eta} + \frac{\partial H}{\partial\zeta} = O(\Delta\tau,\ \Delta\tau\Delta\xi,\ \Delta\tau\Delta\eta,\ \Delta\tau\Delta\zeta,\ \Delta\xi^2,\ \Delta\eta^2,\ \Delta\zeta^2). \qquad (3\text{-}18)$$

Therefore Equations (3-14) and (3-15) give a method that is second-order accurate in space if $\Delta\xi$, $\Delta\eta$, and $\Delta\zeta$ are $O(\Delta\tau)$ and first-order accurate in time when used with Equation (3-13). There are at least two simple variations of this algorithm that will produce second-order accuracy in time.

Before proceeding to a discussion of these second-order time-accurate methods, simplify the problem by considering only one spatial dimension. Also, observe from the analysis above that carrying the split flux vectors had no effect on the accuracy analysis. The fact that this is a split-flux method only enters the problem when actually defining the difference operators to satisfy the conditions given by Equations (3-14) and (3-15), which has not yet been done.

The simplified problem that will now be considered is

$$\frac{\partial Q}{\partial t} + \frac{\partial F}{\partial x} = 0. \qquad (3\text{-}19)$$

Because the time accuracy of the method is independent of how the split fluxes are spatially differenced, any standard time discretization can be applied. A broad class of schemes is given by Beam and Warming's formula[12]

$$[I + \frac{\theta\Delta t}{1+\psi}[\frac{\partial}{\partial x}A\cdot]]\Delta Q^n = -\frac{\Delta t}{1+\psi}\frac{\partial F}{\partial x} + \frac{\psi}{1+\psi}\Delta Q^{n-1} + O[(\theta - \frac{1}{2} - \psi)\Delta t^2, \Delta t^3]. \tag{3-20}$$

The scheme given by (3-13) is the backward Euler differencing scheme obtained from (3-20) by setting $\theta=1$ and $\psi=0$. By taking $\theta=1/2$, $\psi=0$, a trapezoidal scheme is obtained that is second order accurate. A three point backward scheme is obtained by setting $\theta=1$, $\psi=1/2$, giving

$$[I + \frac{2}{3}\Delta t \frac{\partial}{\partial x} A^n_\cdot]\Delta Q^n = -\frac{2}{3}\Delta t \frac{\partial F}{\partial x} + \frac{1}{3}\Delta Q^{n-1} + O(\Delta t^3). \tag{3-21}$$

Spatially differencing Equation (3-21) with

$$\delta^i = \frac{\partial}{\partial x} + O(\Delta x) \tag{3-22}$$

$$\delta^e = \frac{\partial}{\partial x} + O(\Delta x^2)$$

will yield

$$[I + \frac{2}{3}\Delta t \delta^i A^n_\cdot]\Delta Q^n = -\frac{2}{3}\Delta t\, \delta^e F + \frac{1}{3}\Delta Q^{n-1} + O(\Delta t\Delta x^2, \Delta t^2\Delta x, \Delta t^3). \tag{3-23}$$

For the sake of completeness, the trapezoidal scheme for Equation (3-19) is

$$[I + \frac{1}{2}\Delta t \delta^i A^n_\cdot]\Delta Q^n = -\Delta t \delta^e F + O(\Delta t\Delta x^2, \Delta t^2\Delta x, \Delta t^3) \tag{3-24}$$

and the backward Euler scheme written for Equation (3-19) is

$$[I + \Delta t \delta^i A^n_\cdot]\Delta Q^n = -\Delta t \delta^e F + O(\Delta t\Delta x^2, \Delta t^2\Delta x, \Delta t^2). \tag{3-25}$$

Although the truncation error has been determined without fully specifying the spatial difference operators, other properties of the various methods cannot be determined until δ^i and δ^e are completely defined. To be consistent with the objective of deriving a finite volume method, δ^i and δ^e should be central differences of quantities at opposing faces of a computational cell. Dependent variable values are only stored at cell centers, so some method must be specified for determining values at cell faces. Also, the difference operators must respect the direction of information transfer and difference F^L and F^R in their respective upwind directions. These two requirements are satisfied by defining

$$\delta^e F_j = \frac{1}{\Delta x}\left[\left(F^L_{j+\frac{1}{2}} - F^L_{j-\frac{1}{2}}\right) + \left(F^R_{j+\frac{1}{2}} - F^R_{j-\frac{1}{2}}\right)\right] \tag{3-26}$$

where $F^L_{j+1/2}$ depends only on information to the left of point j+1/2, i.e. $F^L_{j+1/2}$ depends on $Q_j, Q_{j-1}, \ldots$, and $F^R_{j+1/2}$ depends only on information to the right of point j+1/2, i.e. $F^R_{j+1/2}$ depends on $Q_{j+1}, Q_{j+2}, \ldots$

One method to satisfy the accuracy requirement given by Equation (3-22) for δ^e is to evaluate F^L and F^R by two point flux extrapolations given by

$$F^L_{j+\frac{1}{2}} = \sum_\ell \epsilon^\ell_{j+\frac{1}{2}}\left[\tfrac{3}{2}\lambda^\ell_j F_\ell(Q_j) - \tfrac{1}{2}\lambda^\ell_{j-1} F_\ell(Q_{j-1})\right] \tag{3-27a}$$

$$F^R_{j+\frac{1}{2}} = \sum_\ell (1 - \epsilon^\ell_{j+\frac{1}{2}})\left[\tfrac{3}{2}\lambda^\ell_{j+1} F_\ell(Q_{j+1}) - \tfrac{1}{2}\lambda^\ell_{j+2} F_\ell(Q_{j+2})\right] \tag{3-27b}$$

where

$$\epsilon^{\ell}_{j+\frac{1}{2}} = \left(\frac{|\lambda|+\lambda}{2|\lambda|}\right)^{\ell}_{j+\frac{1}{2}} .$$

If the eigenvalues do not change sign from the j-1/2 face to the j+1/2 face, substitution of Equations (3-27) into Equation (3-26) gives either a second order backward or a second order forward difference approximation to each split flux component yielding

$$\delta^{e} F_j = \left(\frac{\partial F}{\partial x}\right)_j + O(\Delta x^2). \tag{3-28}$$

This is true only if the eigenvalues are of the same sign on both faces of the cell. Also notice that there is some ambiguity in using Equation (3-27) because we use $\lambda^{\ell}_{j+1/2}$ which is at the cell face, but have not specified how to obtain these quantities.

Another alternative for evaluating F^L and F^R so that Equation (3-26) is a second order accurate first derivative of F is to evaluate F^L using a two point dependent variable extrapolation from the left and F^R using a two point dependent variable extrapolation from the right. This is the method of Reference 8 and is used for all calculations reported here. For a particular cell face, the scheme reported here uses

$$Q^L_{j+\frac{1}{2}} = \frac{3}{2} Q_j - \frac{1}{2} Q_{j-1} \tag{3-29}$$

to calculate a set of left eigenvalues, $\lambda^{\ell}(Q^L)$, and left split fluxes, $F_{\ell}(Q^L)$, and uses

$$Q^R_{j+\frac{1}{2}} = \frac{3}{2} Q_{j+1} - \frac{1}{2} Q_{j+2} \tag{3-30}$$

to calculate a set of right eigenvalues, $\lambda^{\ell}(Q^R)$, and right split fluxes, $F_{\ell}(Q^R)$. The flux at the face is then set to

$$F^L = \sum_{\ell} \frac{1}{2} (\lambda^{\ell}(Q^L) + |\lambda^{\ell}(Q^L)|)F_{\ell}(Q^L) \tag{3-31a}$$

and

$$F^R = \sum_{\ell} \frac{1}{2} (\lambda^{\ell}(Q^R) - |\lambda^{\ell}(Q^R)|)F_{\ell}(Q^R) \tag{3-31b}$$

Note that if a left and right eigenvalue have different signs, then the corresponding split flux may be either summed from both sides, if the sign changes from positive to negative, or from neither side, if the sign changes from negative to positive.

To determine the truncation error of this scheme consider the scalar version of Equation (3-19) and assume $\partial F/\partial Q>0$ for all x. Then $F^R=0$ and Equation (3-26) would become

$$\delta^e F_j = \frac{1}{\Delta x}[F(\tfrac{3}{2}Q_j - \tfrac{1}{2}Q_{j-1}) - F(\tfrac{3}{2}Q_{j-1} - \tfrac{1}{2}Q_{j-2})] \tag{3-32}$$

Letting $\Delta Q_j=Q_j-Q_{j-1}$ and using Taylor series expansion about Q_j,

$$F(\tfrac{3}{2}Q_j - \tfrac{1}{2}Q_{j-1}) = F(Q_j + \tfrac{1}{2}\Delta Q_j) = F(Q_j) + \tfrac{1}{2}\Delta Q_j \frac{\partial F}{\partial Q}\Big|_j + \tfrac{1}{8}\Delta Q_j^2 \frac{\partial^2 F}{\partial Q^2}\Big|_j + O(\Delta Q_j^3) \tag{3-33}$$

$$F(\tfrac{3}{2}Q_{j-1} - \tfrac{1}{2}Q_{j-2}) = F(Q_j - (\Delta Q_j - \tfrac{1}{2}\Delta Q_{j-1}))$$

$$= F(Q_j) - (\Delta Q_j - \tfrac{1}{2}\Delta Q_{j-1})\left.\frac{\partial F}{\partial Q}\right|_j + \tfrac{1}{2}(\Delta Q_j - \tfrac{1}{2}\Delta Q_{j-1})^2 \left.\frac{\partial^2 F}{\partial Q^2}\right|_j$$

$$+ O[(\Delta Q_j - \frac{1}{2}\Delta Q_{j-1})^2] \qquad (3\text{-}34)$$

Substituting Equations (3-33) and (3-34) in Equation (3-32), followed by expanding all dependent variable values about x_j and then simplifying yields

$$\delta^e F_j = \left.\frac{\partial F}{\partial x}\right|_j + O(\Delta x^2). \qquad (3\text{-}35)$$

By comparing Equations (3-28) and (3-35) it is clear that extrapolating dependent variables is different from extrapolating flux values only in the higher order terms.

The implicit difference operation δ^i need only be first order accurate and hence it is evaluated using one point dependent variable extrapolation giving

$$\delta^i(A\Delta Q)_j = (A^L(Q_j^n)\Delta Q_j^n - A^L(Q_{j-1}^n)\Delta Q_{j-1}^n)\frac{1}{\Delta x}$$

$$+ (A^R(Q_{j+1}^n)\Delta Q_{j+1}^n - A^R(Q_j^n)\Delta Q_j^n)\frac{1}{\Delta x}. \qquad (3\text{-}36)$$

Metric quantities involved in the evaluation of the Jacobian matrices are taken from the appropriate face, so that $A^L(Q_j^n)$ uses metrics from j+1/2 and $A^R(Q_j^n)$ uses metrics from j-1/2 in Equation (3-36).

For dynamic grid calculations, metric quantities including the cell volumes change during the solution process. For this study, all spatial metrics are evaluated at time level n to be used in the calculation of ΔQ^n. The time metrics at time level n are evaluated from the change in

the grid from t^n to t^{n+1}. After ΔQ^n has been obtained, an approximation is used to account for the change in cell volume from t^n to t^{n+1} given by

$$\frac{J^n}{J^{n+1}} = 1 + \Delta t\left(\frac{\partial(J\xi_t)}{\partial\xi} + \frac{\partial(J\eta_t)}{\partial\eta} + \frac{\partial(J\zeta_t)}{\partial\zeta}\right)^n + O(\Delta t^2). \tag{3-37}$$

In the limit as $\Delta t \to 0$, Equation (3-37) gives the geometric conservation law.[13]

Due to the large range of cell sizes involved in a typical solution, the Courant number in some cells may be several orders of magnitude larger than in other cells. For time-accurate calculations there is little choice but to choose the time step so that the maximum Courant number is acceptable, even though this time step may be much smaller than what could be taken in the majority of cells. If the steady-state solution is of primary interest, however, time-accuracy can be sacrificed to greatly increase the convergence rate by taking different time steps in different cells. This is referred to as local time stepping and is used in this study to obtain steady-state results. The time step for each cell when local time stepping is taken to be

$$\Delta\tau = \frac{\Delta\tau^{\xi}\Delta\tau^{\eta}\Delta\tau^{\zeta}}{\Delta\tau^{\xi}\Delta\tau^{\eta}+\Delta\tau^{\xi}\Delta\tau^{\zeta}+\Delta\tau^{\eta}\Delta\tau^{\zeta}}, \tag{3-38a}$$

where

$$\Delta\tau^k = \frac{(CFL)\Delta k}{\max_{\ell}|\lambda_k^{\ell}|}. \tag{3-38b}$$

All quantities in Equations (3-38a) and (3-38b) are to be evaluated at point (i,j,k).

3.3 Factorizations

The finite volume scheme described by Equation (3-13) is not practical to use because the system of algebraic equations that are generated have a very large bandwidth. There are many possible approximate factorizations of this method that can be used to make the solution process easier, as noted by Steger and Warming,[14] for example. Several factorizations have been recently applied by Whitfield,[9] and by Anderson, Thomas, and Whitfield.[15] One scheme that has been used is the six-factor scheme given by

$$[I+\Delta\tau\delta_\xi^i A_\bullet^L][I+\Delta\tau\delta_\xi^i A_\bullet^R][I+\Delta\tau\delta_\eta^i B_\bullet^L][I+\Delta\tau\delta_\eta^i B_\bullet^R][I+\Delta\tau\delta_\zeta^i C_\bullet^L][I+\Delta\tau\delta_\zeta^i C_\bullet^R]\Delta Q^n \quad (3\text{-}39)$$

$$= -\Delta\tau R^n,$$

where

$$R^n = \delta_\xi^e F^n + \delta_\eta^e G^n + \delta_\zeta^e H^n$$

The solution of this scheme consists of successive solution of six block bidiagonal systems of equations which are

$$[I + \Delta\tau\delta_\xi^i A_\bullet^L]X^1 = -\Delta\tau R^n \quad (3\text{-}40a)$$

$$[I + \Delta\tau\delta_\xi^i A_\bullet^R]X^2 = X^1 \quad (3\text{-}40b)$$

$$[I + \Delta\tau\delta_\eta^i B_\bullet^L]X^3 = X^2 \quad (3\text{-}40c)$$

$$[I + \Delta\tau\delta_\eta^i B_\bullet^R]X^4 = X^3 \quad (3\text{-}40d)$$

$$[I + \Delta\tau\delta_\zeta^i C^L_\bullet]X^5 = X^4 \qquad (3\text{-}40e)$$

$$[I + \Delta\tau\delta_\zeta^i C^R_\bullet]\Delta Q^n = X^5 \qquad (3\text{-}40f)$$

The bidiagonal solution can be vectorized in planes perpendicular to lines along which backward or forward substitution is taking place. For example, the solution of (3-40a), which is lower bidiagonal, is obtained by forward substituting along ξ lines. In this case the vectorization direction is the ξ=constant plane. Another factorization is

$$[I+\Delta\tau(\delta_\xi^i A^L_\bullet+\delta_\xi^i A^R_\bullet)][I+\Delta\tau(\delta_\eta^i B^L_\bullet+\delta_\eta^i B^R_\bullet)][I+\Delta\tau(\delta_\zeta^i C^L_\bullet+\delta_\zeta^i C^R_\bullet)]\Delta Q^n = -\Delta\tau R^n. \qquad (3\text{-}41)$$

The solution is obtained to this three-factor scheme by successive solution of three block tridiagonal systems of equations, and can be vectorized similarly to the six-factor scheme. This method requires half the solution passes of the six-factor scheme, but each pass is more costly since it requires solution of a block tridiagonal system. This method also requires more storage than the six-factor because two sets of flux Jacobians are required in memory at the same time, while the six-factor only needs one at a time. Yet another factorization is given by

$$[I+\Delta\tau(\delta_\xi^i A^L_\bullet+\delta_\eta^i B^L_\bullet+\delta_\zeta^i C^L_\bullet)][I+\Delta\tau(\delta_\xi^i A^R_\bullet+\delta_\eta^i B^R_\bullet+\delta_\zeta^i C^R_\bullet)]\Delta Q^n = -\Delta\tau R^n \qquad (3\text{-}42)$$

This two-factor scheme is very attractive in that it consists of solution of a sparse block lower triangular system followed by solution of a sparse block upper triangular system of equations given by

$$[I + \Delta\tau(\delta_\xi^i A_\bullet^L + \delta_\eta^i B_\bullet^L + \delta_\zeta^i C_\bullet^L]X^1 = -\Delta\tau R^n \qquad (3\text{-}43a)$$

$$[I + \Delta\tau(\delta_\xi^i A_\bullet^R + \delta_\eta^i B_\bullet^R + \delta_\zeta^i C_\bullet^R]\Delta Q^n = X^1. \qquad (3\text{-}43b)$$

Solution of (3-43a) is done by a simple forward substitution and solution of (3-43b) by a simple back substitution. As noted in Reference 15, the forward and backward substitution steps cannot be vectorized along any coordinate line or constant coordinate plane. This is due to the fact that $X^1_{i,j,k}$ in (3-43a) depends on $X^1_{i-1,j,k}$, $X^1_{i,j-1,k}$ and $X^1_{i,j,k-1}$. However, Janus[16] has subsequently derived an algorithm for vectorizing the substitution step by operating on all points in a diagonal plane in computational space simultaneously. A diagonal plane is one on which i+j+k = constant. The solution of Equation (3-43) is a pass through computational space starting at the lower corner, i.e. (i,j,k)=(1,1,1), and sweeping through by diagonal planes until the upper corner, $(i,j,k)=(i_{max}, j_{max}, k_{max})$ is reached. The second pass, given by Equation (3-43b) starts at the upper corner and sweeps back to the lower corner. Using this technique the solution of Equation (3-43) is fully vectorizable. One disadvantage of this two-factor algorithm is that three sets of Jacobian matrices need to be stored simultaneously.

A stability analysis for the six-factor, three-factor and two factor schemes was presented by Anderson, et al., in Reference 15. The analysis indicated that the six-factor scheme had the poorest stability properties and was stable up to a Courant number of about 10. The two-factor scheme was least sensitive to Courant number and was stable for all Courant numbers up to 35, which was the maximum investigated. The present study includes calculations with both the six-factor and the

two-factor methods which tend to verify the superiority of the two factor results for higher Courant numbers. These results will be presented in Section 3.5.

3.4 Boundary Conditions

Characteristic variable boundary conditions are derived in Reference 17 for stationary grids and Reference 8 for dynamic grids. As in these references, a layer of points outside the boundaries, called phantom points, are used here to implement the characteristic variable boundary conditions. Because there is only one point outside the boundary, the computation of fluxes at boundary faces is modified to use one point dependent variable extrapolation at boundary faces both from inside and outside the domain. The change in dependent variables, ΔQ^n, is taken as zero at phantom points. The result of this boundary treatment is that the boundary conditions are only first order accurate. The assumption is made that this will not affect global accuracy of the second order scheme.

3.5 Time Accuracy

In this section the time-accuracy of the split flux algorithms previously discussed will be examined by comparing computed unsteady results for different factorizations, different time discretizations, and different time step sizes. All calculations are for a NACA0012 airfoil oscillating in pitch about its quarter chord point at a Mach number of 0.755 and a reduced frequency of 0.1628, where reduced frequency, or Strouhal number, is defined as

$$k = \frac{\hat{\omega}\hat{c}}{\hat{V}_\infty} \tag{3-44}$$

with $\hat{\omega}$ = oscillatory frequency of airfoil motion

$\hat{V}_\infty$ = free-stream velocity

$\hat{c}$ = chord length of airfoil

The mean angle of attack, α_0, of the airfoil was 0.016 degrees and the unsteady angle of attack amplitude, α_1, was 2.51 degrees. The angle of attack history of the airfoil is given by

$$\alpha(t) = \alpha_0 + \alpha_1 \sin(\hat{\omega}\hat{t}), \tag{3-45}$$

which in nondimensional variables is given by

$$\alpha(t) = \alpha_0 + \alpha_1 \sin(M_\infty kt) \tag{3-46}$$

Experimental data is available for this case from Landon,[18] and a comparison of computed results with the experimental data will also be presented.

The grid used for these calculations was a 'C' grid with 221 points on the airfoil and in the wake and 20 points from the airfoil to the far-field boundaries. The far-field boundaries were placed 25 chords upstream and 30 chords above, below, and downstream of the airfoil. There were 161 points actually on the airfoil surface. The grid was generated using the transfinite interpolation option of the grid code written by Thompson. Figures (3-2a) and (3-2b) show the entire grid and a closeup of the airfoil. The maximum spacing between points on the airfoil surface is 1.9% of the chordlength and occurs at the 60% chord position. From experience with steady calculations on this grid it has been found that this grid resolution is insufficient to resolve weak

shocks, but clustering the grid at shock locations is impractical for unsteady calculations in which the shock position changes by 20% of the chord during the calculation. Solution adaptive gridding offers a solution to this problem, but is beyond the scope of this investigation.

The calculations were started with initial conditions of free stream values everywhere, and then 500 iterations of local time stepping with CFL (Equation (3-38)) equal to 15 were used to establish the steady flow field before the unsteady motion was started. The local time stepping was replaced by a fixed time step, the same at all points, when the unsteady calculation began. The unsteady calculations were continued until the airfoil had gone through four cycles of pitching motion to allow unsteady transients to decay. Airfoil motion for this and all cases presented here was implemented by rotating the entire grid as a rigid body about the pitch axis.

Results from the two-pass algorithm applied to the oscillating NACA0012 case described above are presented in Figures (3-3) through (3-5). Figures (3-3a thru h) show the pressure coefficients on the airfoil surface at eight time instants during the fourth cycle of oscillating pitch. Three time step sizes are shown using the second-order time-accurate three point backward scheme given by Equation (3-23), and two time step sizes using the first-order time-accurate backward Euler scheme given by Equation (3-25). In Figure (3-3a) the airfoil is 25° into the cycle, and although the angle of attack is increasing through 1.09°, there is a remnant of the lower surface shock wave moving forward and weakening. This phenomenon, and the similar occurrence involving the collapse of the upper surface shock when the an-

gle of attack is decreasing (Figure 3-3e), is where the variation between the different methods and time steps is most visible. The extremes in the shock locations given by the various curves are always given by the 0.01 time step case and the 0.20 time step case. This is true at each instant plotted in Figures (3-3a-h). In all cases, the shock wave given by the larger time step lags the motion of the shock wave given by the smaller time step. Taking the shock location as the position where the coefficient of pressure curve crosses the critical pressure coefficient value, Figure (3-4) shows the shock location for all the cases shown in Figure (3-3a). Notice from Figure (3-4) that decreasing the time step an order of magnitude from $\Delta\tau = 0.10$ to $\Delta\tau = 0.01$ changed the shock location by approximately the same amount as reducing the time step from $\Delta\tau = 0.20$ to 0.10. This indicates that reduction of the time step below $\Delta\tau=0.01$ *should not be expected* to change the shock location appreciably. Returning to Figure (3-3), another difference between results using different time step sizes is apparent. For those cases with relatively large shock wave speeds, the larger time steps show more compression downstream of the shock and a large wavelength 'ringing' behavior, but in parts (c) and (g), where the shock has nearly reached the point of maximum downstream travel, the smaller time step produces a higher pressure coefficient behind the shock, with no ringing, however. The $\Delta\tau=0.01$ case also generally produces slightly sharper shocks than the larger time steps.

Comparing the first-order time-accurate results with the second-order time-accurate results in Figure (3-3) shows little difference. The first-order $\Delta\tau=0.05$ pressures are between the second-order $\Delta\tau=0.01$ and

second-order $\Delta\tau$=0.10 pressures, while the first-order $\Delta\tau$=0.10 results are slightly more different from the $\Delta\tau$=0.01 results than are the second-order $\Delta\tau$=0.10 results. Since the second-order $\Delta\tau$=0.01 case can be assumed closer to the correct values, this indicates that the second-order method gives slightly better results for large time step sizes, but no appreciable difference is shown for this test case.

The difference in pressure coefficients for the different time step sizes and methods discussed above make relatively little difference to the lift coefficient history of the airfoil, as shown in Figure (3-5a), but make more difference to the moment coefficient history, as shown in Figure (3-5b). The ragged peaks are due to not calculating lift and moment at the same time in each cycle. One reason for the small difference in lift is that the increased area under the pressure coefficient curve due to the lagging shock position of the larger time step cases is counterbalanced by the overcompression behind the shock. This behavior imposes an additional moment on the airfoil, however, and is responsible for the larger amplitudes of the $\Delta\tau$=0.10 and $\Delta\tau$=0.20 moment coefficient histories.

The discussion above has dealt with the time step sizes used for different calculations. Time step size by itself has little meaning for application to general problems that may have different grids and flow conditions. A parameter that is much more meaningful for numerical solution of hyperbolic systems is the Courant number. The Courant number is the number of computational cells that a wave will propagate through in one time step. For a given time step, $\Delta\tau$, Equations (3-38a,b) give

a value for the CFL parameter that will be used as a measure of Courant number for the three-dimensional problem.

$$CFL = \Delta\tau \left[\frac{\max_{\ell} |\lambda_{\xi}^{\ell}|}{\Delta\xi} + \frac{\max_{\ell} |\lambda_{\eta}^{\ell}|}{\Delta\eta} + \frac{\max_{\ell} |\lambda_{\zeta}^{\ell}|}{\Delta\zeta} \right] \tag{3-47}$$

The maximum CFL for the $\Delta\tau$=0.01 case was approximately 10, the maximum CFL for the $\Delta\tau$=0.10 case was about 100, and for the $\Delta\tau$=0.20 case the maximum CFL was about 200. The maximum CFL occurs in the first cell off the airfoil at about 2.5% chords downstream of the leading edge. At the 25% chord location, the CFL is about half its maximum value, and at the trailing edge it is one-fourth its maximum. The local CFL decreases quickly as the cells become larger away from the airfoil. The maximum CFL in the second row of points off the airfoil surface is only 75% of the maximum CFL in the first row.

All results presented thus far were obtained using the two-pass, or two-factor, method. The six-pass, or six-factor, method has also been applied to the oscillating NACA0012 airfoil. Results obtained for $\Delta\tau$=0.01 and $\Delta\tau$=0.05 are similar to those obtained from the two-pass method, but for the $\Delta\tau$=0.10 case the pressure distribution displayed oscillations as illustrated in Figure (3-6a,b). As previously discussed, the maximum CFL for this case is near 100 and occurs not at the leading edge but slightly downstream of it at approximately the location where those oscillations occur. The oscillations are present on both the upper and lower surface, but are much larger in magnitude on the lower surface throughout the cyclic motion of the airfoil, even though the local CFL on the upper surface at times exceeds that of the lower

surface as in Figure (3-6a). The reason for this is not understood, but may be due to the asymmetry of the six-pass method. These results verify the trend predicted by the stability analysis of Anderson, et al.[15] discussed earlier. It is apparent from the figure that in regions away from the oscillations, the six-pass results match the two-pass results very well.

The trapezoidal scheme given by Equation (3-24) was attempted for this problem, but it was found to be unstable for all tested values of CFL greater than one using local time stepping, and no full calculations were performed.

A comparison of computed pressure coefficients for the pitching NACA0012 with the experimental results of Landon[18] is given in Figure (3-7). Figures (3-8a,b) are plots of the experimental versus the computed lift and moment coefficient histories. Computed results are plotted for both the nominal mean angle of attack, α_0=0.016°, and for a mean angle of attack of α_0=0.375°. The use of a mean angle of attack different from the near zero angle of attack reported in Reference 18 is motivated by the differences in the experimental C_p curves at points that are 180° apart in the oscillatory motion of the airfoil (compare Figures (3-7b) and (3-7f)), and by the obvious bias towards positive lift coefficients shown in Figure (3-8a). The specific value used for α_0 was obtained by using the slope of the unsteady lift versus angle of attack curve to determine the change in α_0 required to match the experimental peak lift values. The α_0=0.375° calculation matches the experiment much more closely than the nominal. In particular, the experimental data in Figure (3-7a) shows an already developed upper sur-

face shock in addition to the decaying lower surface shock. The α_0=0.016° case gives the lower surface shock too far downstream and too strong, while the upper surface shock has not yet been resolved. The remaining parts of Figure (3-7) also illustrate better agreement for the α_0=0.375° case. The α_0=0.375° case matches the experimental lift history better than the α_0=0.16° case in Figure (3-8a), but both computations fail to match the negative portion of the moment coefficient history in Figure (3-8b).

CHAPTER IV

EULER SOLUTIONS ON BLOCKED GRIDS

4.1 Basic Concepts

Various approaches have been presented for making the task of grid generation about complex geometries more simple, such as the Chimera grid scheme of Dougherty, et al.,[19] and Benek, et al.[20] Figure(4-1a) shows a schematic of a Chimera grid. The Chimera approach to gridding provides for multiple bodies that are gridded independently and communicate between grids by interpolating in regions of overlap. The patched grid approach of Rai[21] requires that grids meet along a common boundary as shown in Figure (4-1b), but allows for discontinuity in the grid across the boundary. The blocked grid scheme advocated by Thompson,[22] Figure (4-1c), is a subset of patched grids that assumes complete continuity (or at least slope continuity) of the grid across block boundaries. This scheme makes the task of information transfer across block boundaries much simpler than when grid lines are not continued into adjacent blocks because complex interpolation is not required at grid boundaries. Though blocked grids require matched interface grid boundaries that are not required by patched grids, blocked grids still allow very complicated three-dimensional configurations to be easily gridded. The grid used by Lasinski, et al.[23] to calculate flow about a tri-element "augmentor wing" airfoil is an example of a blocked grid used to model a complex three-body problem in two dimensions. Hessenius and Pulliam[24] presented steady inviscid two-dimensional calculations and unsteady one-dimensional calculations on blocked grids. An implicit

central difference method was used at field points and flux splitting was used at the block-to-block boundaries. The blocked grid concept has been applied to three-dimensional problems by Weatherill and Forsey[25] and by Miki and Takagi.[26] The common theme of these gridding methods is the use of different grids, or coordinates systems, in different regions, thereby allowing the most appropriate grid structure to be used in each region. The primary conceptual difference between the Chimera grids, patched grids, and blocked grids is the degree of independence between the various subgrids. The idea of using different coordinates systems in different regions is not new. In 1969, Thoman and Szewczyk[27] calculated viscous flow over a circular cylinder by embedding a cylindrical coordinate system inside a rectangular mesh. The cylindrical coordinates allowed better resolution near the cylinder, while the rectangular mesh was more appropriate for the wake region.

The Euler code presented here will accept any arrangement of arbitrarily sized blocks. Only one block at a time is stored in memory while all other blocks are stored in high speed secondary memory that is accessed like a disk. Dynamic memory management is used to adjust the amount of memory requested while working on a particular block to equal the amount of memory needed. Details of the block handling and block-to-block information transfer techniques and an analysis of the error introduced at block boundaries will also be presented in this chapter. Calculations for transonic flow over an airfoil using blocked

and unblocked grids will be used to validate the method. The method will be applied to calculation of three-dimensional transonic flow about a rectangular planform supercritical wing of aspect ratio two and compared with experiment to illustrate the application of the code in Chapter V.

4.2 Block Boundary Conditions

Consider the simple blocked grid arrangement shown by Figure 4-2. Solving on this block grid corresponds to partitioning the set of equations that would be solved if the entire grid were one block. Using the two-pass method given by Equation (3-43), the partitioned matrix equations have the following structure

$$\begin{bmatrix} I + \Delta\tau L_{I,I} & 0 \\ \Delta\tau L_{II,I} & I + \Delta\tau L_{II,II} \end{bmatrix} \begin{bmatrix} X_I \\ X_{II} \end{bmatrix} = \begin{bmatrix} \Delta\tau R_I \\ \Delta\tau R_{II} \end{bmatrix} \tag{4-1a}$$

$$\begin{bmatrix} I + \Delta\tau U_{I,I} & \Delta\tau U_{I,II} \\ 0 & I + \Delta\tau U_{II,II} \end{bmatrix} \begin{bmatrix} \Delta Q_I \\ \Delta Q_{II} \end{bmatrix} = \begin{bmatrix} X_I \\ X_{II} \end{bmatrix} \tag{4-1b}$$

Equation (4-1a) is the matrix form of the lower block triangular system of equations represented by Equation (3-43a), and Equation (4-1b) is the matrix form of the upper block triangular system of equations represented by Equation (3-43b). The partitioning of the matrices is the mathematical analog of breaking the original grids into blocks I and

II. Note that $\mathbf{I} + \Delta\tau\mathbf{L}_{I,I}$ and $\mathbf{I} + \Delta\tau\mathbf{L}_{II,II}$ are lower block triangular matrices and that $\mathbf{I} + \Delta\tau\mathbf{U}_{I,I}$ and $\mathbf{I} + \Delta\tau\mathbf{U}_{II,II}$ are upper block triangular matrices. The rectangular matrix $\Delta\tau\mathbf{L}_{II,I}$ contains coefficients of quantities in block I that are required to make spatial difference expressions for cells in block II complete. Similarly, $\Delta\tau\mathbf{U}_{I,II}$ contains coefficients of quantities in block II that are required to make difference expressions for cells in block I complete. Although Equation (3-43) uses backward Euler time differencing, this matrix representation would be identical if either three-point backward or trapezoidal time differencing were used. The conditions required to solve the blocked grid problem and obtain exactly the same results as for the unblocked problem will be discussed first. Then some simplifications that can be used and the error resulting from these simplifications will be presented. Expanding Equation (4-1a) gives

$$(\mathbf{I} + \Delta\tau\mathbf{L}_{I,I})\mathbf{X}_I = \Delta\tau\mathbf{R}_I \tag{4-2}$$

$$(\mathbf{I} + \Delta\tau\mathbf{L}_{II,II})\mathbf{X}_{II} = \Delta\tau\mathbf{R}_{II} - \Delta\tau\mathbf{L}_{II,I}\mathbf{X}_I \tag{4-3}$$

Equation (4-2) illustrates that the intermediate solution obtained from the forward pass through block I does not depend upon the solution, $\mathbf{X}_{II}$, in block II. There is a dependency on dependent variable values in block II, however, that is not clearly displayed by the notation in Equation (4-2). The elements of $\mathbf{R}_I$ that correspond to the first and second cells inside the block boundary are affected by dependent variable values from time t^n in the first two cells across the block boundary in block II. This is due to the fact that evaluation of flux at a face generally will require two points on either side of the face.

Therefore, one requirement for obtaining exactly the same answer from the blocked calculated as from the unblocked is to have dependent variable values available from the first two cells of neighboring blocks.

Equation (4-3) shows that if the result of the forward pass in block II is to be identical for the blocked and unblocked cases, then the solution from the forward pass in block I, $\mathbf{X}_I$, must be available. Though not shown by Equation (4-3), the actual elements of $\mathbf{X}_I$ that are required are those in the first cell off the block boundary. Now expanding Equation (4-1b) for the backward pass gives

$$(\mathbf{I} + \Delta\tau\mathbf{U}_{I,I})\Delta\mathbf{Q}_I = \mathbf{X}_I - \Delta\tau\mathbf{U}_{I,II}\Delta\mathbf{Q}_{II} \tag{4-4}$$

$$(\mathbf{I} + \Delta\tau\mathbf{U}_{II,II})\Delta\mathbf{Q}_{II} = \mathbf{X}_{II} \tag{4-5}$$

The situation here is similar to that for the forward pass, assuming that the correct $\mathbf{X}_I$ and $\mathbf{X}_{II}$ are available. The backward pass can be completed first in block II to obtain $\Delta\mathbf{Q}_{II}$ without results from block I. The backward pass can then be performed in block I to obtain $\Delta\mathbf{Q}_I$ since $\Delta\mathbf{Q}_{II}$ is available.

The sequence of operations required to reproduce unblocked results is summarized in Figure (4-3), and Figure (4-4) shows how the discussion above could be extended to more complicated arrangements of blocks. The grids depicted by Figures (4-3) and (4-4) can be considered to be in the computational domain. The transformation that maps the blocks back to physical space could map these rectangular arrays of points into a 'C' grid or an 'O' grid or any other conceivable shape obtainable by warping or stretching the original rectangle. Although it is possible to write the coordinate transformation for each block separately, nothing would

be gained by doing so. Any blocked grid that maps into computational space in such a way as to allow assembly of the blocks with all block-to-block interfaces correctly aligned can be represented by a single coordinate transformation, except in the case where block faces are double-valued to allow a solid surface to be enclosed between blocks. An example where blocking the grid would not be necessary except to allow impermeable surface boundary conditions on a missile fin is given in Figure (4-5). For the class of problems for which a single coordinate transformation could be used to generate the entire grid, blocking is still a useful concept. Computer memory sizes are not projected to become infinite for a few years yet, and until this occurs, blocked grids allow very large problems to be solved with one piece at a time in memory. Also, as discussed in Section 4.3, most charging algorithms heavily weight memory usage so that it is economically attractive to reduce the amount of memory used even if total computational time increases as a result.

The original motivation for this study of blocked grids was the capability of gridding complex geometries. The advantage of blocked grids for complex geometries is the ability to embed a block of one topology inside another block with a totally different topology. (Here the word topology is loosely used to refer to the type of grid system as typified by the location of any cuts necessary to unwrap the physical grid into a rectangular block in computational space with no interior boundaries.) Figure (4-1c) is an example of this type of blocked grid system. The blocks that make up this grid and their correspondences are shown in Figure (4-6). For this grid and for most blocked grids about

truly complex geometries, there is no equivalent one-block or unblocked grid. For many block arrangements no sequence of operations exists that will provide values at boundaries when necessary. The question of whether the multiblock solution can reproduce the unblocked solution is moot for these grids, and the correct question becomes whether it is possible to transfer information between blocks in such a way as to produce a stable, conservative, and consistent scheme with no degradation in accuracy.

Equations (4-1a,b) apply to the case where there exists a global unblocked grid equivalent to the blocked grid, and hence are not strictly applicable to cases where such an unblocked grid does not exist. Because blocked grids have complete continuity across block boundaries it will always be possible, however, to trace any grid line until it ends at a far-field boundary, an impermeable surface, a reflection plane, or closes on itself. Since multiple lines can originate from a single line as it passes through a block boundary, this tracing is not unique for grid lines. As noted by Norton, Thompkins, and Haimes,[28] however, if cell centers are traced then ambiguities are resolved and the tracing is unique. For schemes with all unknowns along a computational line, such as the six-factor and three-factor methods, it is possible to write a set of equations for each of the three lines passing through each cell and solve these as if no block boundaries were present. This fact has little practical value in terms of obtaining a solution for the two-factor scheme, since solving these lines in the correct order to have necessary information available for the solution of the next line is not always possible. It does mean that when considering

any particular block-to-block interface the grid can be locally re-blocked so that both blocks become part of the same new block. This is the rationale for using Equations (4-1a,b) as a standard of correct block-to-block information transfer, even though an equivalent globally unblocked grid may not exist.

As a very simple example of this consider the one-block "O" grid schematic in Figure (4-7). To map the physical grid in Figure (4-7a) into the rectangular block in the computational domain shown in Figure (4-7b), a cut must be made along line ab which is identical to cd in the physical domain. The boundary conditions that should be used on faces ab and cd fall into the general class of block-to-block boundary conditions under discussion. The only peculiarity of this case is that the block on both sides of the boundary is the same. This simple one block example illustrates the difficulty in supplying correct values at block boundaries. In order to sweep from face ab to cd, the solution at face cd must be used as a boundary condition at face ab. Following the rationale described in the previous paragraph, the grid can be reblocked by placing the cut along line ef instead of ab making ab an interior boundary to the new block. If no error is incurred on the outer boundary of the new block then Figure (4-7c) is identical to Figure (4-2), and therefore Equation (4-1) is applicable. Of course, the fallacy in this argument is that boundaries ef and gh have the same problem that ab and cd had originally, and therefore there will be some error at these boundaries. This is why the following arguments concerning error at block-to-block boundaries can only be considered valid in a small region local to the boundary.

The value of $\mathbf{X}_I$ in Equation (4-3) and of $\Delta\mathbf{Q}_{II}$ in Equation (4-4) are the quantities that will not necessarily be available in cases with no unblocked equivalent. The simplest approximation for these quantities is to set their coefficients, $\mathbf{U}_{I,II}$ and $\mathbf{L}_{II,I}$ to zero. To evaluate the effect of this, first determine the correct solution for $\Delta\mathbf{Q}_I$ and $\Delta\mathbf{Q}_{II}$. From Equations (4-2) and (4-3)

$$\mathbf{X}_I = \Delta\tau(\mathbf{I} + \Delta\tau\mathbf{L}_{I,I})^{-1}\,\mathbf{R}_I \tag{4-6}$$

$$\mathbf{X}_{II} = \Delta\tau(\mathbf{I} + \Delta\tau\mathbf{L}_{II,II})^{-1}\,[\mathbf{R}_{II} - \Delta\tau\mathbf{L}_{II,I}(\mathbf{I} + \Delta\tau\mathbf{L}_{I,I})^{-1}\,\mathbf{R}_I] \tag{4-7}$$

Substituting (4-7) in (4-5) and solving for $\Delta\mathbf{Q}_{II}$ gives

$$\Delta\mathbf{Q}_{II} = (\mathbf{I}+\Delta\tau\mathbf{U}_{II,II})^{-1}(\mathbf{I}+\Delta\tau\mathbf{L}_{II,II})^{-1}[\Delta\tau\mathbf{R}_{II}-\Delta\tau^2\mathbf{L}_{II,I}(\mathbf{I}+\Delta\tau\mathbf{L}_{I,I})^{-1}\mathbf{R}_I] \tag{4-8}$$

Using Equations (4-6) and (4-8) in Equation (4-4) gives

$$\Delta\mathbf{Q}_I = (\mathbf{I} + \Delta\tau\mathbf{U}_{I,I})^{-1}\{(\mathbf{I}+\Delta\tau\mathbf{L}_{I,I})^{-1}\Delta\tau\mathbf{R}_I \tag{4-9}$$

$$- \Delta\tau^2\mathbf{U}_{I,II}(\mathbf{I}+\Delta\tau\mathbf{U}_{II,II})^{-1}(\mathbf{I}+\Delta\tau\mathbf{L}_{II,II})^{-1}[\mathbf{R}_{II}-\Delta\tau\mathbf{L}_{II,I}(\mathbf{I}+\Delta\tau\mathbf{L}_{I,I})^{-1}\mathbf{R}_I]\}$$

Setting $\mathbf{U}_{I,II}$ and $\mathbf{L}_{II,I}$ to zero in Equations (4-8) and (4-9) yields

$$\Delta\mathbf{Q}_{II} = \Delta\tau(\mathbf{I} + \Delta\tau\mathbf{U}_{II,II})^{-1}(\mathbf{I} + \Delta\tau\mathbf{L}_{II,II})^{-1}\mathbf{R}_{II} \tag{4-10}$$

$$\Delta\mathbf{Q}_I = \Delta\tau(\mathbf{I} + \Delta\tau\mathbf{U}_{I,I})^{-1}(\mathbf{I} + \Delta\tau\mathbf{L}_{I,I})^{-1}\mathbf{R}_I \tag{4-11}$$

The error committed in not passing the implicit solution across block boundaries is

$$\mathbf{E}_{\Delta Q_I} = -\Delta\tau^2(\mathbf{I} + \Delta\tau\mathbf{U}_{I,I})^{-1}\mathbf{U}_{I,II}(\mathbf{I} + \Delta\tau\mathbf{U}_{II,II})^{-1}(\mathbf{I} + \Delta\tau\mathbf{L}_{II,II})^{-1}$$

$$[\mathbf{R}_{II} - \Delta\tau\mathbf{L}_{II,I}(\mathbf{I} + \Delta\tau\mathbf{L}_{I,I})^{-1}\,\mathbf{R}_I] \tag{4-12}$$

for the error in $\Delta\mathbf{Q}_I$, and

$$\mathbf{E}_{\Delta Q_{II}} = -\Delta\tau^2(\mathbf{I} + \Delta\tau\mathbf{U}_{II,II})^{-1}(\mathbf{I} + \Delta\tau\mathbf{L}_{II,II})^{-1}\mathbf{L}_{II,I}(\mathbf{I} + \Delta\tau\mathbf{L}_{I,I})^{-1}\,\mathbf{R}_I \tag{4-13}$$

for the error in $\mathbf{\Delta Q}_{II}$. To determine the order of magnitude of $\mathbf{E}_{\Delta Q_I}$ and $\mathbf{E}_{\Delta Q_{II}}$, the magnitude of the individual factors in Equations (4-12) and (4-13) must be known. Each element of the matrices $\mathbf{U}_{I,I}$, $\mathbf{U}_{I,II}$, $\mathbf{U}_{II,II}$, $\mathbf{L}_{I,I}$, etc. represents one term of a first order spatial difference in one of the three coordinate directions, and therefore each element is either $O(1/\Delta\xi)$, $O(1/\Delta\eta)$, or $O(1/\Delta\zeta)$. The matrices $(\mathbf{I}+\Delta\tau\mathbf{U}_{I,I})^{-1}$, $(\mathbf{I}+\Delta\tau\mathbf{L}_{I,I})^{-1}$, etc. are $O(1)$ and $\mathbf{R}_I$ and $\mathbf{R}_{II}$ are $O(1)$. Using this in Equations (4-12) and (4-13) results in

$$\mathbf{E}_{\Delta Q_I} = O\left(\frac{\Delta\tau^2}{\Delta\xi}, \frac{\Delta\tau^2}{\Delta\eta}, \frac{\Delta\tau^2}{\Delta\zeta}\right) \tag{4-14a}$$

$$\mathbf{E}_{\Delta Q_{II}} = O\left(\frac{\Delta\tau^2}{\Delta\xi}, \frac{\Delta\tau^2}{\Delta\eta}, \frac{\Delta\tau^2}{\Delta\zeta}\right) \tag{4-14b}$$

Since $\mathbf{\Delta Q}_I$ and $\mathbf{\Delta Q}_{II}$ are themselves $O(\Delta\tau)$, the truncation error due to not passing the solution vector across block boundaries is $O(\Delta\tau/\Delta\xi,\ \Delta\tau/\Delta\eta,\ \Delta\tau/\Delta\zeta)$.

For better understanding of the error due to not passing the implicit solution across block boundaries, consider the one-dimensional backward Euler scheme, Equation (3-25), rewritten here for convenience.

$$[\mathbf{I} + \Delta t\delta^i\mathbf{A}^n]\Delta\mathbf{Q}^n = -\Delta t\delta^e\mathbf{F} + O(\Delta t\Delta x^2,\ \Delta t^2\Delta x,\ \Delta t^2) \tag{4-15}$$

Taking δ^i as a backward spatial difference and dividing through by Δt gives

$$\frac{\Delta Q_j^n}{\Delta t} + \frac{A_j^n\Delta Q_j^n - A_{j-1}^n\Delta Q_{j-1}^n}{\Delta x} = -\delta^e F^n + O(\Delta x^2,\ \Delta t\Delta x,\ \Delta t) \tag{4-16}$$

setting $A_{j-1}^n = 0$ yields

$$\frac{\Delta Q_j^n}{\Delta t} + \frac{A_j^n \Delta Q_j^n}{\Delta x} = -\delta^e F \qquad (4\text{-}17)$$

$$\left[\left(\frac{\partial Q}{\partial t}\right)^{n+1} + O(\Delta t)\right] + O\left(\frac{\Delta t}{\Delta x}\right) = -\left[\left(\frac{\partial F}{\partial x}\right)^{n+1} + O(\Delta t, \Delta x^2)\right]$$

giving a truncation error of $O(\Delta t, \Delta t/\Delta x, \Delta x^2)$. The three point backward scheme, Equation (3-24) is

$$\frac{3\Delta Q_j^n - \Delta Q_j^{n-1}}{2\Delta t} + \frac{A_j^n \Delta Q_j^n - A_{j-1}^n \Delta Q_{j-1}^n}{\Delta x} = -\delta^e F^n + O(\Delta x^2, \Delta t \Delta x, \Delta t^2) \qquad (4\text{-}18)$$

Setting $A_{j-1}^n = 0$ yields

$$\frac{3\Delta Q_j^n - \Delta Q_j^{n-1}}{2\Delta t} + \frac{A_j^n \Delta Q_j^n}{\Delta x} = -\delta^e F^n \qquad (4\text{-}19)$$

$$\left[\left(\frac{\partial Q}{\partial t}\right)^{n+1} + O(\Delta t^2)\right] + O\left(\frac{\Delta t}{\Delta x}\right) = -\left[\left(\frac{\partial F}{\partial x}\right)^{n+1} + O(\Delta t, \Delta x^2)\right]$$

giving the same truncation error on block boundaries as the backward Euler.

It is obvious from the analysis above that not transferring the solution vector across block boundaries results in an inconsistent scheme at the boundary unless $\Delta t/\Delta x \to 0$. There is also a conservation error at the boundary of $O(\Delta t/\Delta x)$ due to the "implicit flux," $A\Delta Q$, being defined differently in the adjacent blocks. The conservation error could be eliminated by setting $A\Delta Q = 0$ in both blocks at the boundary face, but this adds another cell with an inconsistent differencing.

Another approach for passing the solution vector across block boundaries is to approximate $\mathbf{X}_I$ in Equation (4-3) and $\mathbf{\Delta Q}_{II}$ in Equation

(4-4) using whatever information is currently available from other blocks. The values used in this study are the results from both passes in adjacent blocks, at whatever time level was most recently calculated in those blocks. This means that $\mathbf{\Delta Q}_I^n$ or $\mathbf{\Delta Q}_I^{n-1}$ may be used to approximate $\mathbf{X}_I^n$ in Equation (4-3), and $\mathbf{\Delta Q}_{II}^n$ or $\mathbf{\Delta Q}_{II}^{n-1}$ may be used to approximate $\mathbf{\Delta Q}_{II}^n$ in Equation (4-4), depending on the order in which the blocks are solved.

The effect of using a time lagged value of ΔQ is easily illustrated for the one-dimensional backward Euler method. Using $\Delta Q^n = \Delta Q^{n-1} + O(\Delta t^2)$ in Equation (4-16) yields

$$\frac{\Delta Q_j^n}{\Delta t} + \frac{A_j^n \Delta Q^n - A_{j-1}^n \Delta Q_{j-1}^n}{\Delta x} = -\delta^e F^n + O(\Delta x^2, \Delta t \Delta x, \Delta t, \frac{\Delta t^2}{\Delta x}) \qquad (4\text{-}20)$$

The time lagged ΔQ resulted in additional truncation error of $O(\Delta t^2/\Delta x)$.

Using the solution vector, $\mathbf{\Delta Q}_I^n$, *to approximate the intermediate solution,* $\mathbf{X}_I^n$, in Equation (4-3) also results in an $O(\Delta t^2/\Delta x)$ truncation error in the calculation of $\mathbf{X}_{II}^n$ and in the subsequent calculation of $\mathbf{\Delta Q}_{II}^n$, as shown below. From Equation (4-4),

$$\mathbf{X}_I = \mathbf{\Delta Q}_I + \Delta\tau(\mathbf{U}_{I,I}\mathbf{\Delta Q}_I + \mathbf{U}_{I,II}\mathbf{\Delta Q}_{II}) \qquad (4\text{-}21)$$

This matrix equation is represented in operator notation by

$$X = \Delta Q + \Delta\tau\delta^i A \Delta Q \qquad (4\text{-}22)$$

which yields

$$\mathbf{X}_I = \mathbf{\Delta Q}_I + O(\Delta\tau^2) \qquad (4\text{-}23)$$

Using Equation (4-23) in Equation (4-3) and solving for $\mathbf{X}_{II}$ results in

$$\mathbf{X}_{II} = \Delta\tau(\mathbf{I} + \Delta\tau\mathbf{L}_{II,II})^{-1}[\mathbf{R}_{II} - \mathbf{L}_{II,I}\mathbf{\Delta Q}_I] + O(\frac{\Delta\tau^3}{\Delta\xi}, \frac{\Delta\tau^3}{\Delta\eta}, \frac{\Delta\tau^3}{\Delta\zeta}) \qquad (4\text{-}24)$$

The truncation error of $O(\Delta\tau^2/\Delta\xi, \Delta\tau^2/\Delta\eta, \Delta\tau^2/\Delta\zeta)$ in X_{II} will obviously carry over as the same order of error when Equation (4-24) is used in Equation (4-5) to calculate $\mathbf{\Delta Q}_{II}$. The order of the error is not affected if X^n is approximated by ΔQ^{n-1} since $\Delta Q^n = \Delta Q^{n-1} + O(\Delta\tau^2)$, and therefore Equation (4-23) still holds.

To summarize the results of the previous error analysis, setting the solution vector values passed to other blocks equal to zero results in $O(\Delta t/\Delta x)$ truncation error, while approximating the required solution vector values by whatever values are currently available from adjoining blocks results in $O(\Delta t^2/\Delta x)$ truncation error. In both the $\Delta Q = 0$ case and the ΔQ approximated case, there is a conservation error due to evaluating the flux at the block boundary differently in adjacent cells.

Throughout the above analysis the assumption was made that all values entering the explicit flux balance, $\delta^e F^n$, were correctly synchronized to be time level n data. Although it is not difficult to code the algorithm so that this is true, for many of the calculations in this study the flux vectors were formed using the latest available information from other blocks. This technique is referred to as using unsynchronized dependent variables. Using some time level n+1 information to form the difference $\delta^e F^n$, that should be totally from time level n data introduces an $O(\Delta t/\Delta x)$ error and a conservation error at the block boundary face.

For steady state calculations all of the errors discussed above vanish as steady state is approached because they are all proportional to ΔQ.

4.3 Coding for Blocked Grids

The design principles used for writing the unsteady, blocked grid, implicit Euler code were, in order of priority:

1. To allow any possible arrangements of blocks with no change to the code.
2. Allow specification of any type of boundary condition, i.e. impermeable surface, far-field, block-to-block, etc. on any patch of a block surface.
3. Maximize vectorization.
4. Minimize memory requirements.
5. Attain most efficient use of high speed secondary memory (SSD on CRAY X-MP).

One important advantage of blocked grids is the ability to solve large problems by working on only one block of the problem at a time while all the rest of the data is stored on disk or a similar device. To take full advantage of this, the code should have adjustable dimension arrays so that arrays associated with blocks of any dimension can be packed into memory with no wasted space. One way of accomplishing this in the FORTRAN computer language is the ribbon vector method. To use the ribbon vector method, the program calculates the equivalent one dimensional array length for all adjustable dimension arrays. Starting locations are then assigned for each of these arrays in the blank common block, making sure to allow enough space between the start of one array and the next to store the entire array. Most computer systems provide a

user callable subroutine that will allow the user to set the amount of memory available to the program. This process is referred to here as dynamic memory management. On systems with dynamic memory management blank common should contain one array singly dimensioned to a length of one. After the user program has determined the total number of words required in the ribbon vector, the program will call the dynamic memory management routine to allocate that many extra words. Because blank common is stored as the last item of the users program in memory, the extra allocated space goes to blank common.

Specific arrays, singly or multiply dimensioned, in the ribbon vector can be easily referred to and used inside subroutines by passing the array as a parameter in the calling statement and using standard FORTRAN adjustable dimension arrays in the subroutines. Figure (4-8) gives an example of ribbon vector usage.

As discussed in Section 4.2, certain information must be transferred between blocks to obtain reasonable results. This information is invariably in the first two cells of neighboring blocks and may consist of the dependent variable values only or the dependent variables and the most recently available solution vector value. Since only one block is contained in memory at a time, special provisions must be made for transferring needed values from other blocks. The approach used here is to store a set of resident boundary condition arrays permanently in memory for each block surface patch that joins another block. These resident arrays are updated to the next time level from information in each block while that block is in memory. By doing this it is never necessary to read or write a block more than once per iteration through the

entire grid. Each block is dimensioned to have enough phantom points to store all boundary condition information. Block boundary condition information is copied into the block's phantom point locations from the resident boundary condition arrays for subsequent calculations. This greatly simplifies vectorization of calculations as opposed to using logic to pull points from the permanent boundary arrays as needed.

Doubly storing the dependent variable values in this way also allows synchronization of terms used in the explicit flux balance. The method used to insure that time level n data is always used at block boundaries is given below. As a starting condition let all blocks and the resident BC (Boundary Condition) arrays contain level n data. The algorithm is as follows:

1. Bring current block into memory and update block BC phantom points from all resident BC arrays.
2. Store information from current block into all resident BC arrays associated with higher numbered blocks.
3. Solve for Q^{n+1} in current block.
4. Store information from current block into all resident BC arrays associated with blocks numbered less than the current block and resident BC arrays for the current block.

The high speed secondary memory on the CRAY X-MP, referred to as SSD, is used to store all blocks not currently in memory. The SSD is accessed using standard FORTRAN input and output methods. To make the most efficient use of SSD, all SSD data files were unblocked. BUFFER IN

and BUFFER OUT statements were used to transfer all data associated with a block in a single unformatted buffer command.

4.4 Two-Dimensional Calculations on Blocked Grids

This section presents results from steady and unsteady calculations on blocked grids. Convergence and stability characteristics are examined for the steady case, and the converged steady solution is shown to not depend on the blocking of the grid. The error in unsteady results due to block boundary positioning is studied for the same airfoil and flow conditions presented in Section 3.5 and results with ΔQ^n=0 at block boundaries and also with ΔQ^n approximated by whatever information is available from adjoining blocks are presented.

The steady calculations were for a NACA0012 airfoil at Mach 0.80 and angle of attack of 1.25 degrees. The grid used first, and the grid that would later be split up to form block grids for comparison, was the one-block "C" grid described in Section 3.5 for use in unsteady calculations. Figure (4-9) shows the pressure distribution obtained after 1000 local time steps at a CFL of 15 using backward Euler time differencing. The strong upper surface shock was sharply captured, but the lower surface shock is not properly resolved. Clustering grid points in the neighborhood of the expected lower surface shock would sharpen it, but this was felt to be unnecessary for this study of blocked versus unblocked results. The blocked grid tests were chosen to provide worst cases by placing block boundaries in regions where the flowfield is rapidly changing. Figure (4-10) illustrates the division of the original grid into four blocks by cutting the grid at the leading and trailing

edges. This is a critical positioning of block boundaries due to the high gradients in the leading and trailing edge stagnation regions, particularly during startup from the initial conditions of free-stream values everywhere. The first block boundary treatment used was to set $\Delta Q^n = 0$ at the boundary and to use the latest available (unsynchronized) dependent variable values from adjoining blocks. Although the starting transients for this case produced highly unrealistic pressure values particularly at the leading edge, the calculation remained stable using local time stepping at a CFL of 15, and steady results identical to the one-block solution were obtained. Figure (4-11) shows a three-block grid chosen to investigate possible interaction between shock waves and the block boundaries. Steady results for this grid were also identical to the one-block case using the same block boundary treatment. These tests show that stability is insensitive to block boundary positioning and that no error is introduced in the steady solution due to blocking.

The convergence history for the one-block, three-block, and four-block steady calculations as measured by the maximum change in density is plotted in Figure (4-12). Another indicator of convergence is the iteration number at which the number of supersonic points stops changing, or is frozen. The number of supersonic points for the one-block case is frozen at 474 iterations; for the four-block case at 604 iterations; and for the three-block case at 599 iterations. For the cases considered approximately 25% more iterations are required to obtain the same degree of convergence with the blocked grids as with an unblocked grid. This disadvantage is more than offset in terms of cost to obtain a solution, however, by the greatly reduced memory requirements for

blocked grid calculations. Table 1 shows a comparison of various job statistics from the three diffferent cases run on the NASA-Ames CRAY X-MP. Note that even though CPU times for the blocked grid cases were higher than the unblocked cases, the cost in terms of accounting units per step for the blocked grid cases were one-third that of the unblocked.

Instead of setting $\Delta Q = 0$ and using the unsynchronized dependent variable values at block boundaries, the solution vector, ΔQ, could be approximated and synchronized dependent variable values could be used. In Section 4.2 it was shown that this should produce less error at block boundaries for unsteady problems. The effect on convergence to steady state of this more accurate boundary treatment is illustrated in Figure (4-13) for the three-block case. The combination of unsynchronized dependent variables with ΔQ approximated is not shown because it was unstable at a CFL of 15. The more accurate boundary treatment obviously does not improve convergence to steady state. Its effect on time-accuracy will be discussed below.

The same four-block and three-block NACA0012 grids used for the steady calculations discussed above were used to calculate unsteady flow at Mach 0.755 and a reduced frequency of 0.1628. The mean angle of attack was 0.016 degrees and the amplitude of the unsteady pitching motion was 2.51 degrees. These are the same conditions used in Section 3.5. The time step was taken to be $\Delta\tau = 0.05$, and backward Euler time differencing was used for all unsteady block calculations.

Pressure distribution for the one-block, three-block and four-block grids are shown in Figures (4-14a) through (4-14h). These results were

obtained by using unsynchronized dependent variables from adjoining blocks and setting $\Delta Q = 0$ at the block boundary. The four block results are nearly indistinguishable from the one block, but the three-block results show a considerable error in shock location everywhere except in Figures (4-14d) and (4-14h). In Figures (4-14d,h) the shock wave has reached its position of maximum downstream travel on the upper and lower surface, respectively, and is nearly stationary. The shock wave position given by the three-block calculation lags the correct location in all cases that have an appreciable shock velocity. The excellent agreement of the four block case is due the small variation with time dependent variables at the block boundaries. Even though large spatial gradients are present at the leading and trailing edge of the airfoil, the pitching motion does not cause rapid changes in a particular cell in this region.

The analysis of Section (4.3) showed that by approximating ΔQ at block boundaries and synchronizing the dependent variables used from adjoining blocks, the error at the boundary could be reduced from $O(\Delta t/\Delta x)$ to $O(\Delta t^2/\Delta x)$. Figures (4-15a) through (4-15h) show a comparison between pressure distributions obtained using approximated ΔQ's with synchronized dependent variables, $\Delta Q=0$ with synchronized dependent variables, and $\Delta Q=0$ at the boundary and unsynchronized dependent variables. The combination of approximated ΔQ with unsynchronized dependent variables was not obtained due to stability problems. The $\Delta Q = 0$ with unsynchronized dependent variables results are the same as those in Figure (4-14). Using synchronized dependent variables, but maintaining the rough $\Delta Q=0$ approximation did not significantly improve the comparison

with one-block results. For example, at the instant in time shown in Figure (4-15a), the $\Delta Q=0$ with synchronized dependent variables comparison is not as good as the $\Delta Q=0$ with unsynchronized dependent variables. Examination of Figure (4-15) reveals the dramatic improvement yielded by the approximated ΔQ and synchronized dependent variable block boundary conditions. The largest difference between the one block results and results from using approximated ΔQ and synchronized dependent variables occurs when the lower surface shock moves upstream from block one through the block boundary roughly parallel to the shock front and into blocks two and three (See Figure (4-11) for the grid geometry). The lower surface shock has just left block one in Figure (4-15a). The upper surface shock in Figure (4-15e) has roughly the same relative position and motion as the lower surface shock in Figure (4-15a), but for this case the approximated ΔQ results show no error in shock position.

The results presented in this section from steady and unsteady calculations on blocked grids have demonstrated the effects on convergence to steady state and on time-accuracy of various block boundary conditions. All of the block boundary conditions represented led to the same steady solution, but the convergence rate was slower on blocked grids than unblocked grids. Block boundary conditions that are formally more time-accurate slowed convergence more than the less accurate conditions for the cases presented here. Cost comparisons for the steady calculations showed that the reduced memory requirements of blocked grids make

their use attractive even if more computer time must be spent to obtain the same level of convergence. Comparison of unsteady calculations on blocked and unblocked grids verified earlier analysis that showed that approximating ΔQ on the block boundaries and using synchronized values of the dependent variables introduces less error than setting $\Delta Q=0$ and using unsynchronized dependent variables.

CHAPTER V

THREE-DIMENSIONAL CALCULATIONS

This chapter presents a comparison of steady and unsteady calculations with experimental results for a rectangular supercritical wing of aspect ratio two.[29] The grid for the wing was generated as a single continuous block of 100x27x25 points and then split into four blocks as shown in Figure (5-1). The overall grid is a "C" mesh in the streamwise direction and half an "O" mesh in the spanwise direction. Points are clustered near the leading edge and near the wing tip. Blocks 1 and 3 include most of the lower and upper surfaces of the wing, respectively, while block 2 wraps around the wing tip. Each of these three blocks are 81x27x9. Block 4 includes all points downstream of the wing and is 20x27x25. The wind tunnel test[29] was conducted in freon so that $\gamma = 1.131$ for the calculations.

Figure (5-2) shows steady state pressure results at four span stations for which experimental data were available for a Mach number of 0.701 and four degrees angle of attack. The semispan location given on the figures in this chapter is for the center of the cell used to compare with experiment. Even though the span location of the experimental data does not exactly match the cell center location, the experimental data point is well within the boundaries of the computational cell with which it is compared in all cases. The calculated leading edge expansion overshoots the experimental near the wing root, but slightly underexpands at the tip. Agreement at the tip is better than at the root, but the inviscid calculation generally predicts lower upper surface pressures than were measured. Steady calculations were done for this

Mach number at two degrees angle of attack with similar results. At higher Mach numbers the comparison with experimental results worsens. For Mach 0.83 and two degrees angle of attack the Euler code predicts a shock wave at the trailing edge of the wing, but the experiment shows the shock much farther forward. Figure (5-3) is a plot of experimental and calculated results for this case at the 60% semispan location. The fairly strong three-dimensional effects present on this low aspect ratio wing are modelled fairly well, but viscous effects need to be accounted for to significantly improve agreement with experiment.

Unsteady calculations for oscillatory rigid body pitching of the wing were performed to compare with experimental results. The pitch axis of the wing was located at 46% of the chord, and the amplitude of the unsteady angle of attack, α_1, was one degree. Two reduced frequencies, k=0.358 and k=0.714, were studied at a freestream Mach number of 0.7 and a mean angle of attack, α_0, of four degrees. The time step size used for both reduced frequencies was approximately $\Delta t = 0.07$. This time step size resulted in a maximum CFL of approximately 130 in blocks 1 and 3 and approximately 60 in block 4. In the wing tip block, block 2, the maximum CFL was around 500 due to the very small cells near the line singularity leaving the leading and trailing edge. The time step sizes chosen resulted in 360 time steps per cycle of motion for k=0.358 and 180 time steps per cycle of motion for k=0.714. The magnitude and phase of the unsteady pressure coefficients were obtained by Fourier analysis of the last cycle of motion calculated at each frequency. Figure (5-4) presents magnitude and phase results obtained from the third cycle of motion at k=0.358. Two hundred local time step iterations at a CFL of 8 preceded the start of the unsteady motion. The flow-field information

from the last time step of this calculation was used to begin the calculation at k=0.714, and the higher frequency motion was continued for four cycles of motion. Magnitude and phase of the unsteady pressures at k=0.714 are plotted in Figure (5-5).

Figures (5-4) and (5-5) show the characteristic spike in the magnitude of unsteady pressure due to shock wave motion. The position of the computed spike is different from the experiment by the same amount that the placement of the steady shock was in error, as seen by referring back to Figure (5-2). The difference in amplitude between Euler results and experiment is difficult to determine due to the sparseness of experimental data points, but the Euler code seems to overpredict the magnitude near the root and underpredict near the tip. The agreement in phase is generally very good except for the effects of the mislocated shock. An exception to this is the 82% semispan results, for which there may be problems with the experimental results.

Due to the large effect on unsteady forces and moments that can be expected from the shock spike, a relatively small error in shock location can result in relatively large differences in unsteady forces and moments. The shock positioning effects of viscosity are, therefore, very important for unsteady transonic analysis.

CHAPTER VI

CONCLUSIONS

An unsteady implicit Euler equation solution algorithm using a finite volume discretization and flux-vector splitting has been presented. The effect on time-accuracy of different time step sizes, different approximate factorizations, and formal first-order versus second-order time accuracy has been determined by numerical experimentation on an oscillating NACA0012 airfoil in transonic flow. It was found that time step sizes corresponding to Courant numbers of 100 or more can produce time-accurate results if flow variables are not rapidly changing. Due to better stability properties, the two-factor method studied here gave better results than the six-factor method. The second-order time-accurate three point backward scheme yielded only slight improvement for the test cases over backward Euler time differencing, which is only first-order in time.

Another topic covered here was the use of blocked grids to obtain time-accurate Euler solutions. Techniques for transfer of information between blocks were analyzed and verified by comparing multi-block solutions with equivalent one-block solutions. It was shown that approximating the value of the solution vector required at block boundaries with whatever information is currently available from adjoining blocks introduces an $O(\Delta t^2/\Delta x)$ error in the transient solution at the boundary, and gives unsteady results that compare well with unblocked results even for cases with a shock wave passing through the block boundary. Converged steady results, with no body motion, showed no error due to the block boundaries. Convergence to steady state was slowed to some

extent by using blocked grids, but the use of blocked grids is economically attractive due to the greatly reduced computer memory cost.

Steady and unsteady calculations of transonic flow over a rectangular planform supercritical wing using a blocked grid were compared to experimental results. The steady comparison is good for those cases in which viscous effects are negligible, but for higher Mach number cases the inviscid calculation places the shock downstream of the experimental location. Unsteady calculations showed good agreement in terms of magnitude and phase of the pressure on the wing except where the shock wave was misplaced.

TABLE 1

	One Block	Four Block	Three Block
CPU Time/Step	0.278	0.314	0.378
Max Job Size (Wds)	1,178,112	524,288	734,720
Memory*CPU Time/Step	0.363	0.161	0.215
Accounting Units/Step	0.035	0.011	0.011

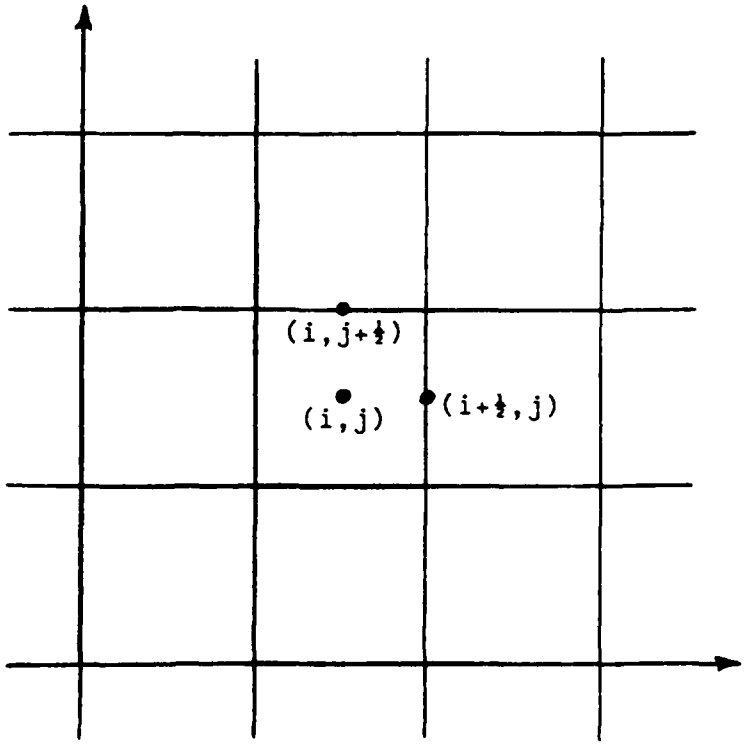

Figure (3-1) Indexing of Cell Centers and Faces

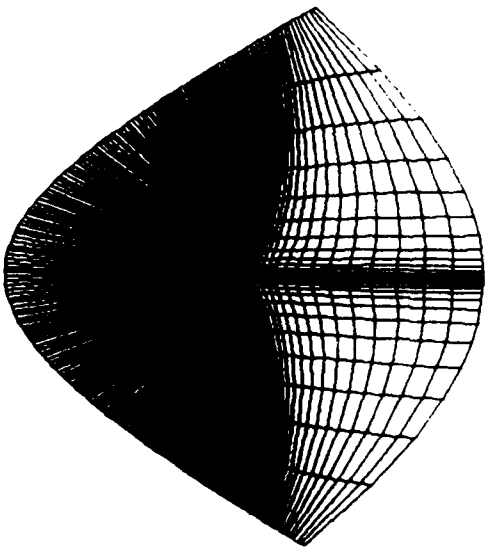

(a) Entire Grid

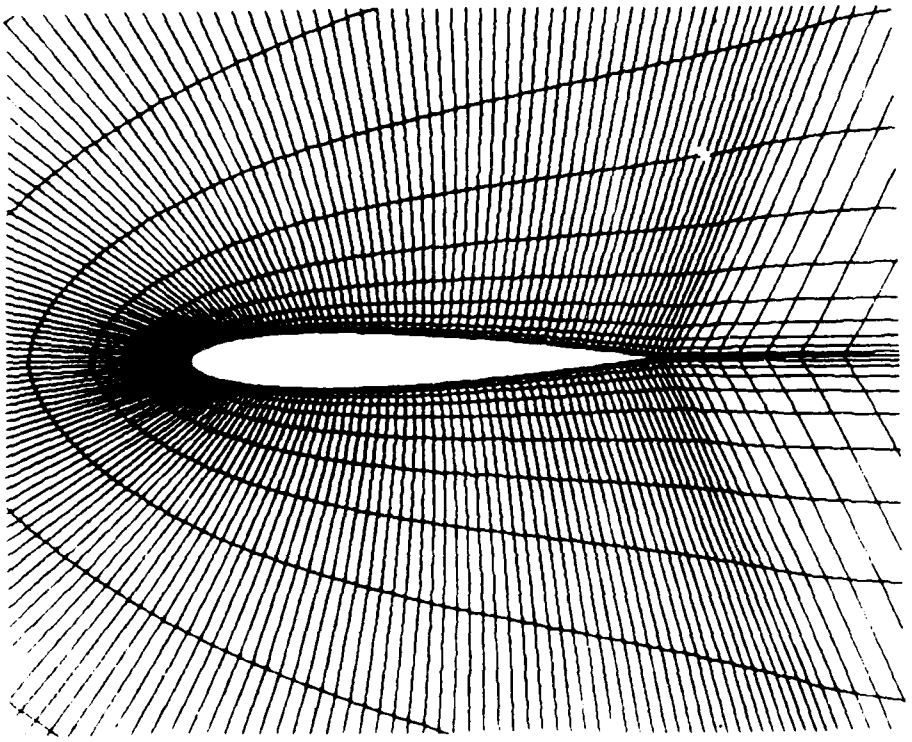

(b) Close-Up of Airfoil

Figure (3-2) NACA0012 221 X 20 'C' Grid

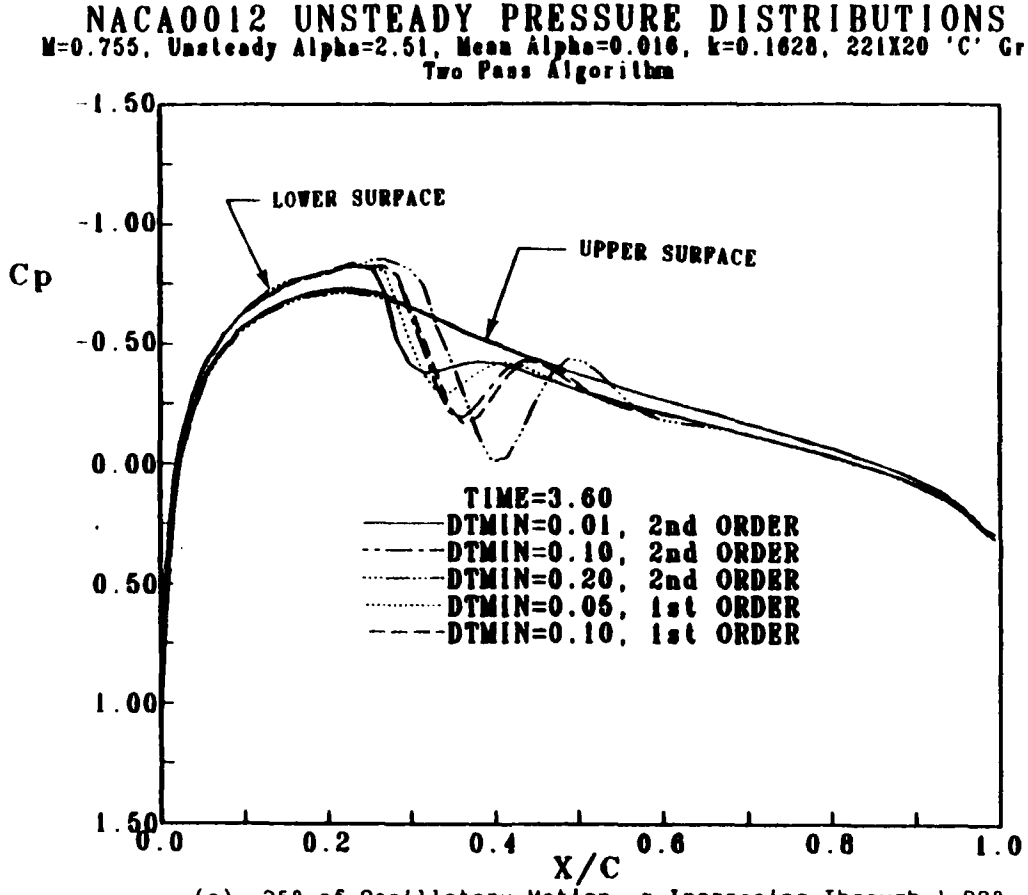

(a) 25° of Oscillatory Motion, α Increasing Through 1.09°

Figure (3-3) Unsteady Airfoil Pressure Coefficients Using Various Time Step Sizes and Time Discretizations

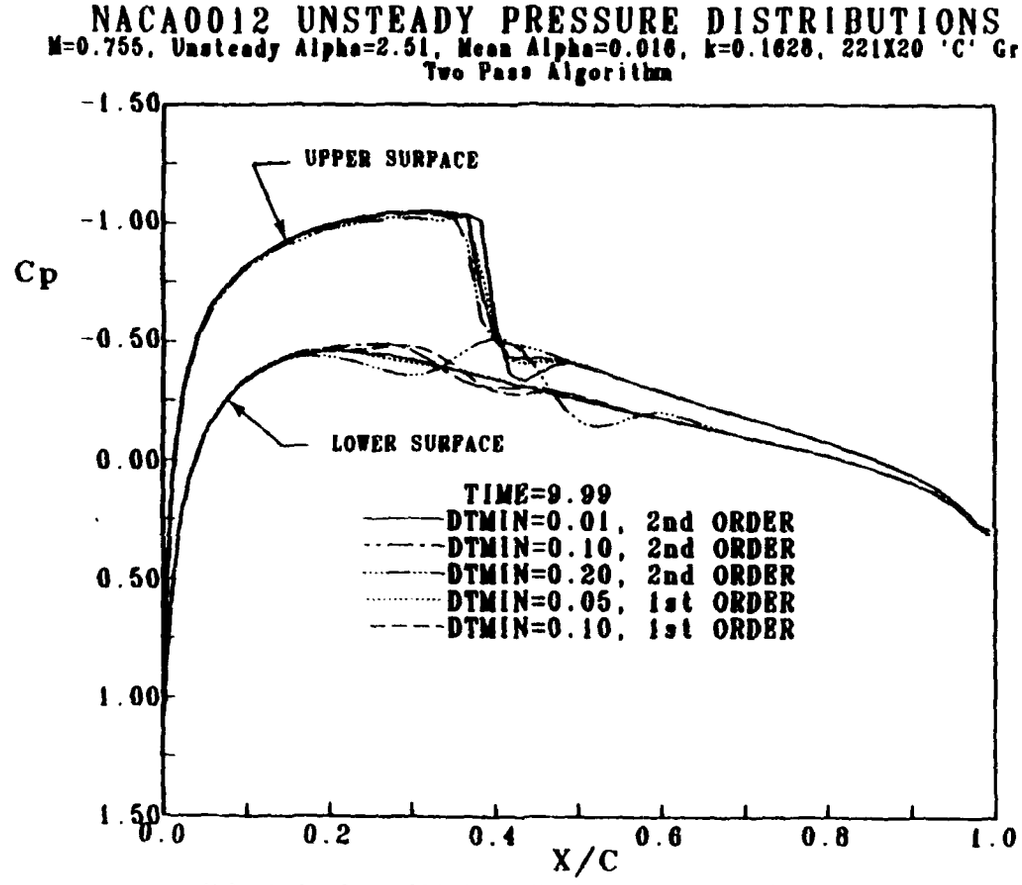

(b) 70° of Oscillatory Motion, α Increasing Through 2.37°

Figure (3-3) continued

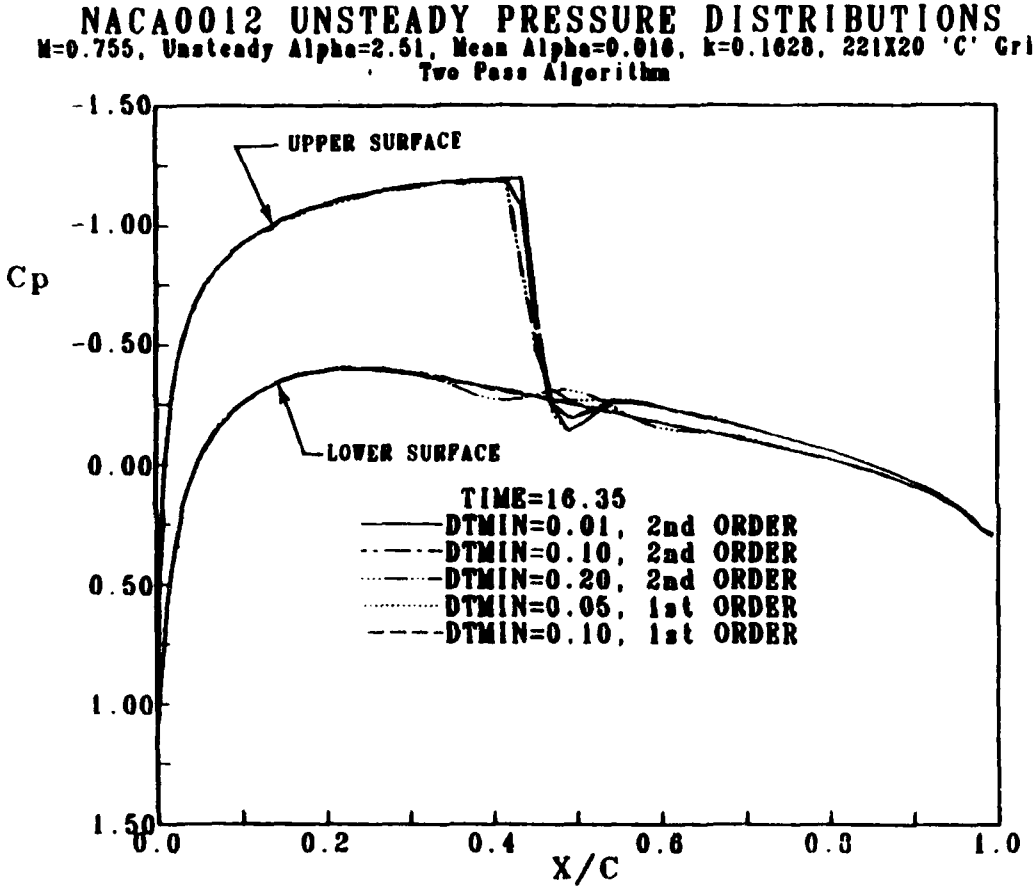

(c) 115° of Oscillatory Motion, α Decreasing Through 2.29°

Figure (3-3) continued

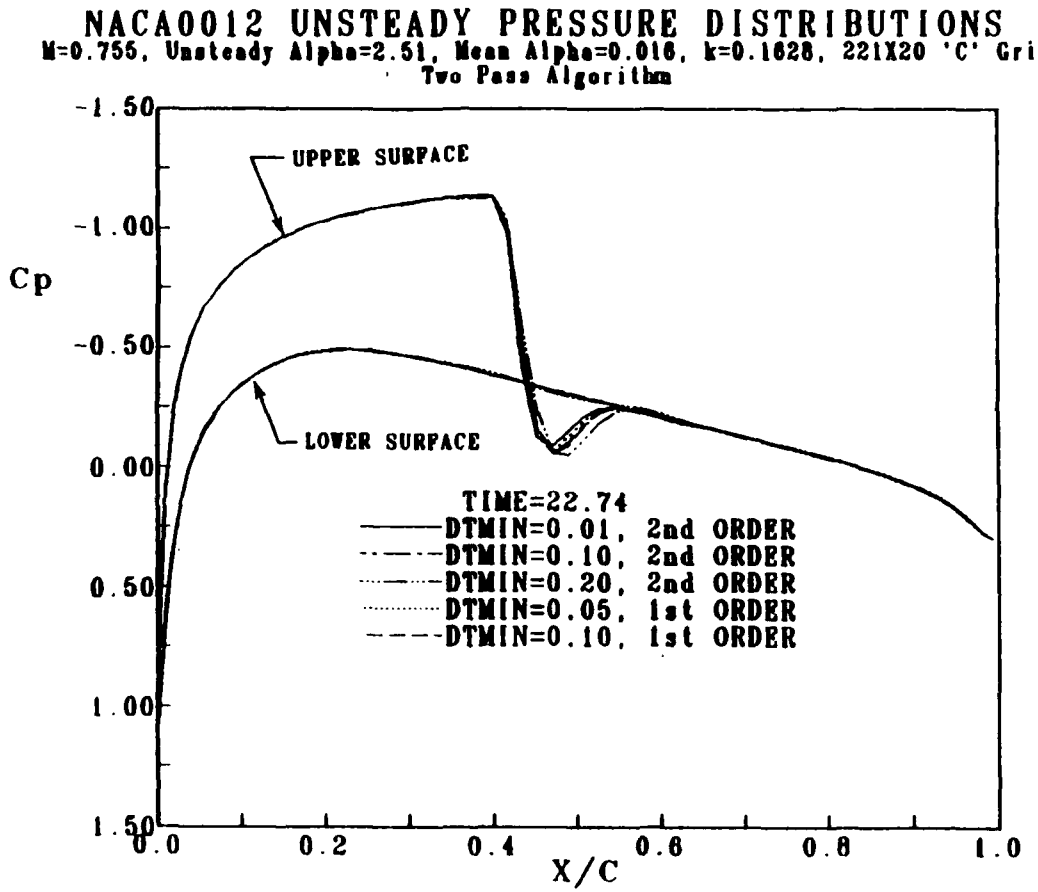

(d) 160° of Oscillatory Motion, α Decreasing Through .87°

Figure (3-3) continued

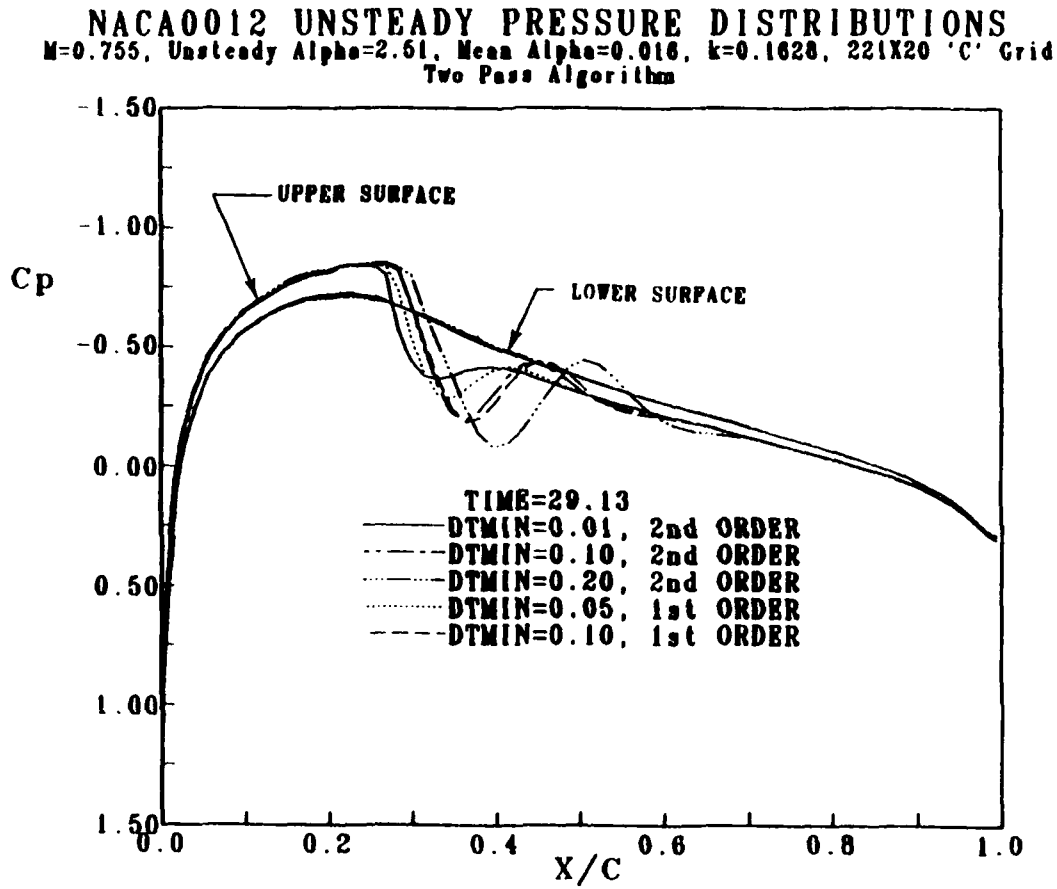

(e) 205° of Oscillatory Motion, α Decreasing Through -1.04°

Figure (3-3) continued

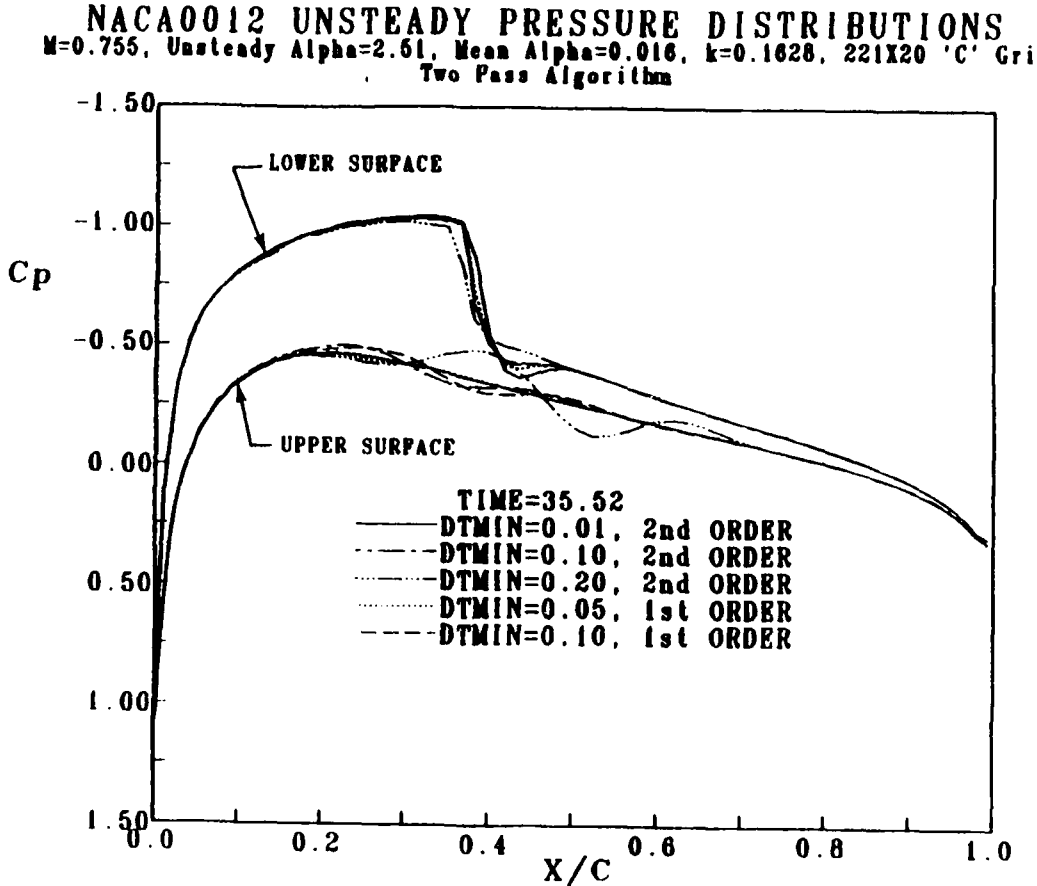

(f) 250° of Oscillatory Motion, α Decreasing Through -2.34°

Figure (3-3) continued

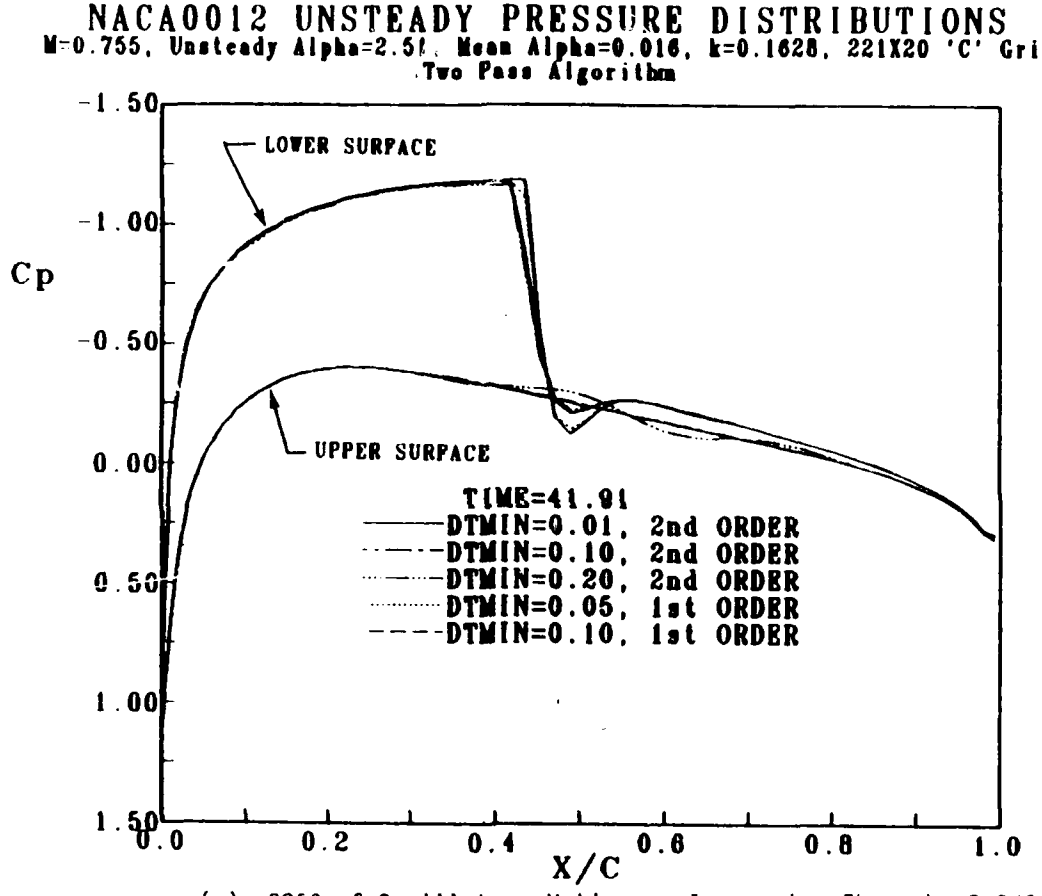

(g) 295° of Oscillatory Motion, α Increasing Through -2.26°

Figure (3-3) continued

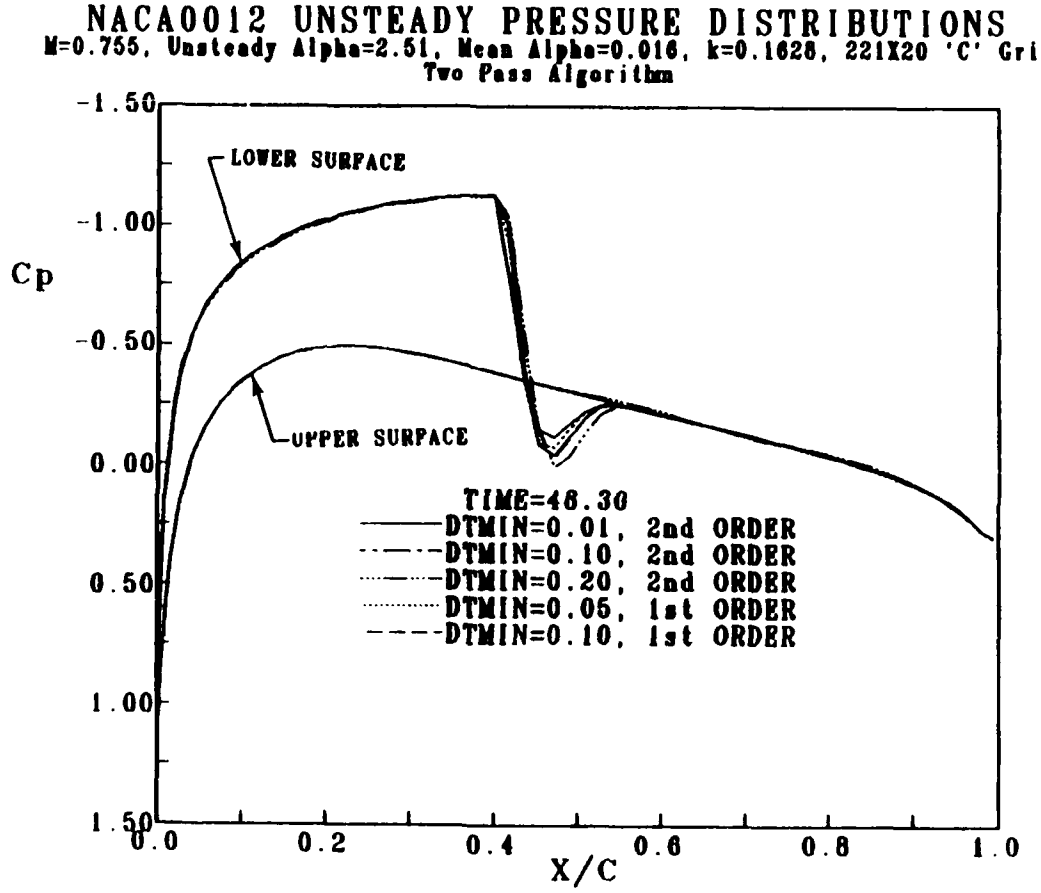

(h) 340° of Oscillatory Motion, α Increasing Through -0.84°

Figure (3-3) continued

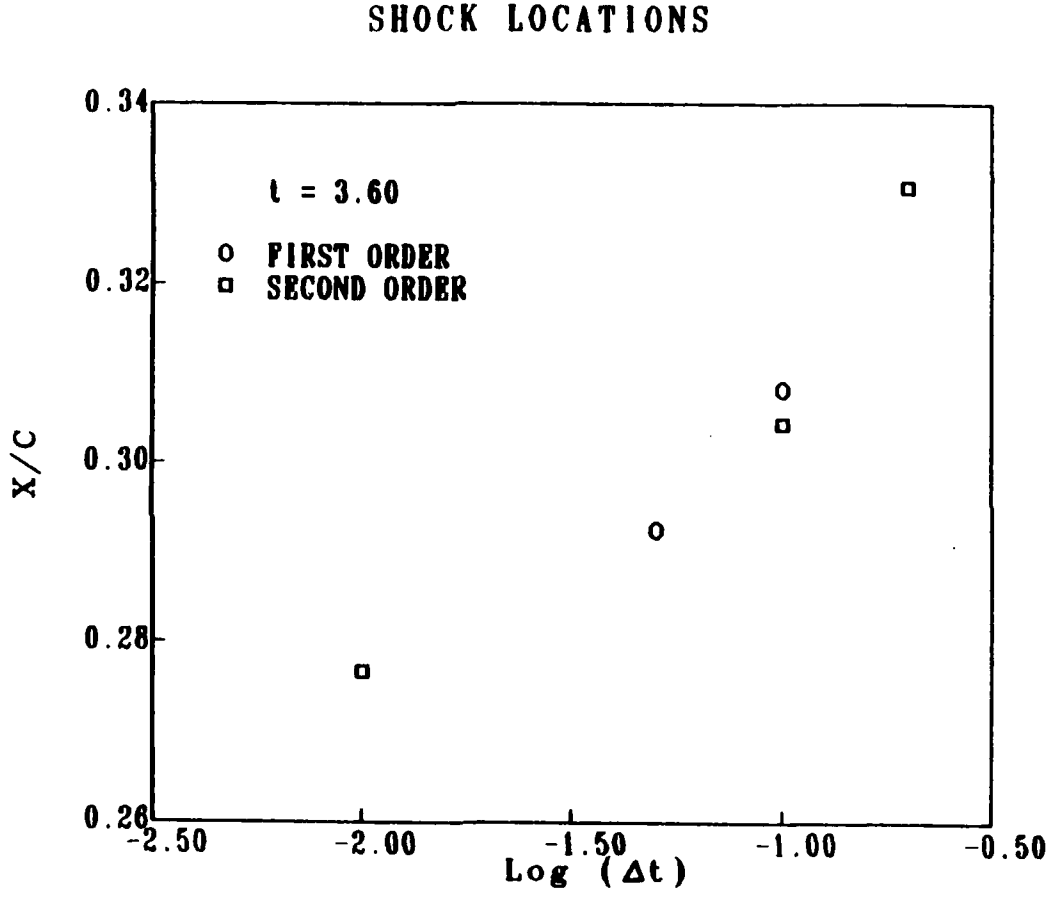

Figure (3-4) Shock Locations Given by Different Time Step Sizes

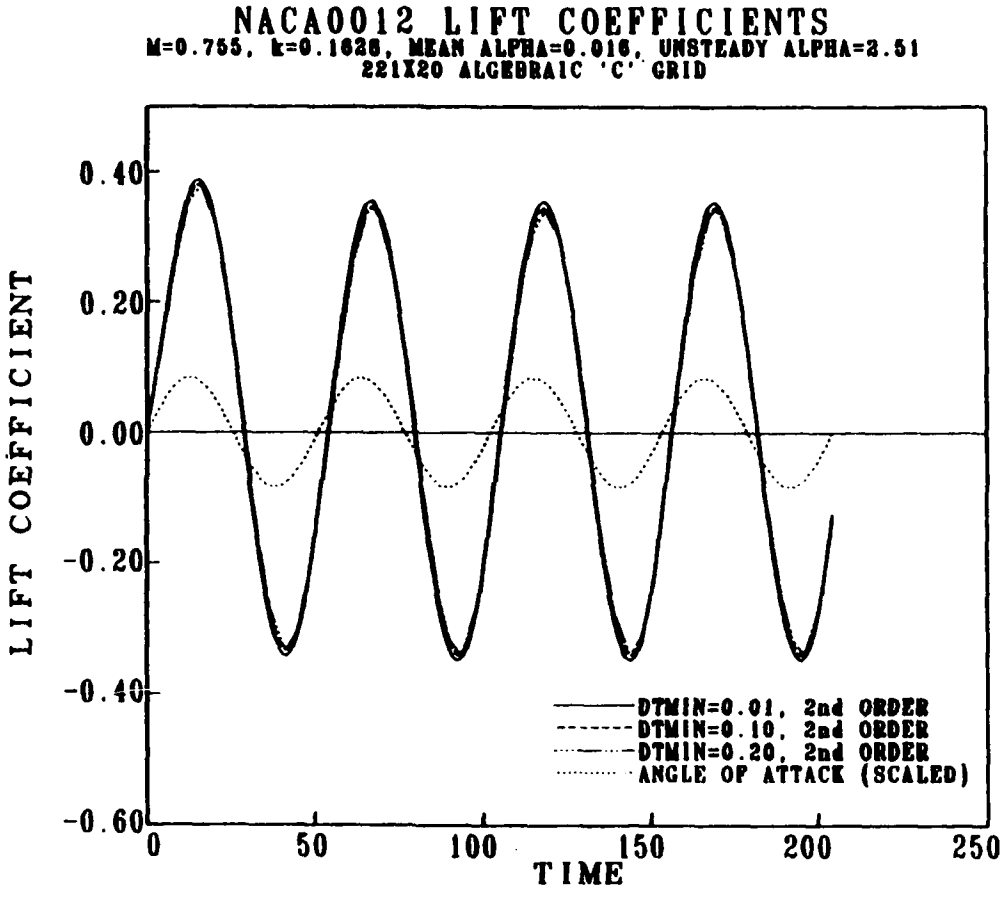

(a) Lift Coefficients

Figure (3-5) Unsteady Airfoil Lift and Moment Coefficients Using Various Time Step Sizes

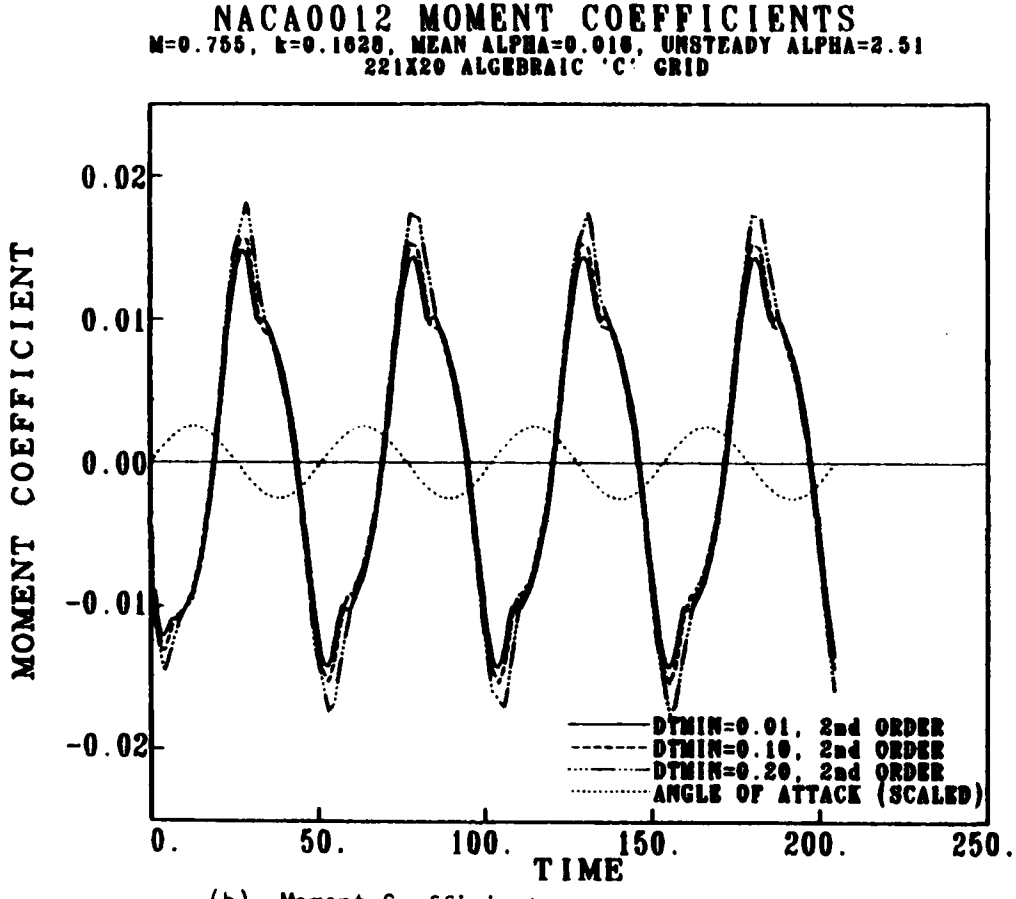

(b) Moment Coefficients

Figure (3-5) continued

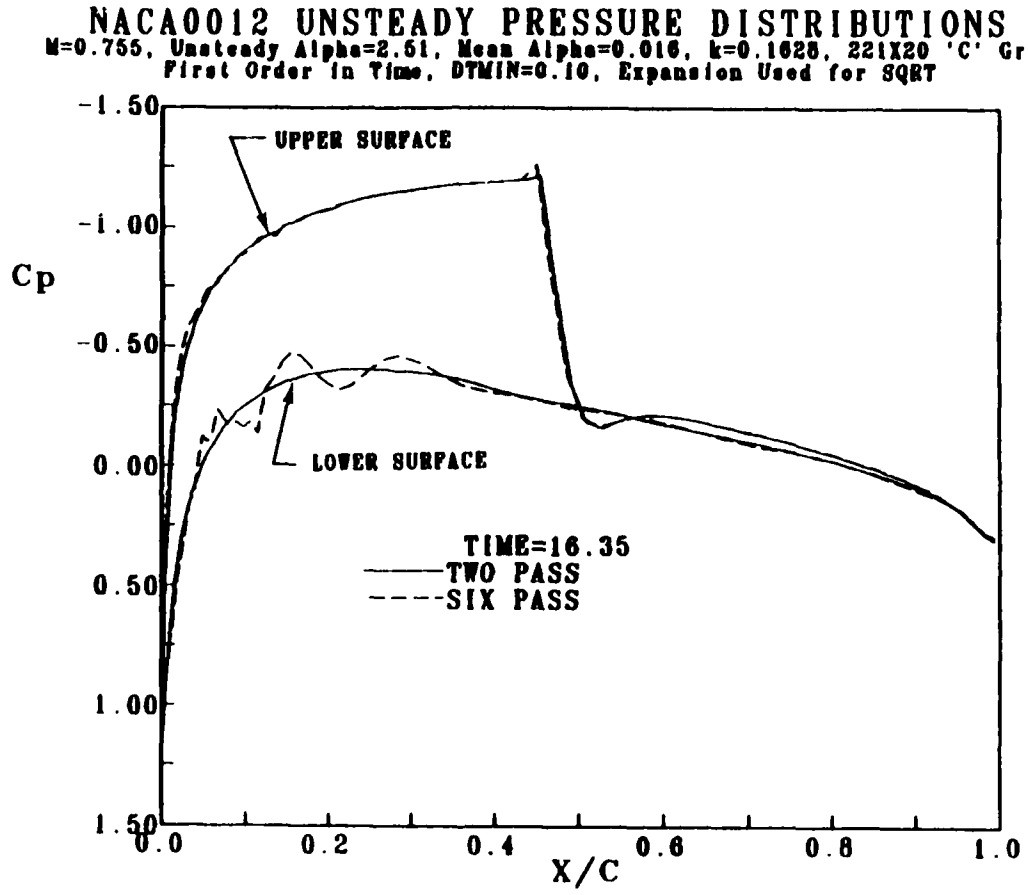

(a) 115° of Oscillatory Motion, α Decreasing Through 2.29°

Figure (3-6) Unsteady Airfoil Pressure Coefficients Using Different Factorizations

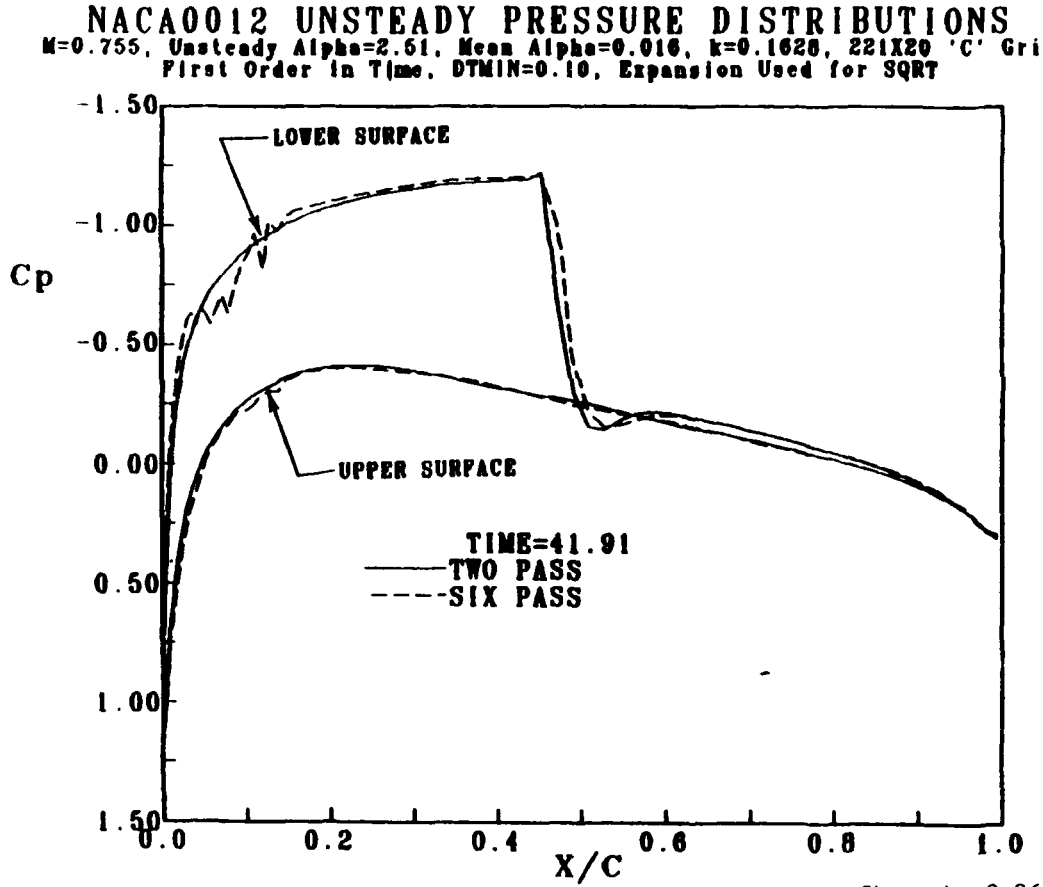

(b) 295° of Oscillatory Motion, α Increasing Through -2.26°

Figure (3-6) continued

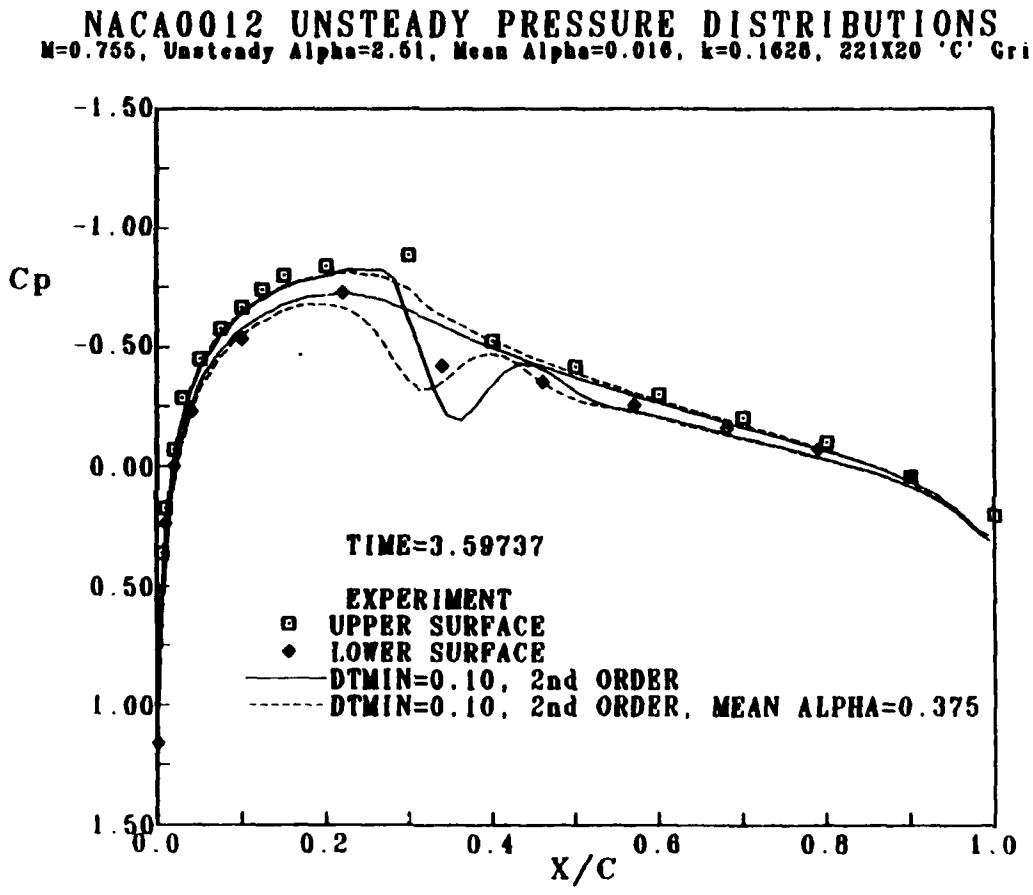

(a) 25° of Oscillatory Motion

Figure (3-7) Comparison of Computed Pressure Coefficients With Experiment

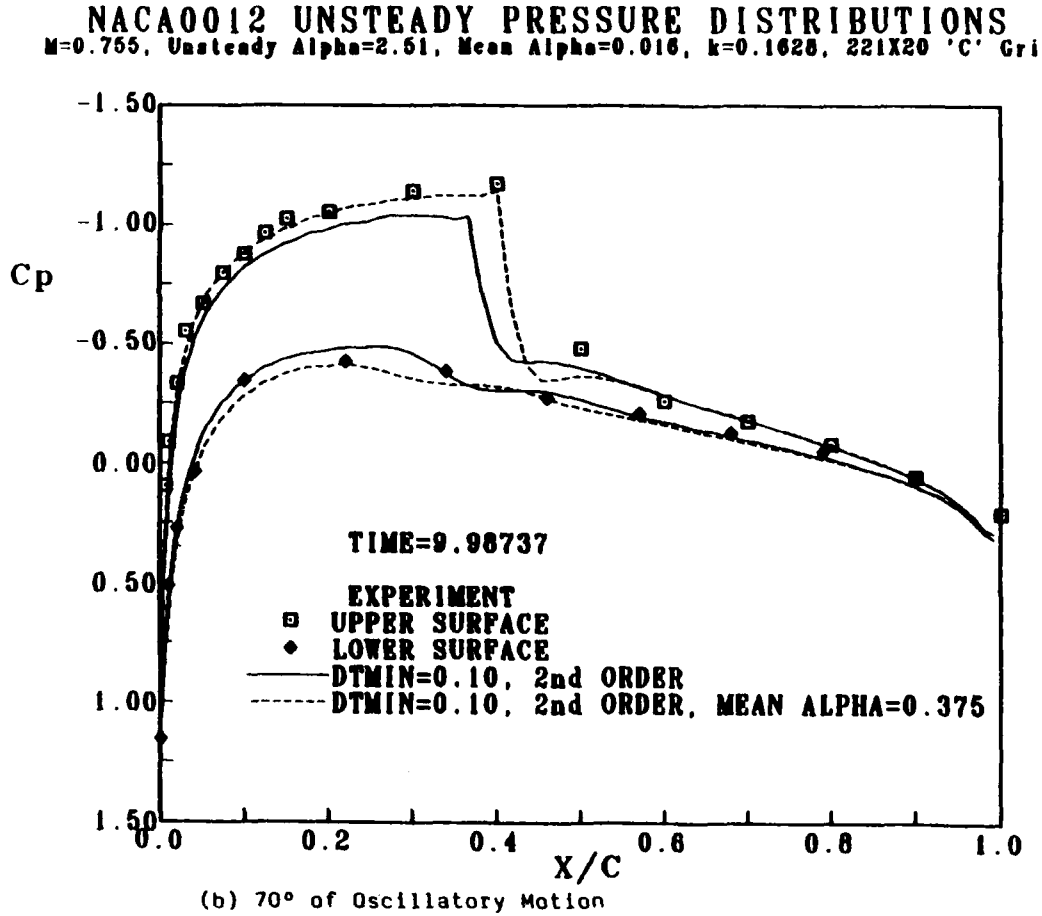

(b) 70° of Oscillatory Motion

Figure (3-7) continued

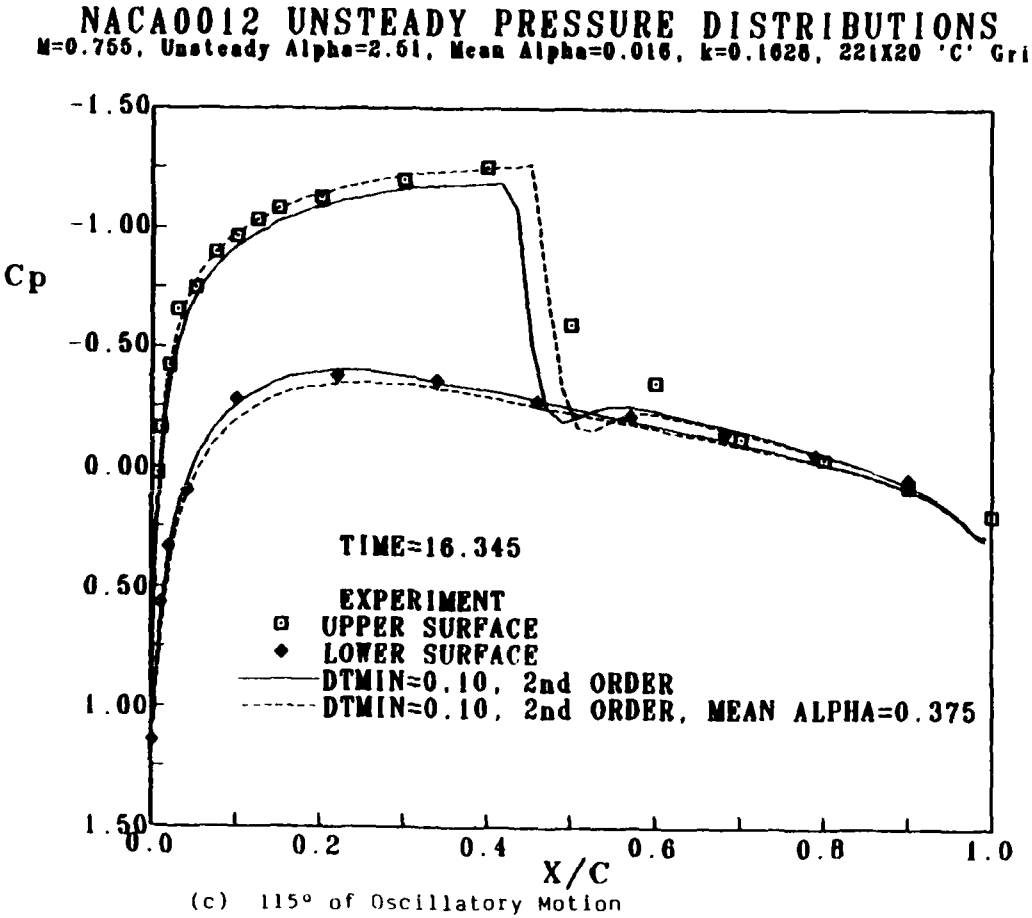

(c) 115° of Oscillatory Motion

Figure (3-7) continued

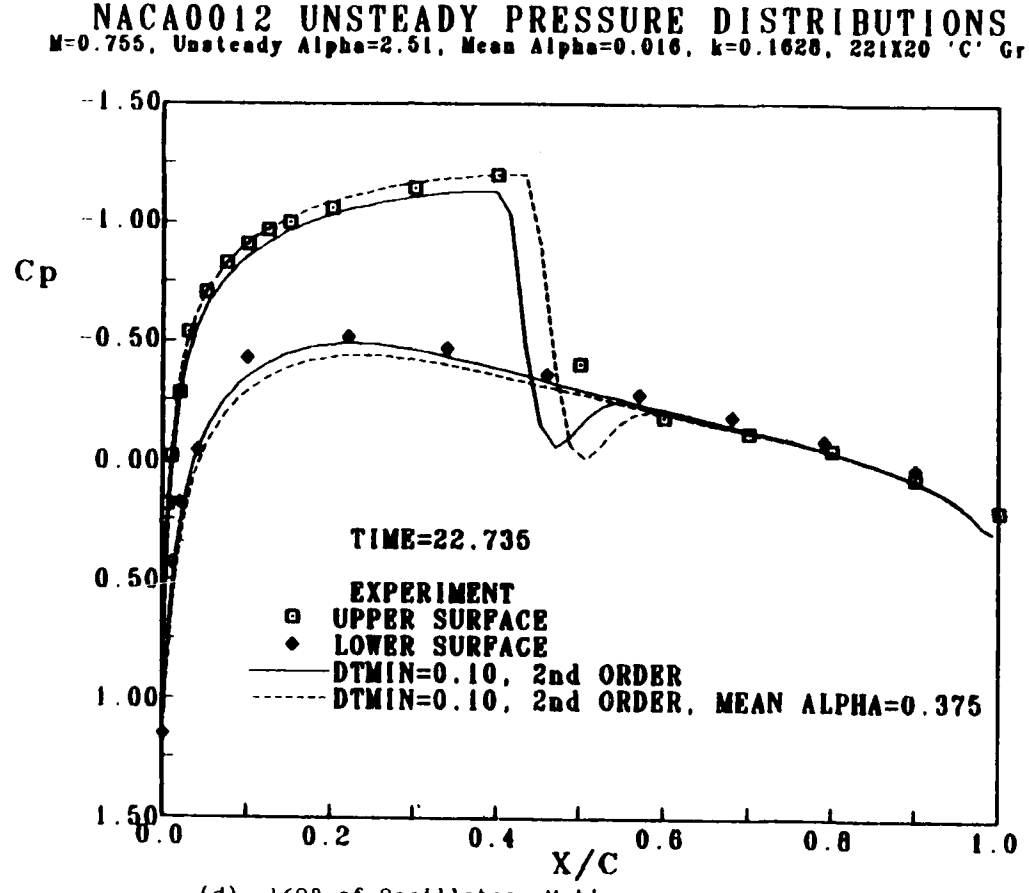

(d) 160° of Oscillatory Motion

Figure (3-7) continued

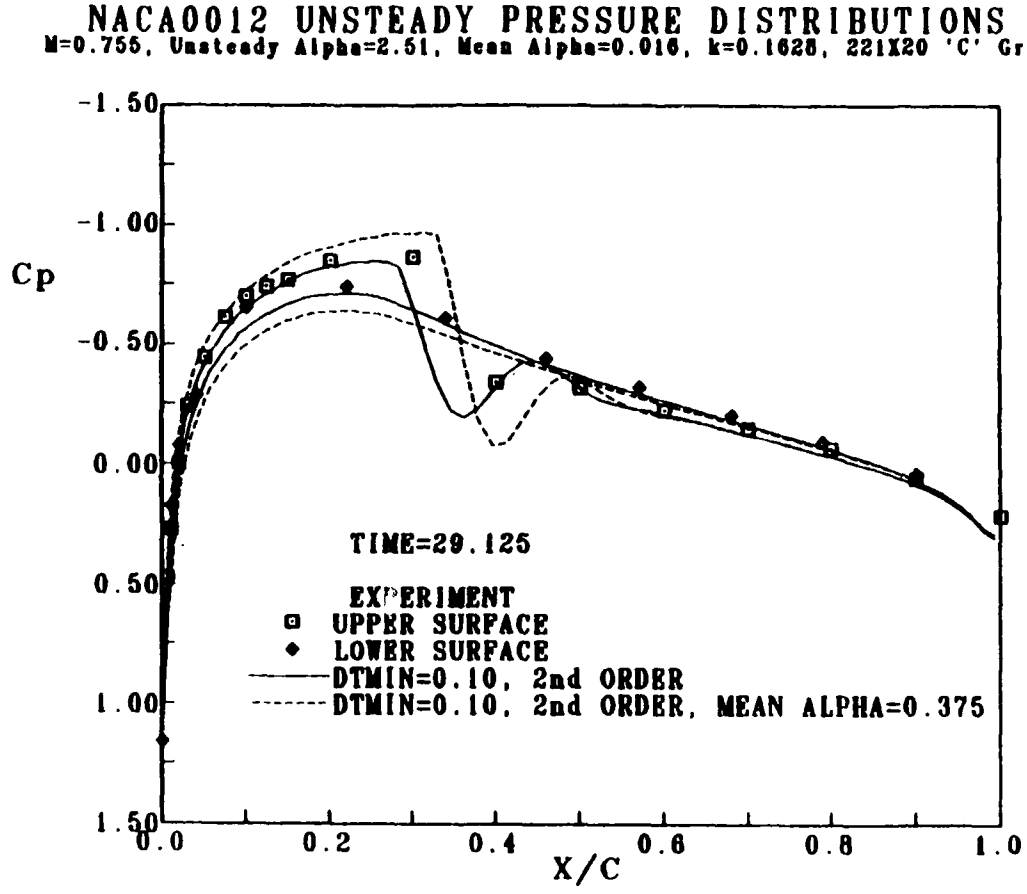

(e) 205° of Oscillatory Motion

Figure (3-7) continued

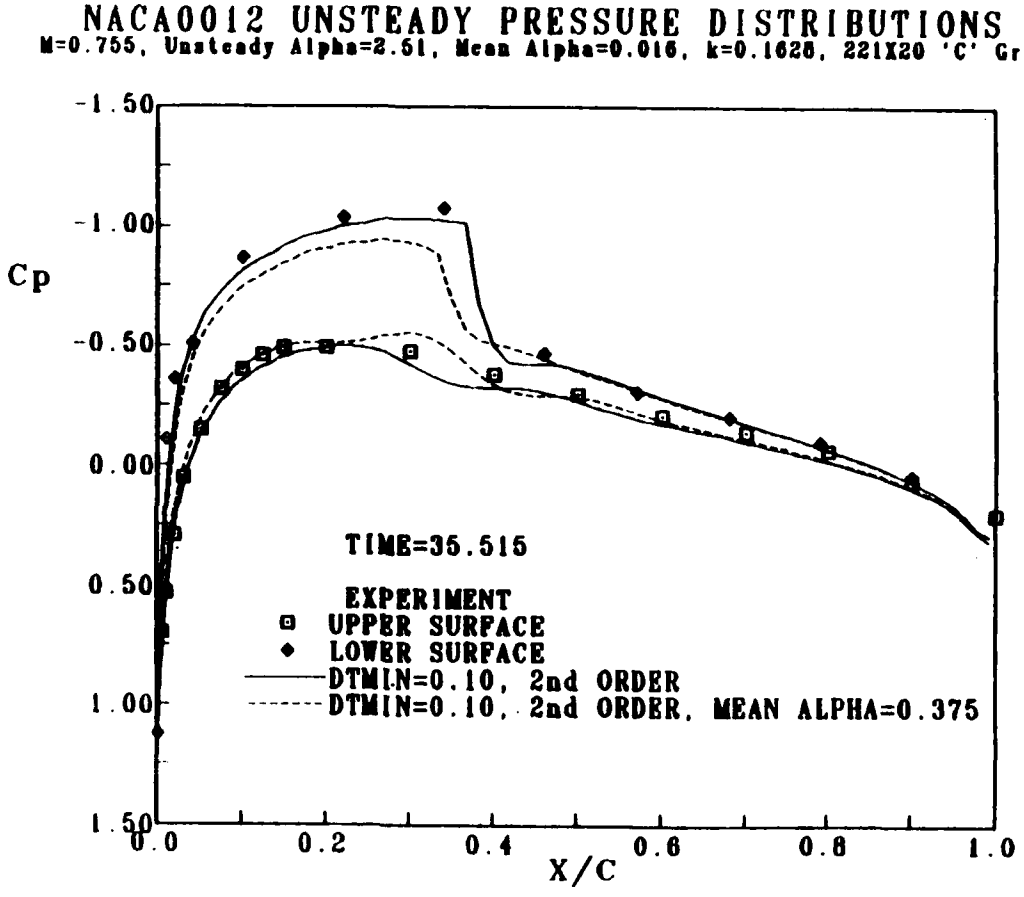

(f) 250° of Oscillatory Motion

Figure (3-7) continued

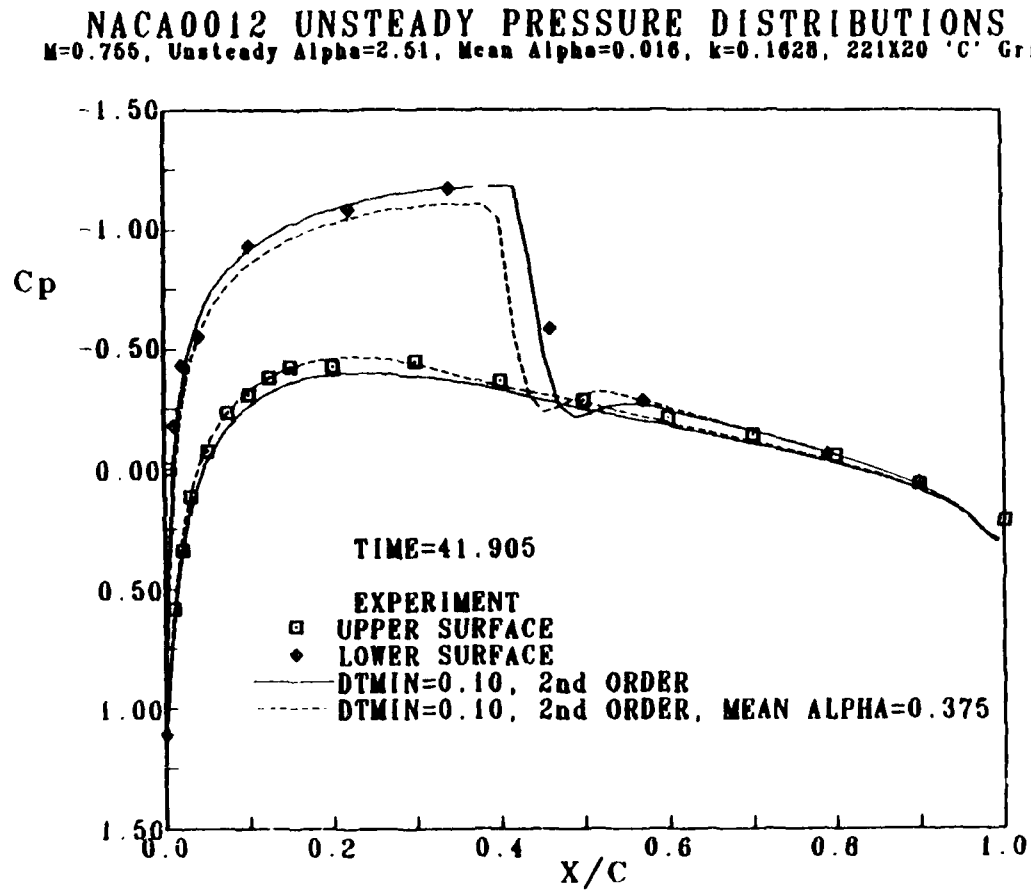

(g) 295° of Oscillatory Motion

Figure (3-7) continued

AD-A173 977 UNSTEADY THREE-DIMENSIONAL EULER EQUATIONS SOLUTIONS ON DYNAMIC BLOCKED GRIDS(U) AIR FORCE ARMAMENT LAB EGLIN AFB FL D M BELK OCT 86 AFATL-TR-86-74 2/2

UNCLASSIFIED F/G 1/1 NL

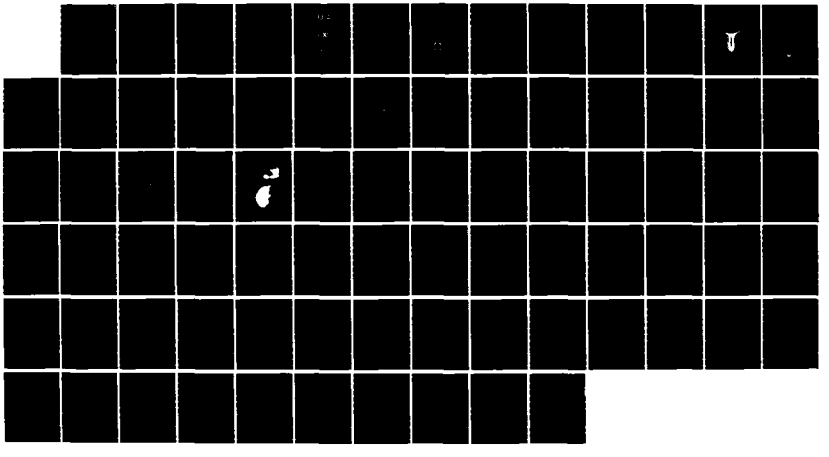

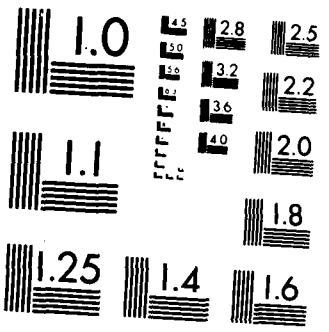

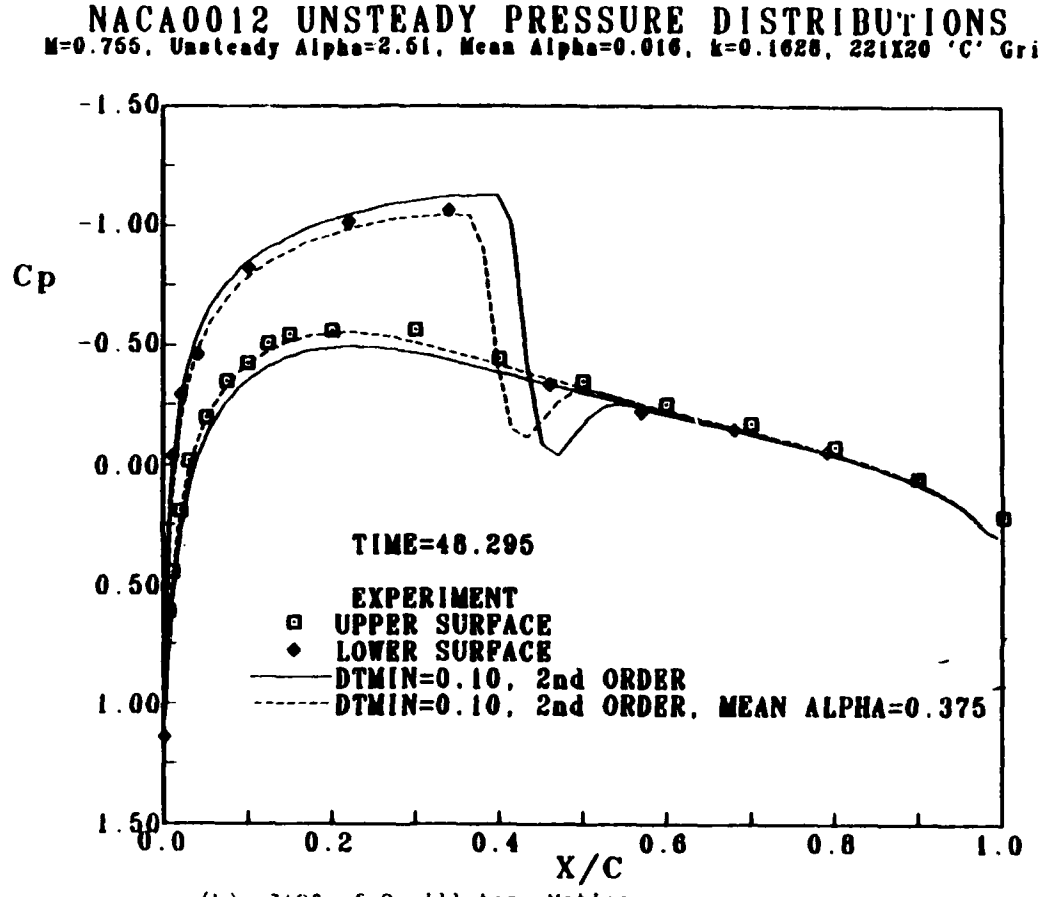

(h) 340° of Oscillatory Motion

Figure (3-7) continued

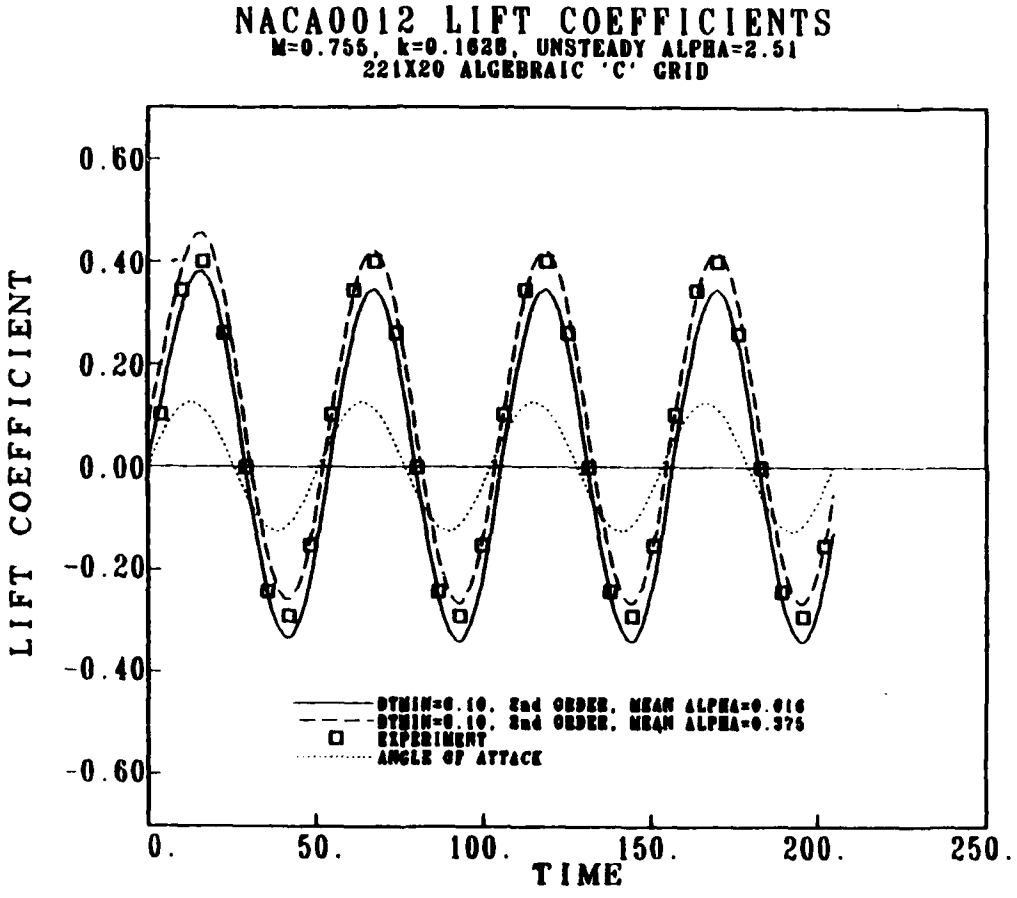

(a) Lift Coefficients

Figure (3-8) Comparison of Computed Lift and Moment Coefficients with Experiment

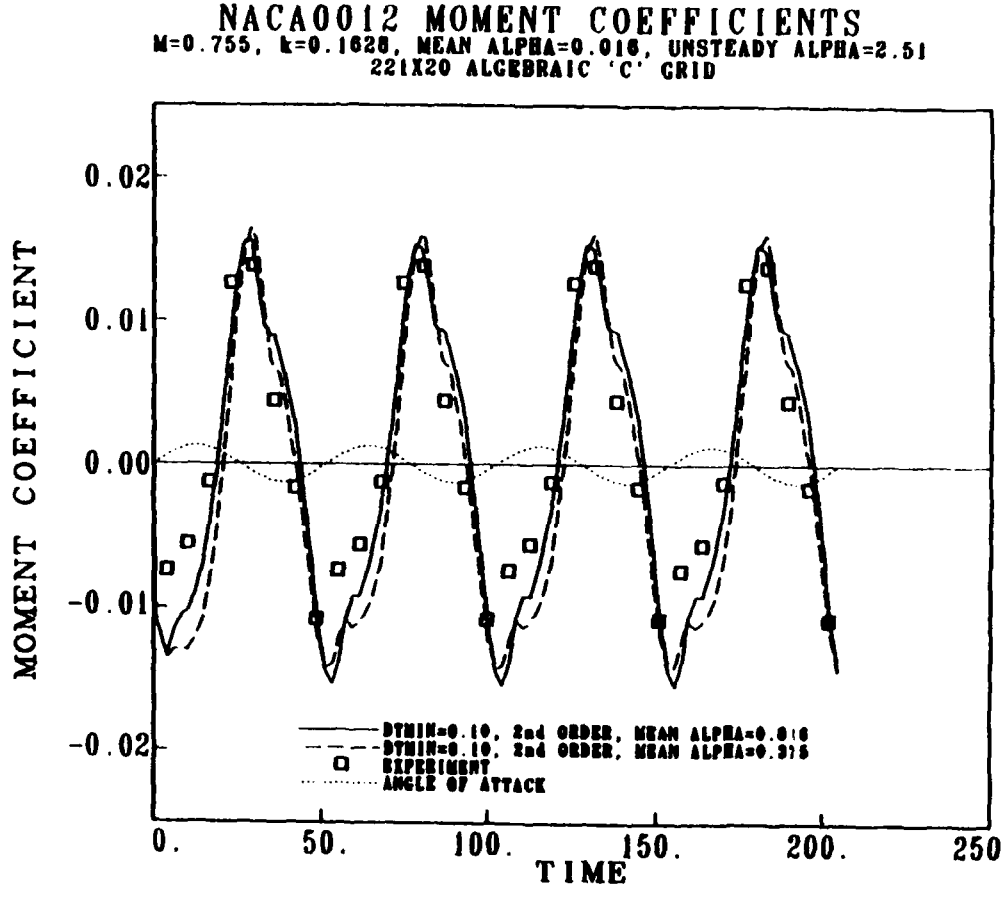

(b) Moment Coefficients

Figure (3-8) Continued

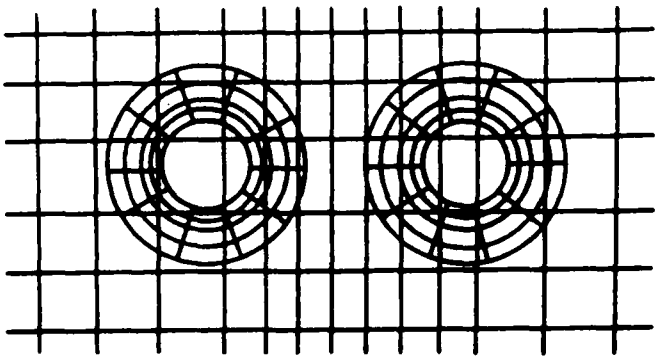

(a) Chimera Grid

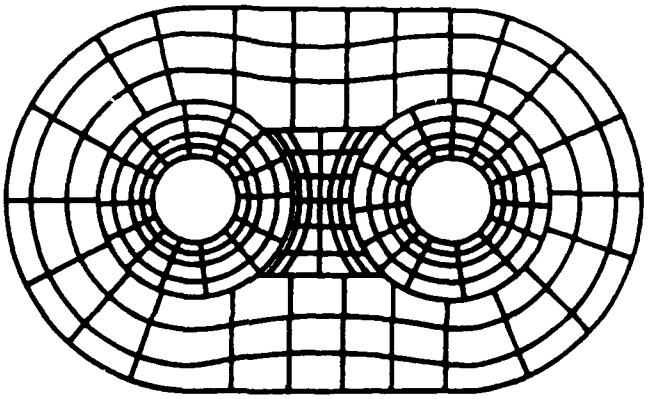

(b) Patched Grid

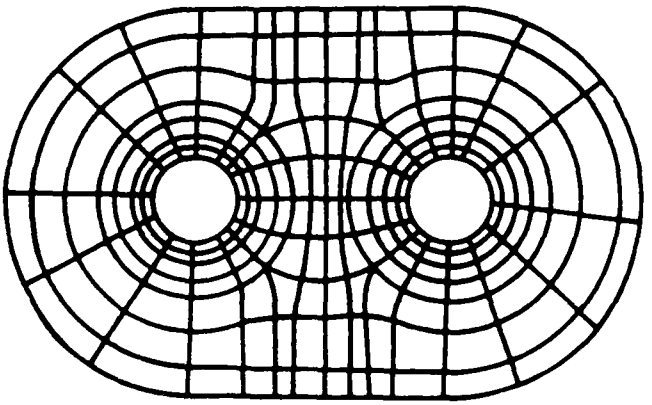

(c) Blocked Grid

Figure (4-1) Various Grid Schemes About Two Cylinders

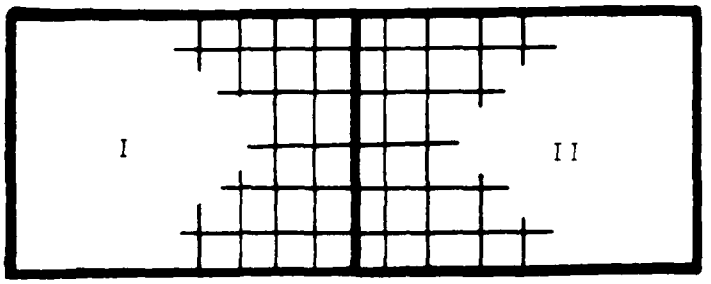

Figure (4-2) Simple Blocked Grid

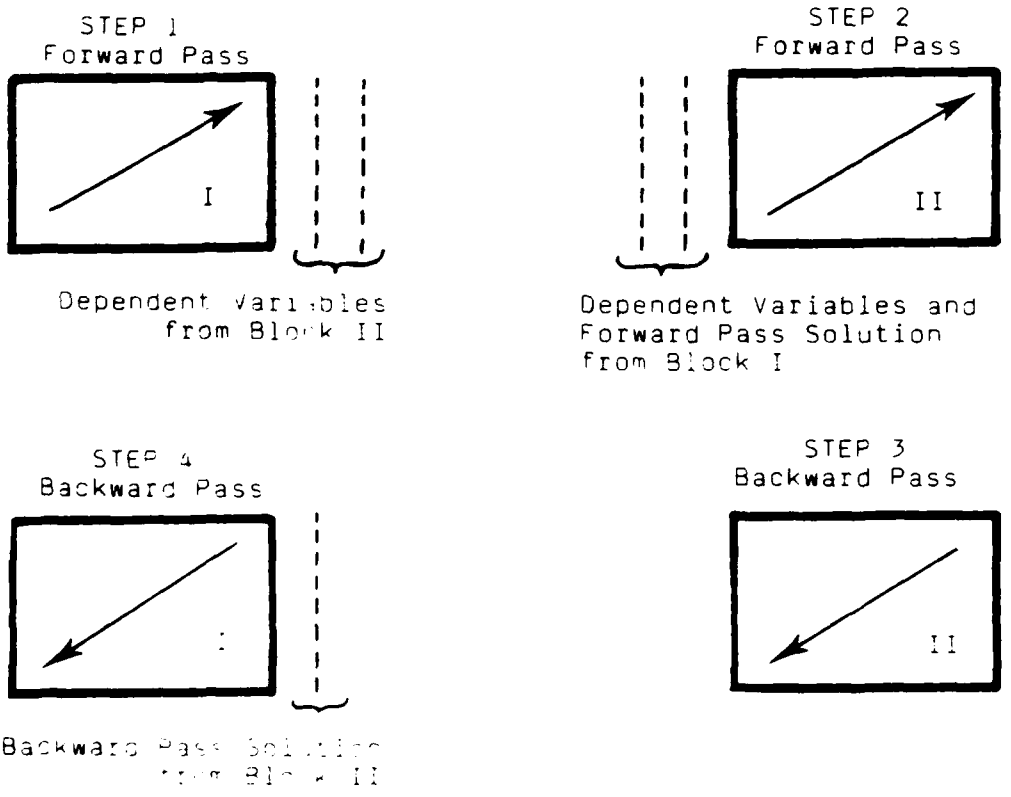

Figure [illegible] Elements of Operations Required to [illegible]

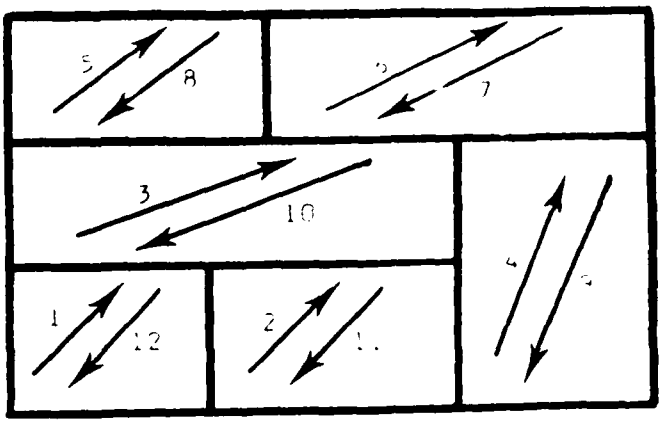

Figure (4-4) Sequence of Operations for a More Complicated Blocking

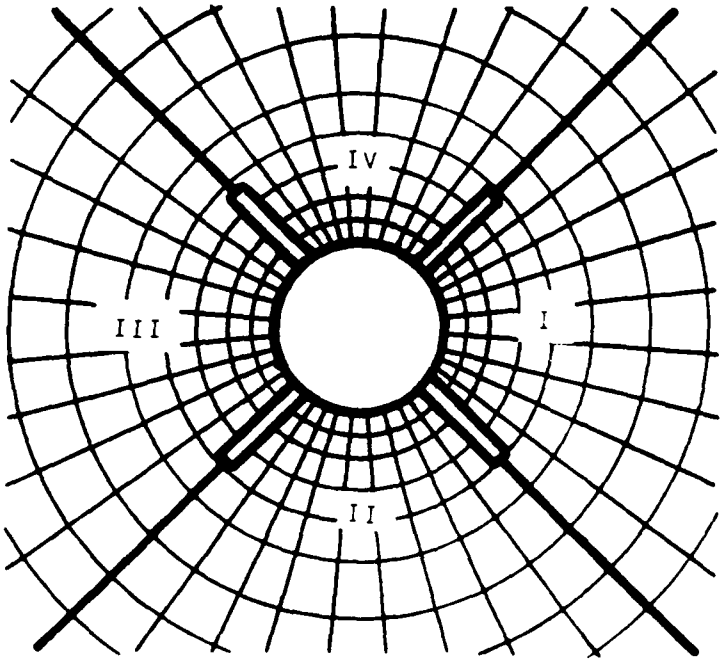

Figure (4-5) Example of Blocking Used to Enclose an Impermeable Surface

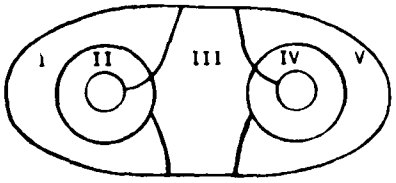

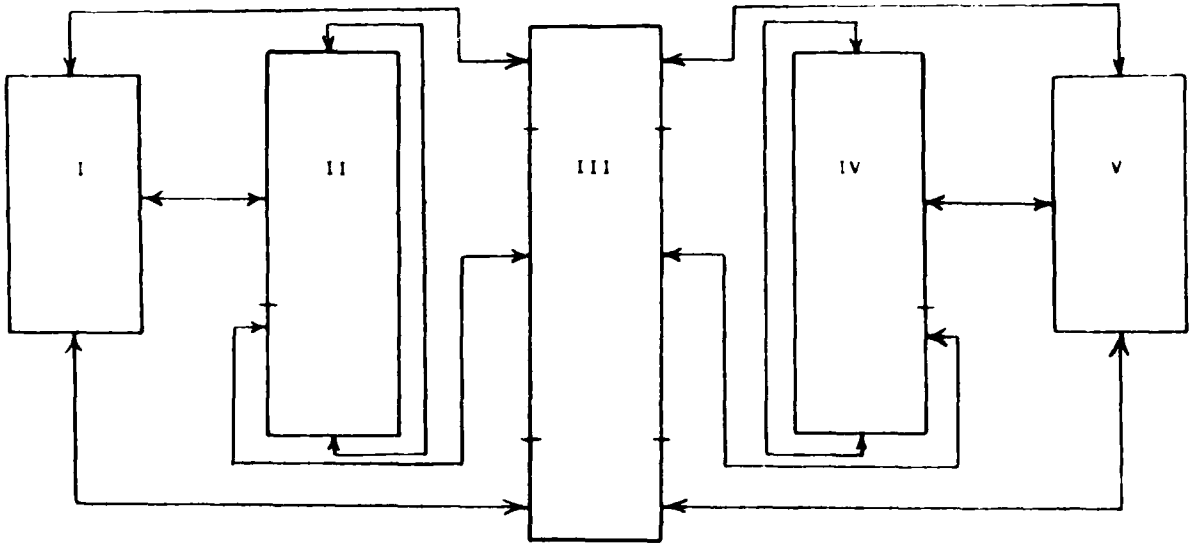

Figure (4-6) Block-to-Block Correspondences

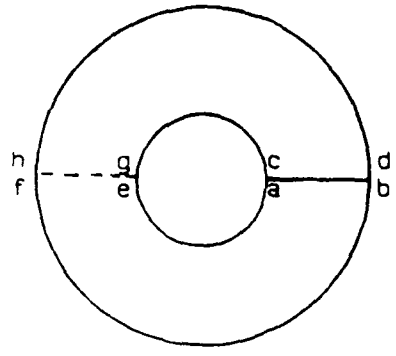

(a) Physical Domain

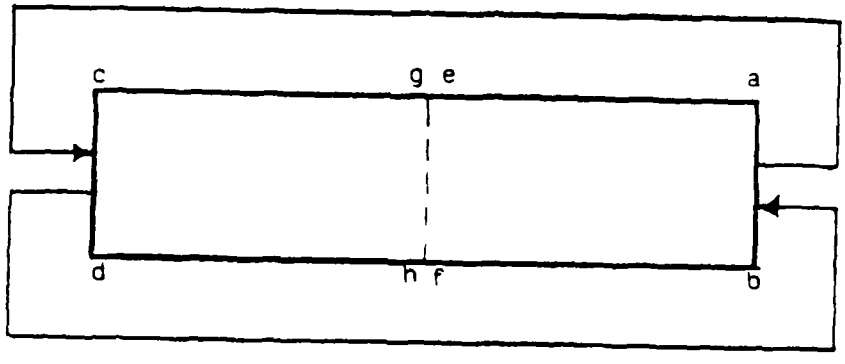

(b) Computational Domain

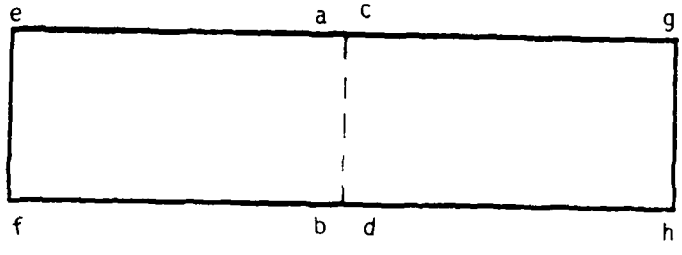

(c) Reblocked Grid in the Computational Domain

Figure (4-7) A One-Block 'O' Grid

```
      PROGRAM RIBBON
      COMMON S(1)

C
C  This program will read three 3-D arrays with dimensions NI,NJ,NK.
C
      READ (5,*) NI, NJ, NK
      ISIZE = NI*NJ*NK
C
C  LX, LY, and LZ are the starting locations for X, Y, and Z.
C
      LX=1
      LY=LX+ISIZE
      LZ=LY+ISIZE
      LAST=LZ+ISIZE-1
C
C  Subroutine GETMEM will increase the available memory
C
      CALL GETMEM (LAST)
      CALL READXYZ(S(LX),S(LY),S(LZ),NI,NJ,NK)
      END
      SUBROUTINE READXYZ(X,Y,Z,NI,NJ,NK)
      DIMENSION X(NI,NJ,NK),Y(NI,NJ,NK),Z(NI,NJ,NK)
      READ(10)X,Y,Z
      DO 20 K=1,NK
      DO 20 J=1,NJ
      DO 20 I=1,NI
      A = X(I,J,K) + Y(I,J,K)
          .
          .
          .
      20  Z(I,J,K) = A*Z(I,J,K)
C
      RETURN
      END
```

Figure (4-8) Use of Adjustable Arrays in FORTRAN

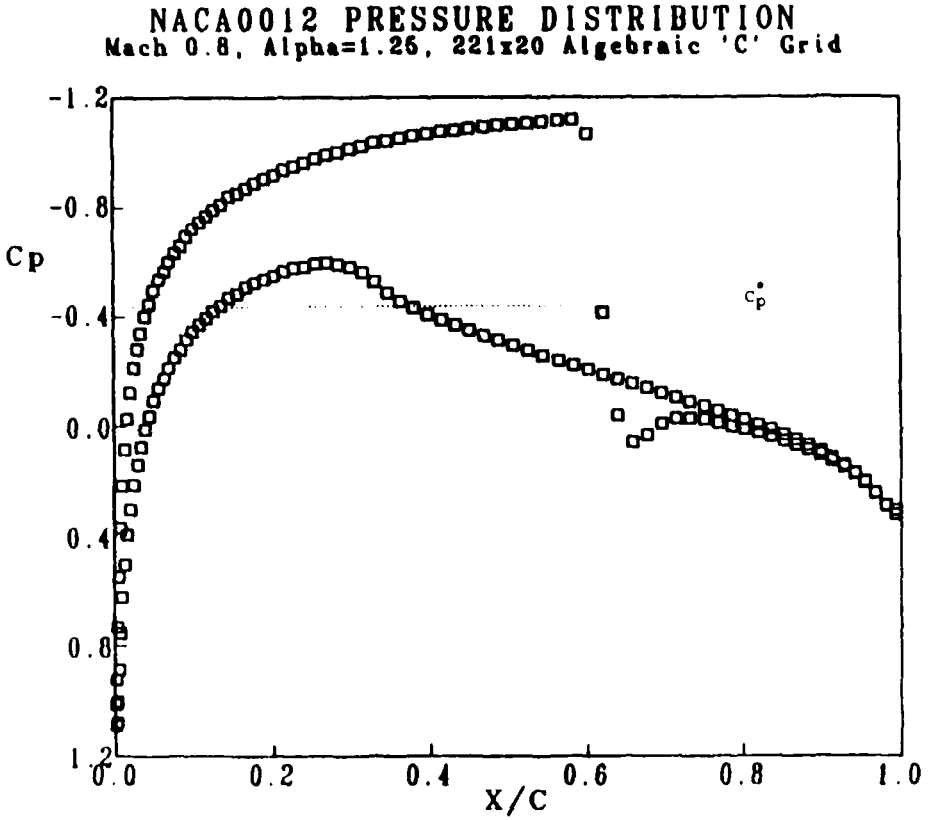

Figure (4-9) NACA0012 Steady Pressure Coefficients

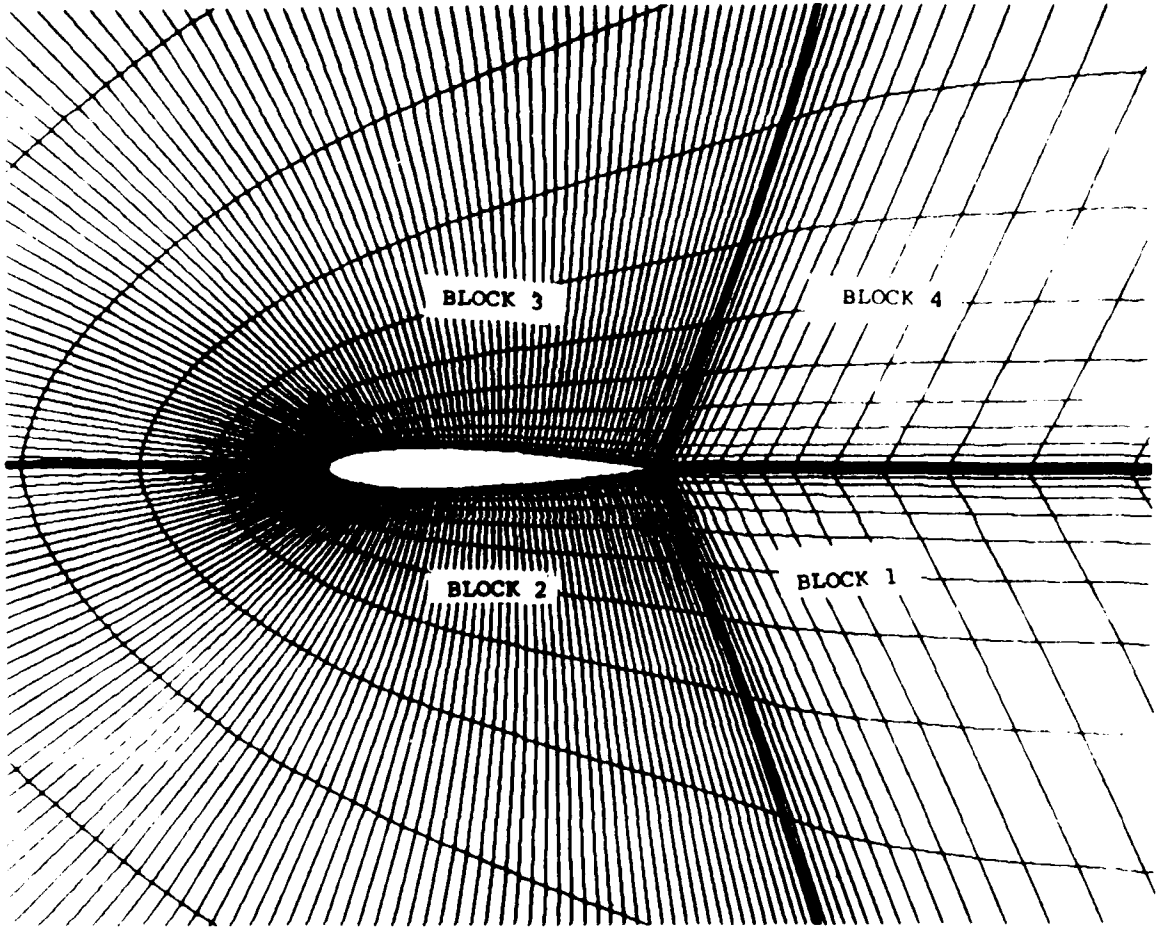

Figure (4-10) NACA0012 Four-Block Grid

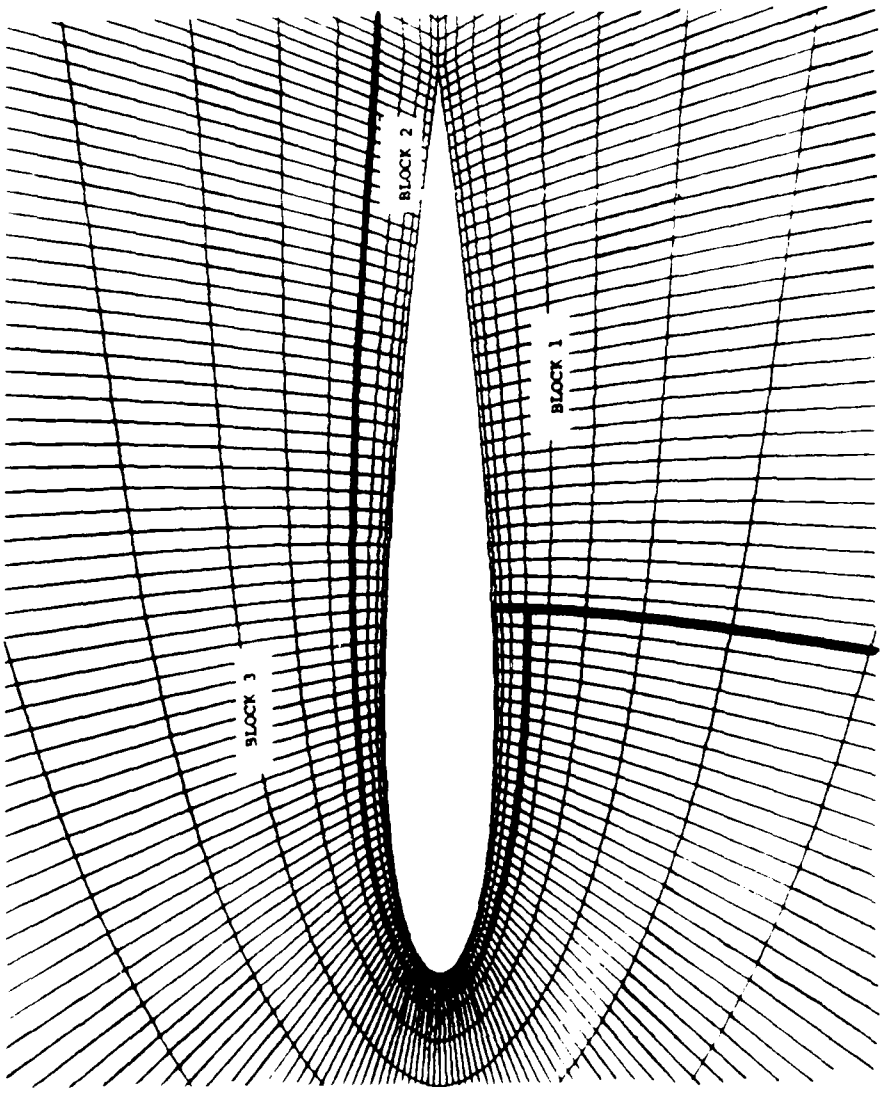

Figure (4-11) NACA0012 Three-Block Grid

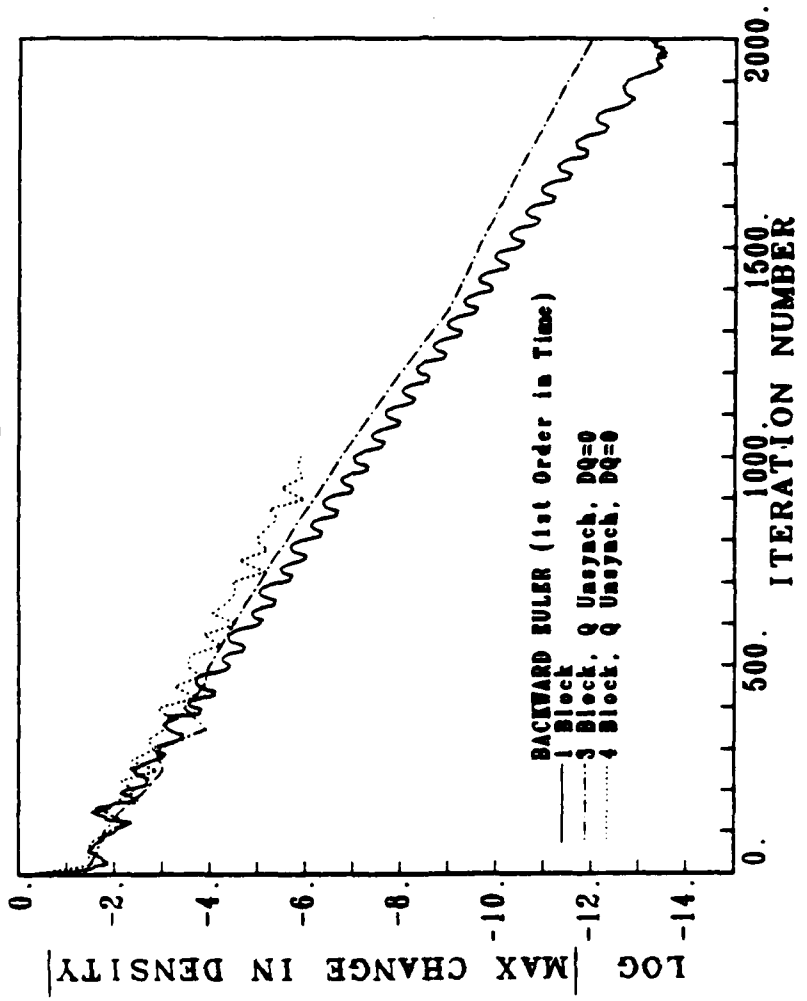

Figure (4-12) Convergence Histories for the One-Block, Three-Block, and the Four-Block Grids

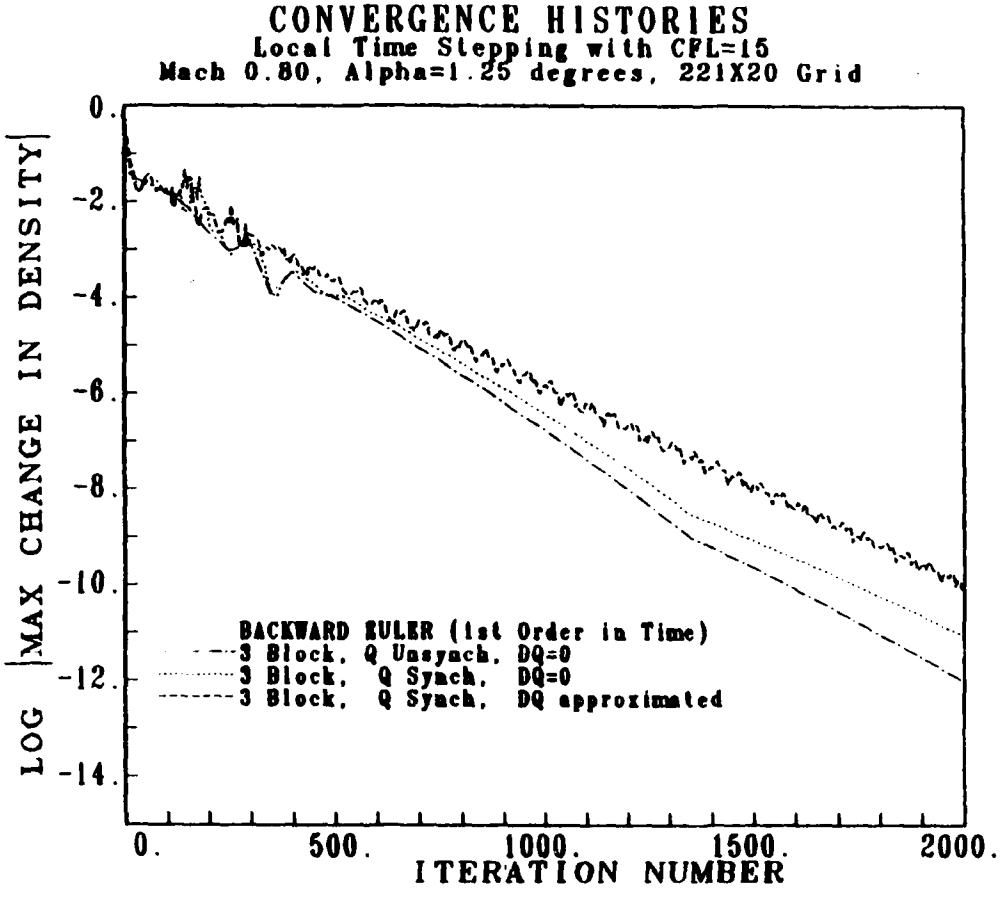

Figure (4-13) Convergence Histories Using Various Block Boundary Conditions

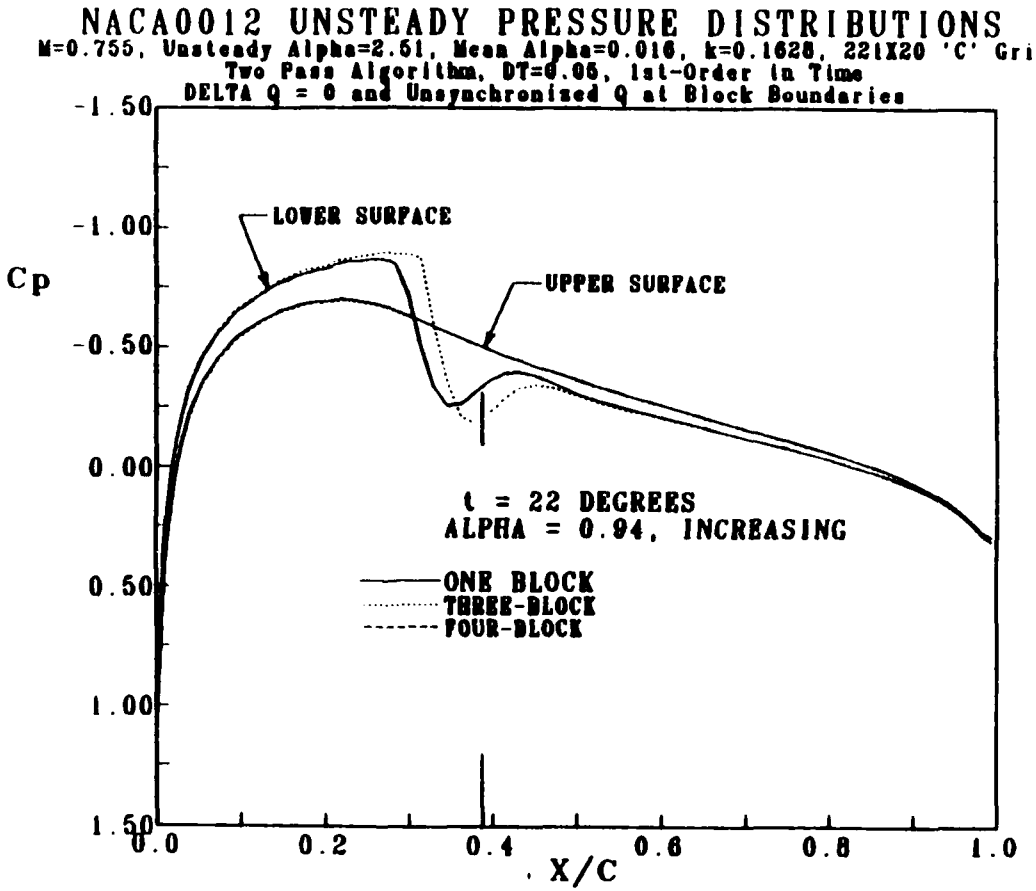

(a) 22° of Oscillatory Motion

Figure (4-14) Unsteady Pressure Coefficients for the One-Block, Three-Block, and Four-Block Grids

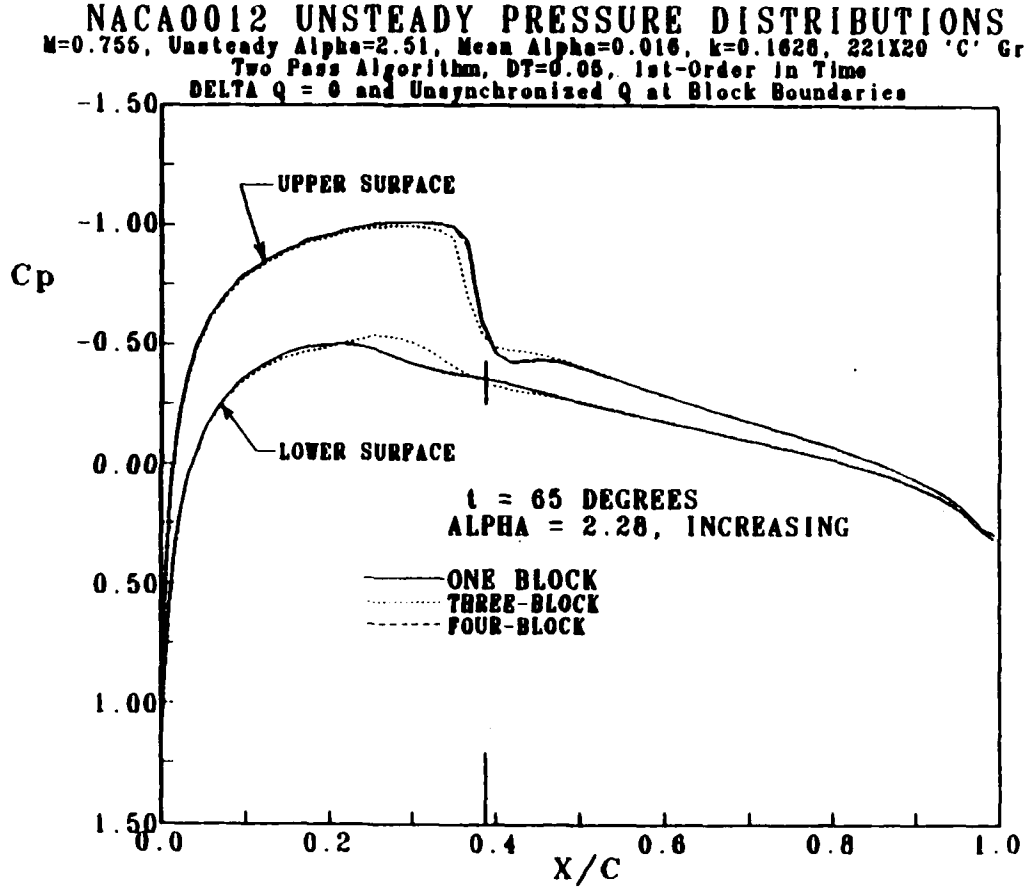

(b) 65° of Oscillatory Motion

Figure (4-14) continued

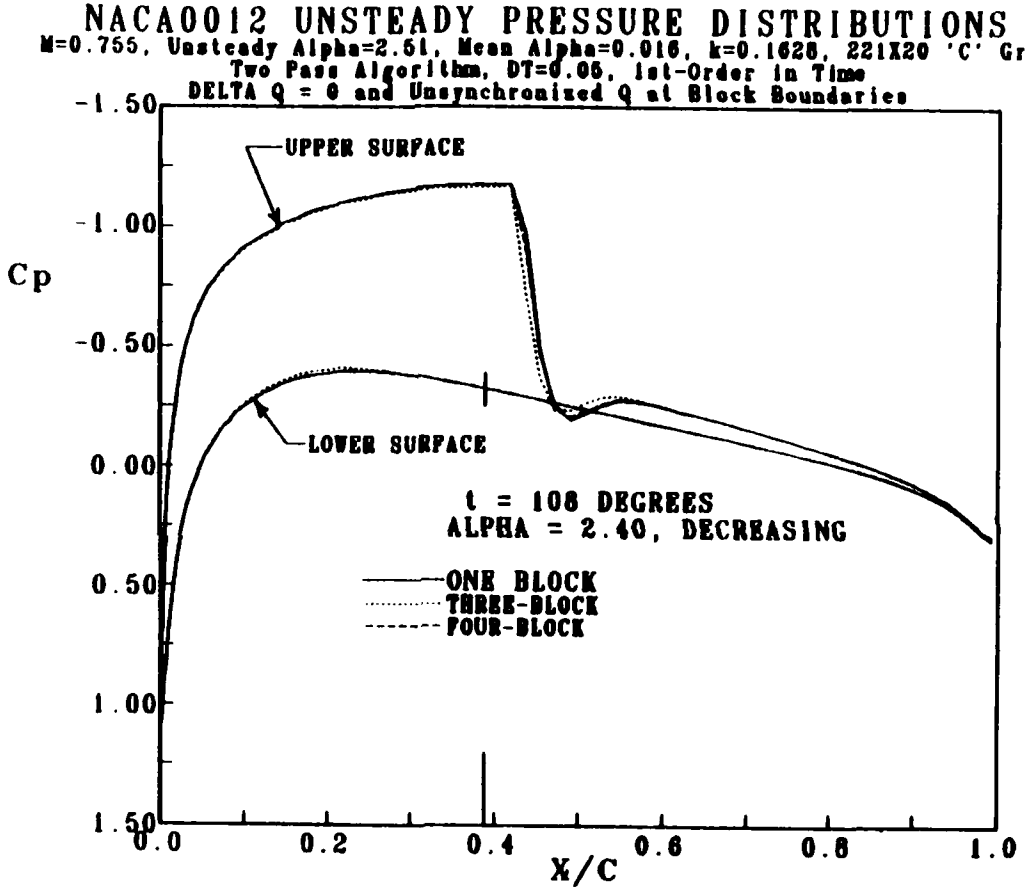

(c) 108° of Oscillatory Motion

Figure (4-14) continued

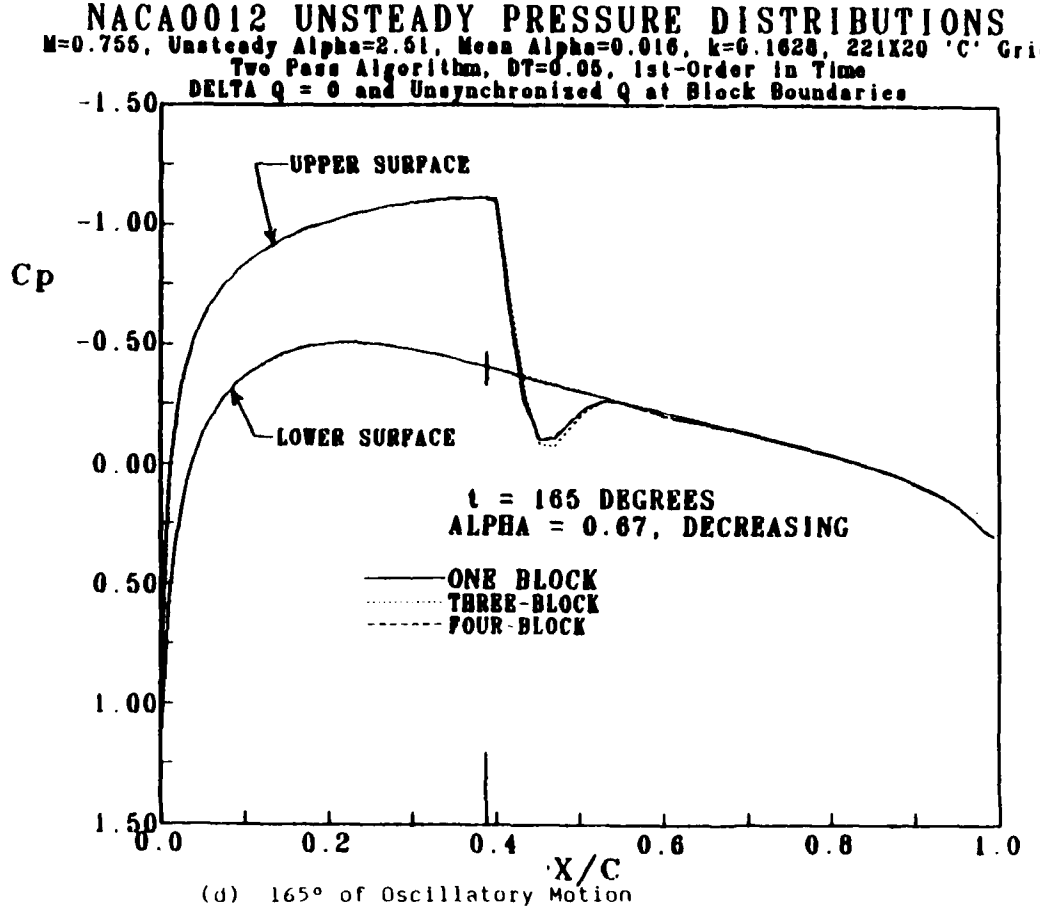

(d) 165° of Oscillatory Motion

Figure (4-14) continued

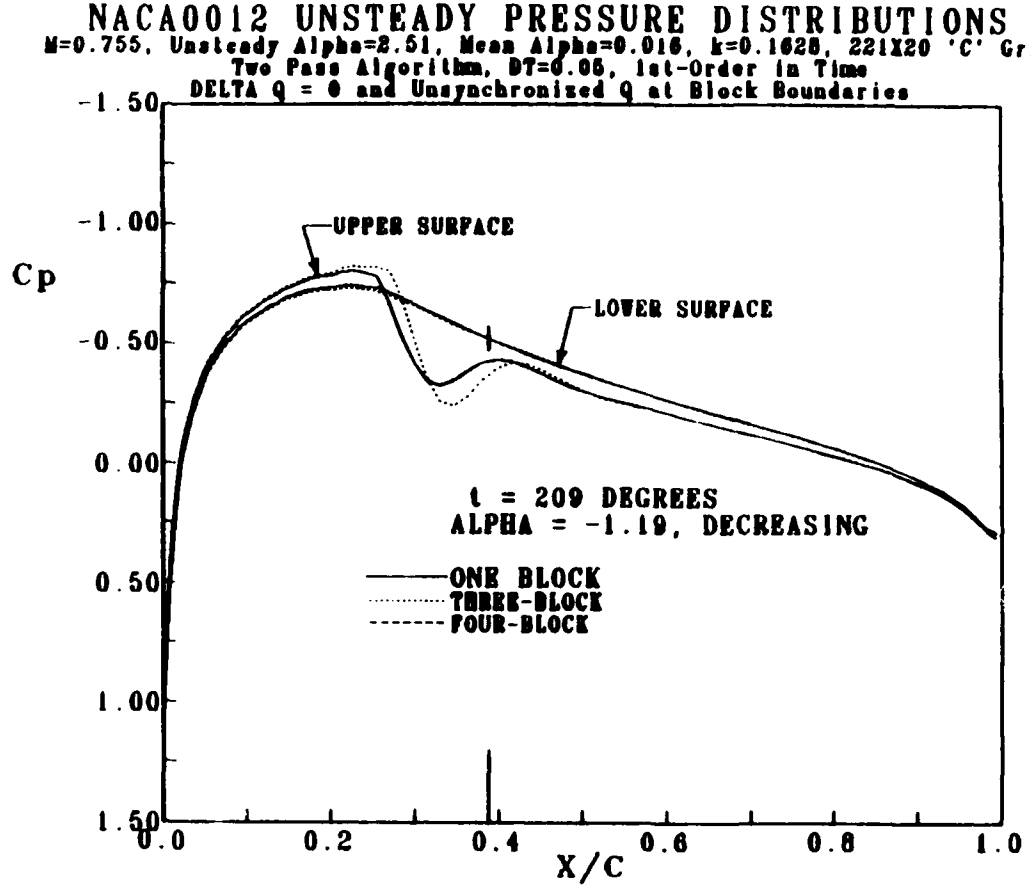

(e) 209° of Oscillatory Motion

Figure (4-14) continued

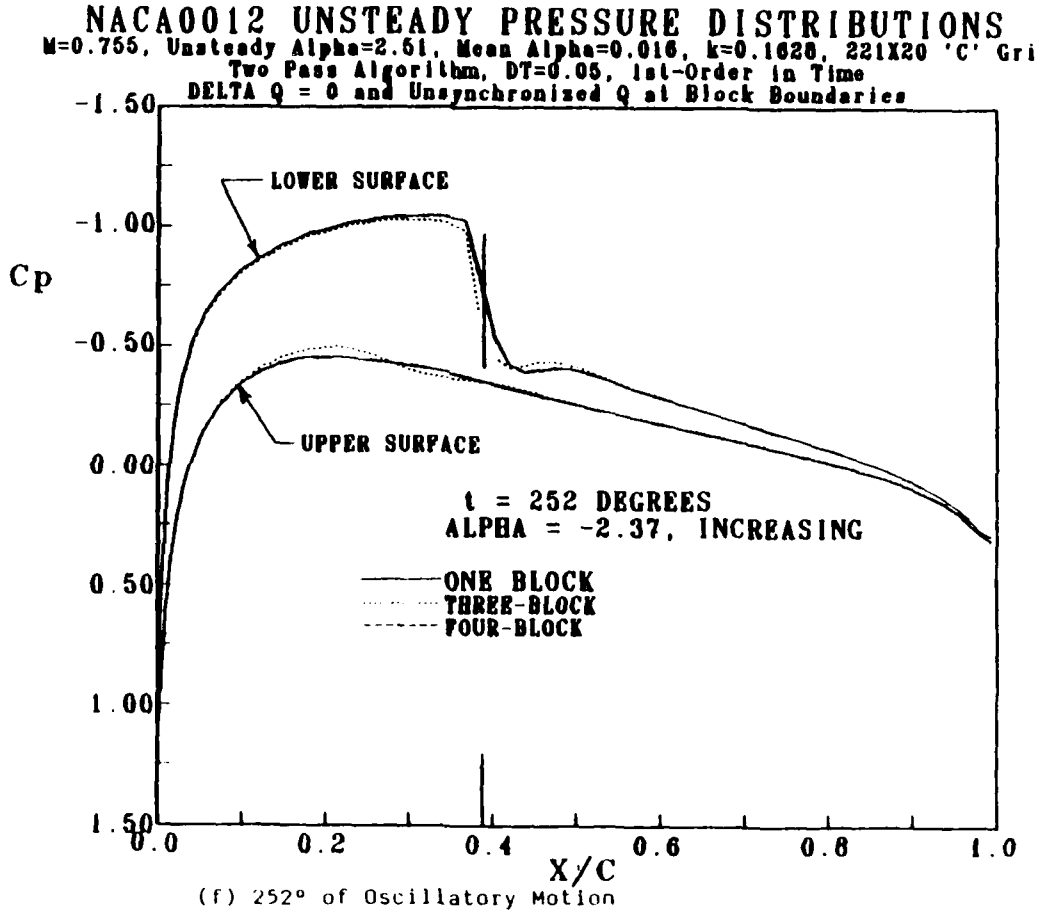

(f) 252° of Oscillatory Motion

Figure (4-14) continued

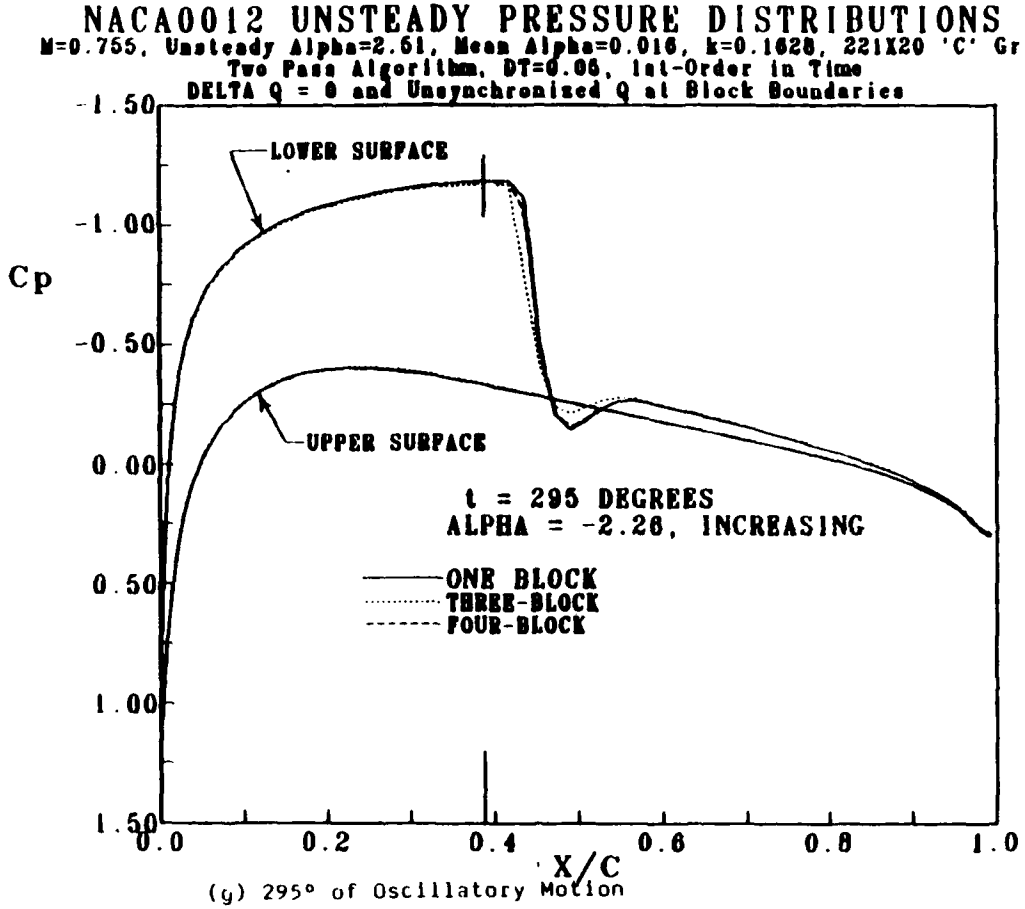

(g) 295° of Oscillatory Motion

Figure (4-14) continued

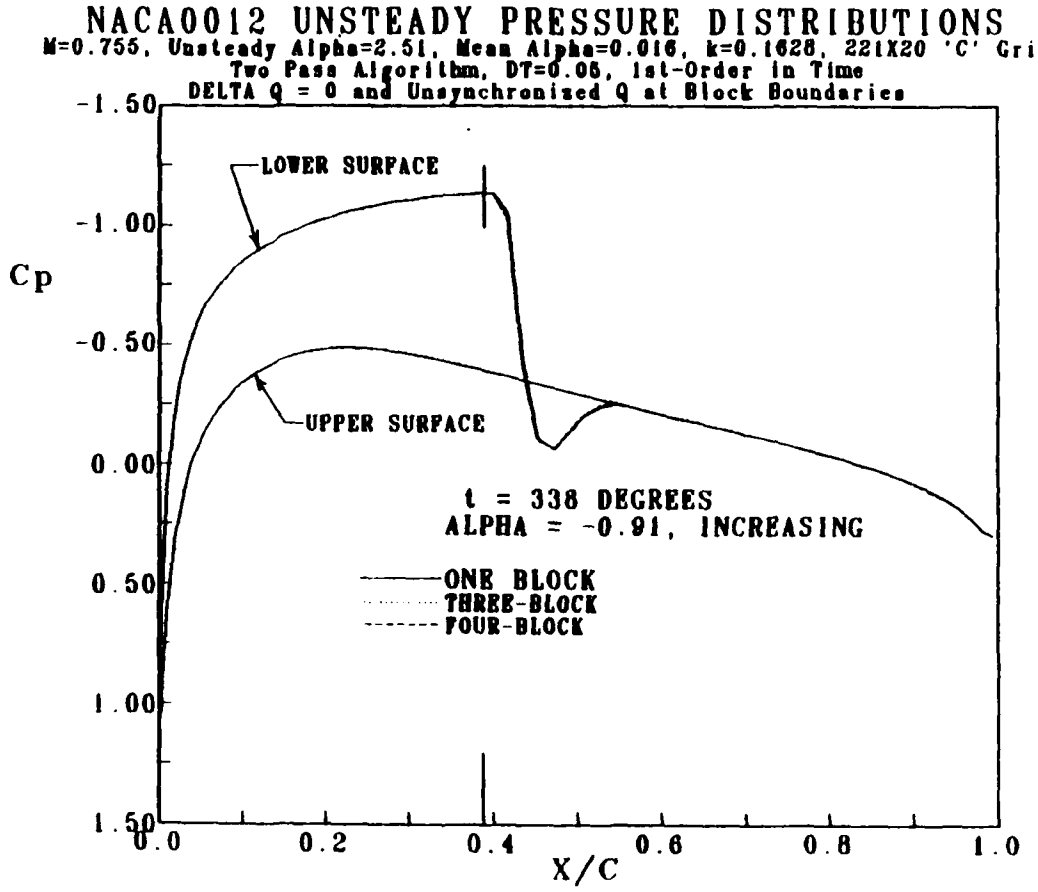

(h) 338° of Oscillatory Motion

Figure (4-14) continued

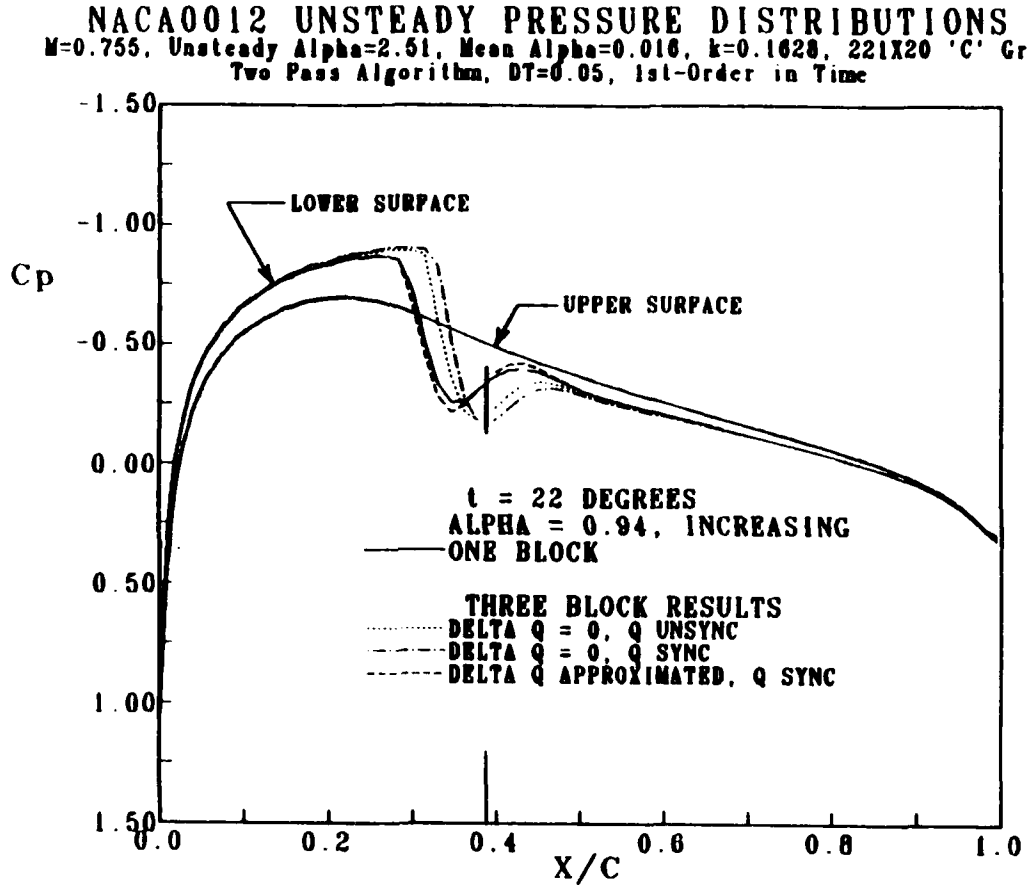

(a) 22° of Oscillatory Motion

Figure (4-15) Unsteady Pressure Coefficients Using Various Block Boundary Conditions

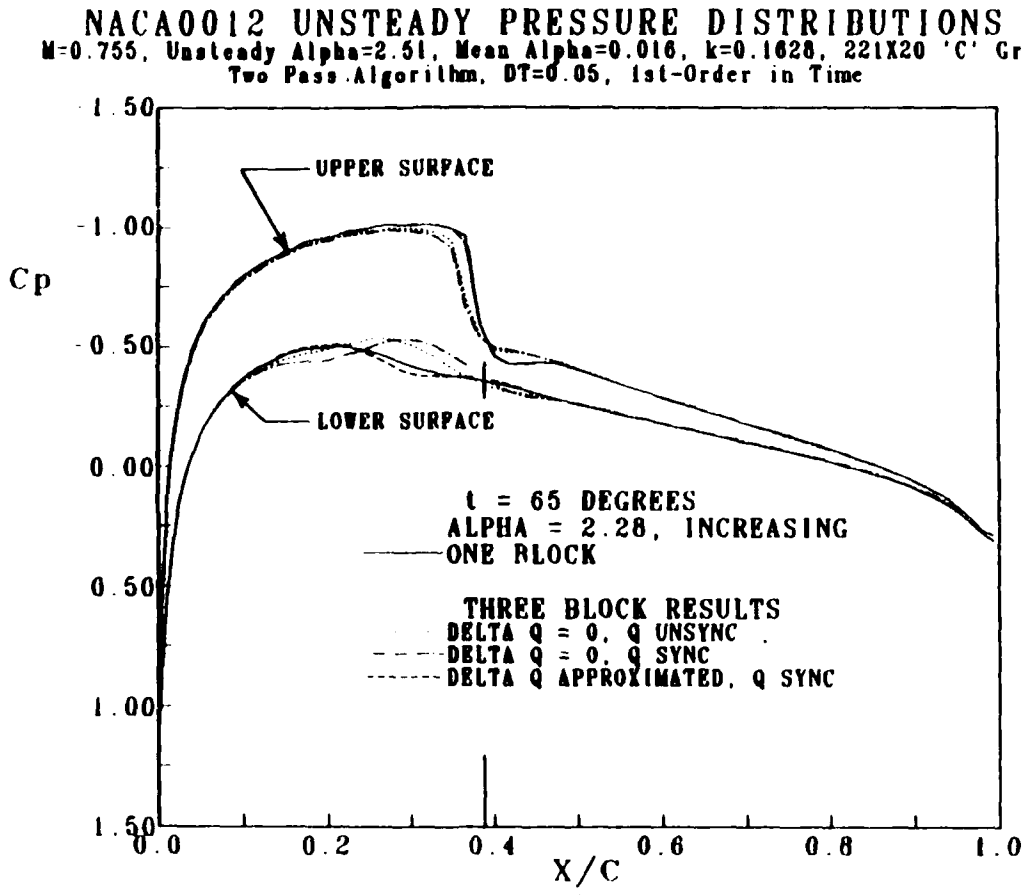

(b) 65° Of Oscillatory Motion

Figure (4-15) continued

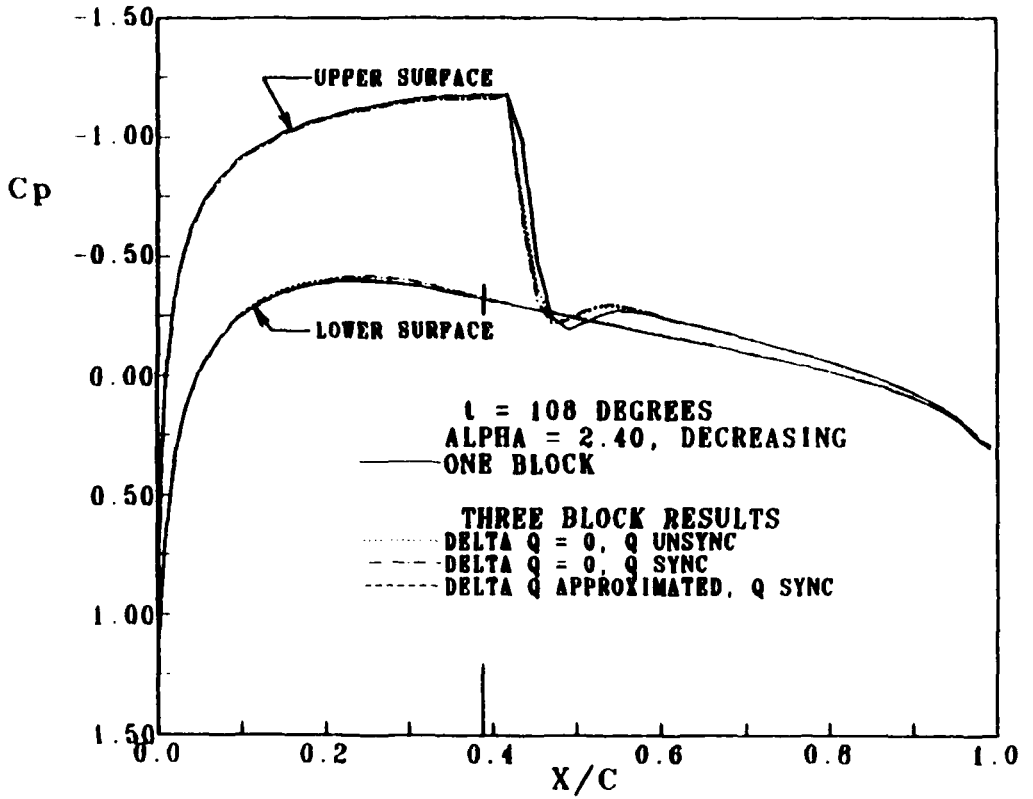

(c) 108° of Oscillatory Motion

Figure (4-15) continued

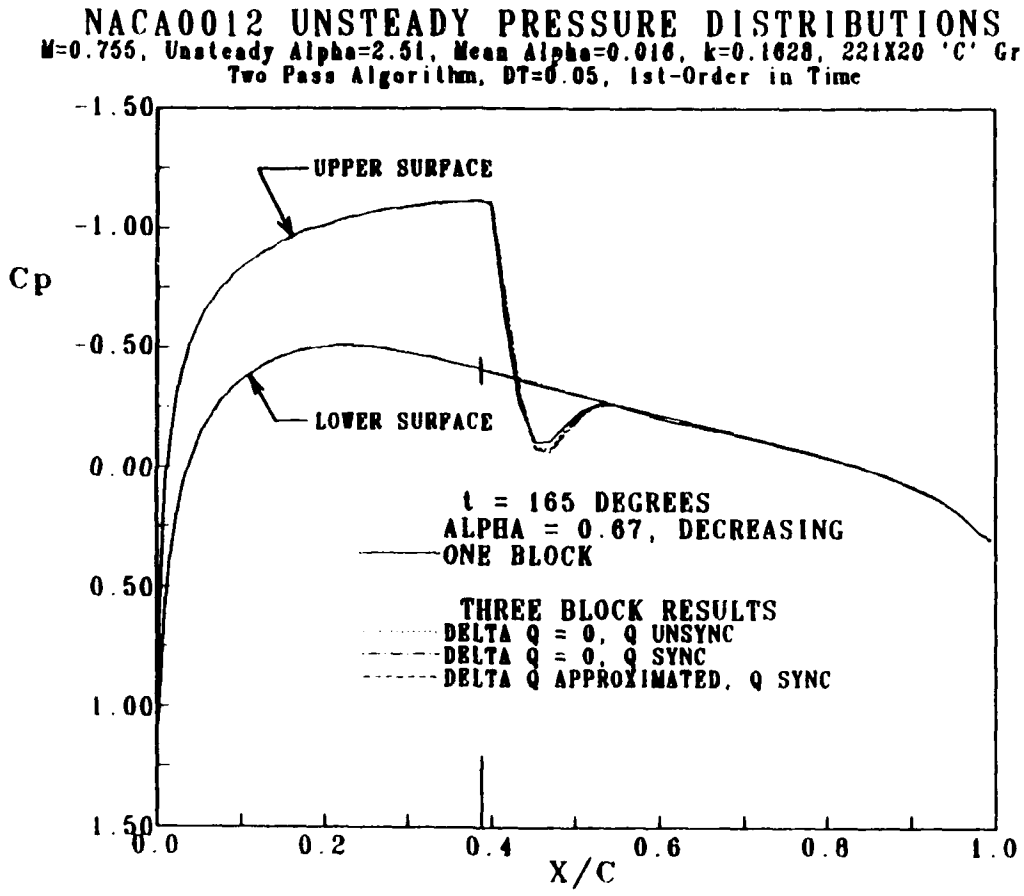

(d) 165° of Oscillatory Motion

Figure (4-15) continued

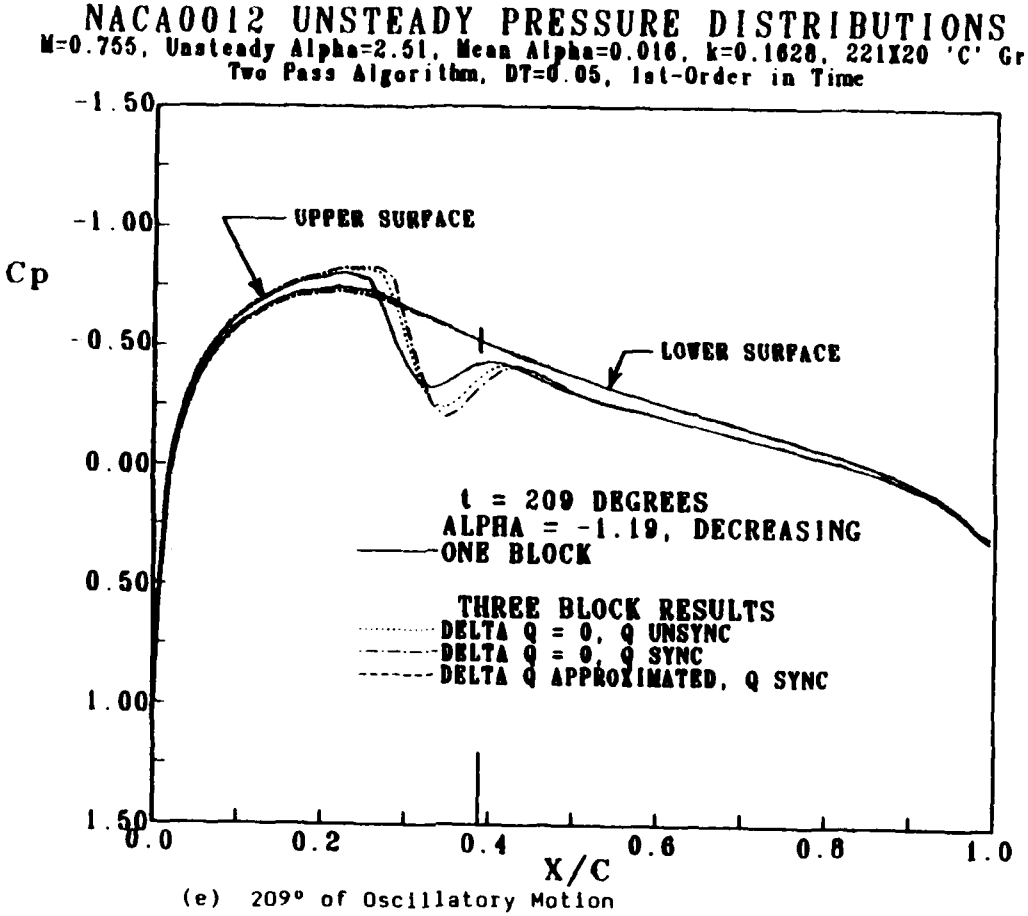

(e) 209° of Oscillatory Motion

Figure (4-15) continued

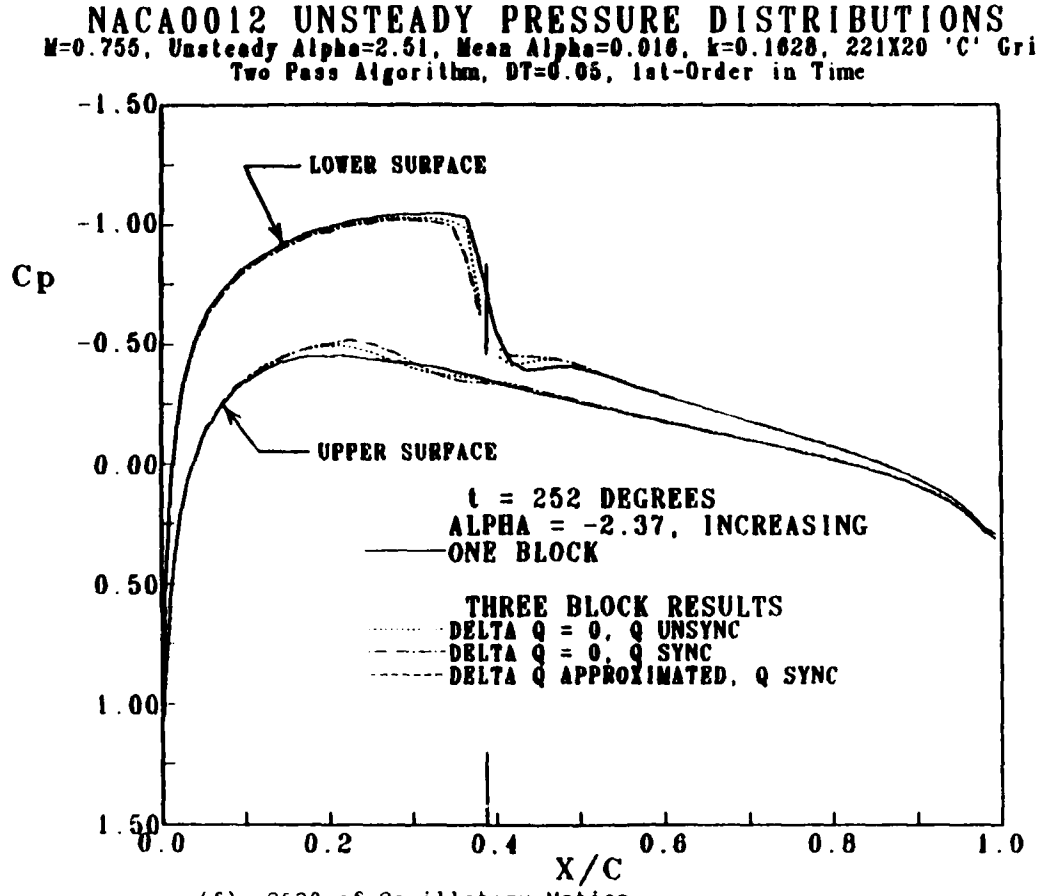

(f) 252° of Oscillatory Motion

Figure (4-15) continued

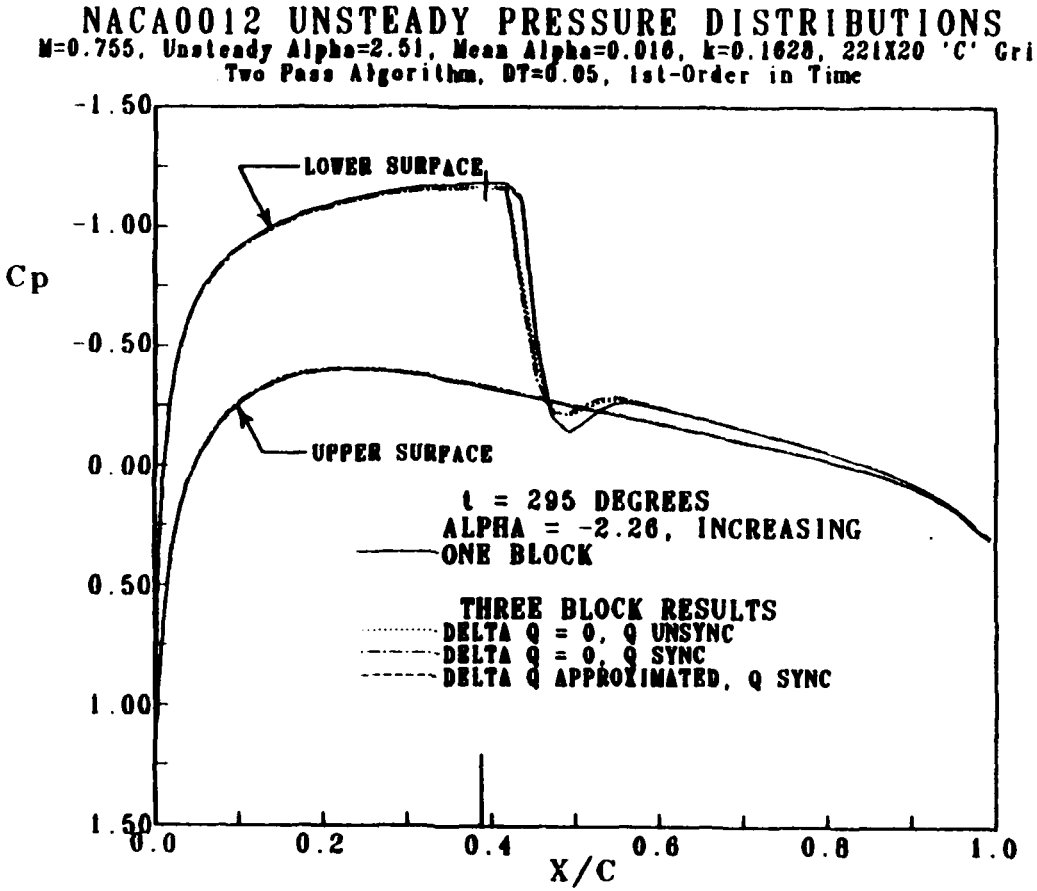

(g) 295° of Oscillatory Motion

Figure (4-15) continued

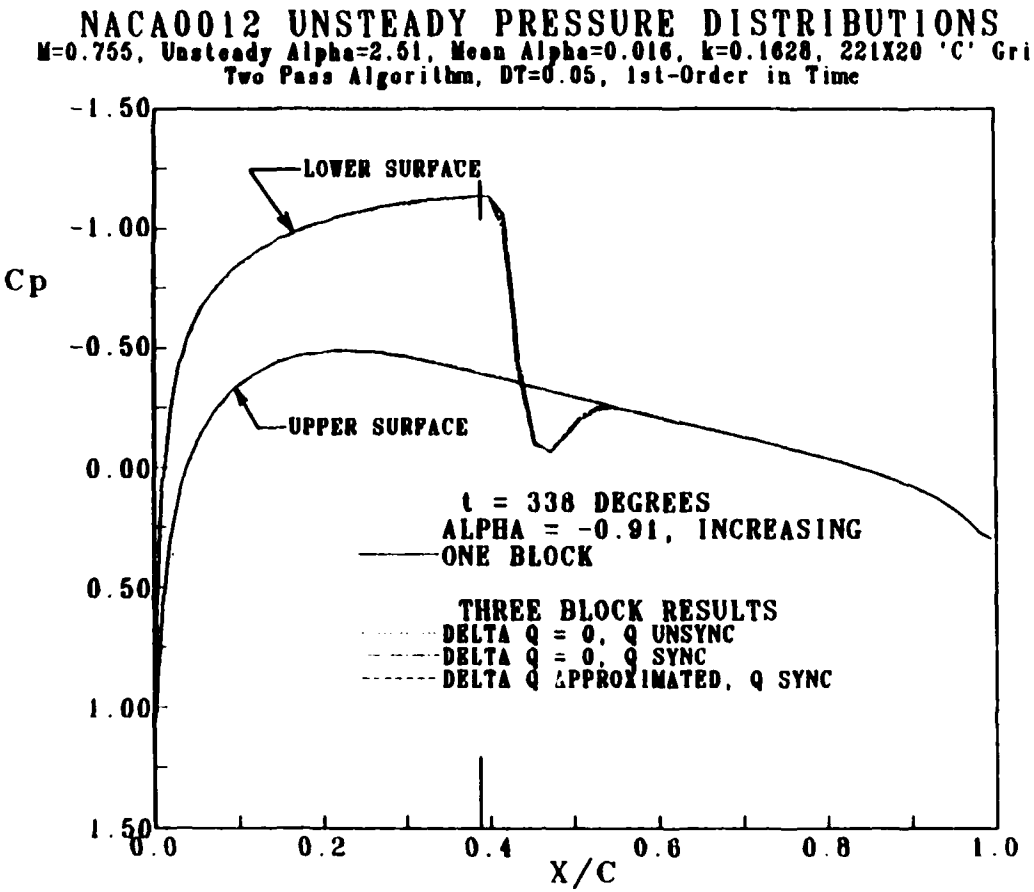

(h) 338° of Oscillatory Motion

Figure (4-15) continued

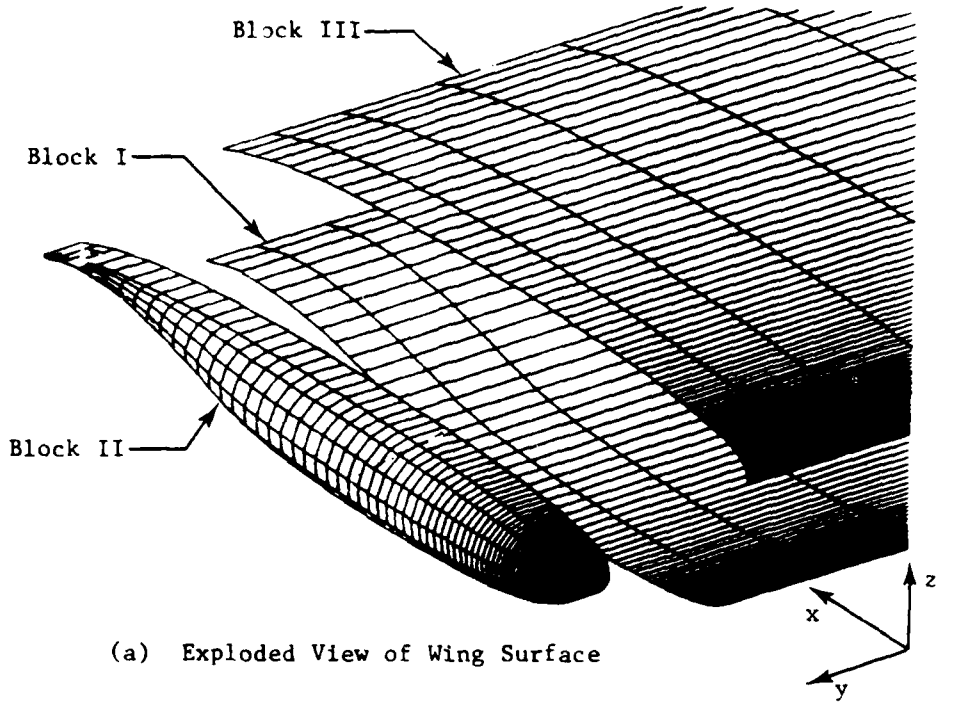

(a) Exploded View of Wing Surface

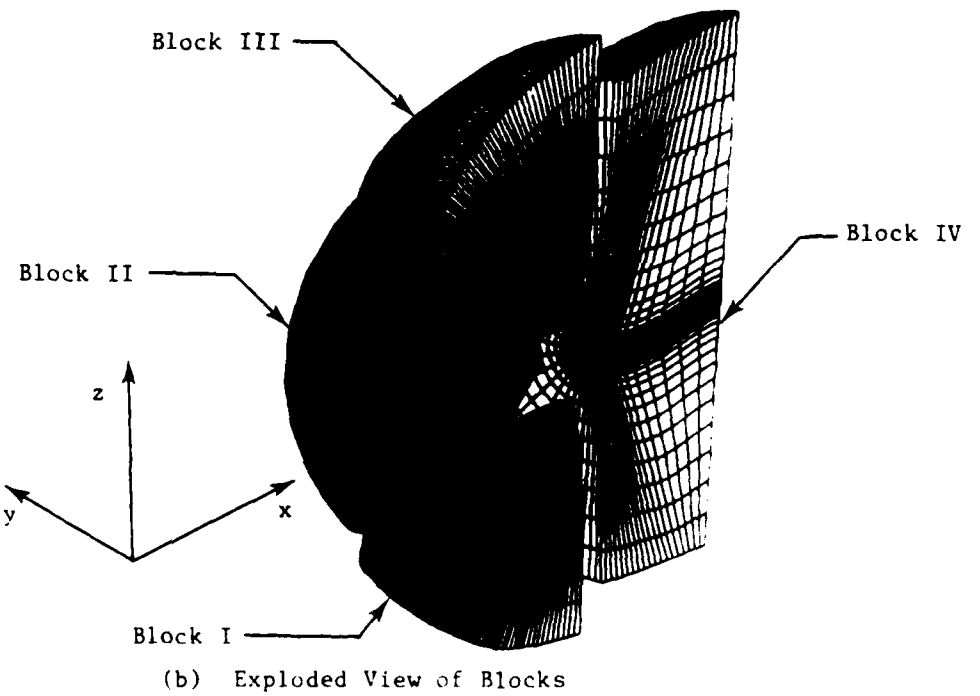

(b) Exploded View of Blocks

Figure (5-1) Blocked Grid Structure Around Rectangular Supercritical Wing

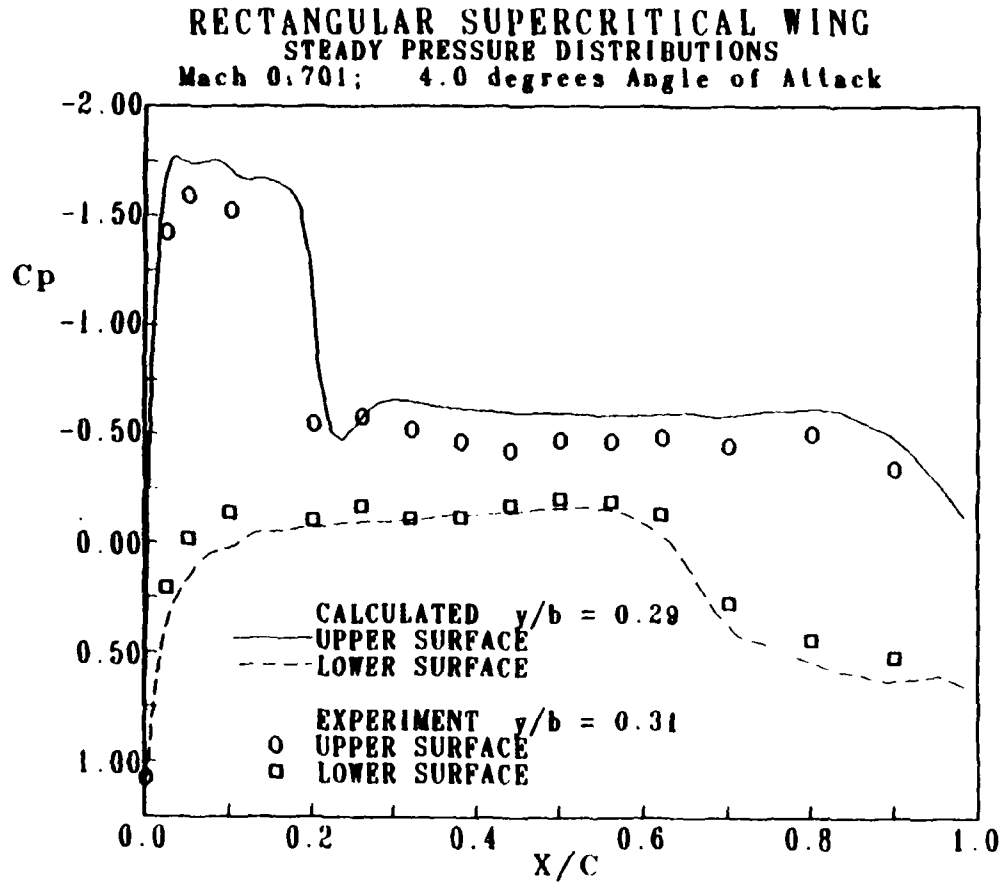

(a) 30% Semispan

Figure (5-2) Steady Rectangular Wing Pressure Coefficients at Mach 0.7

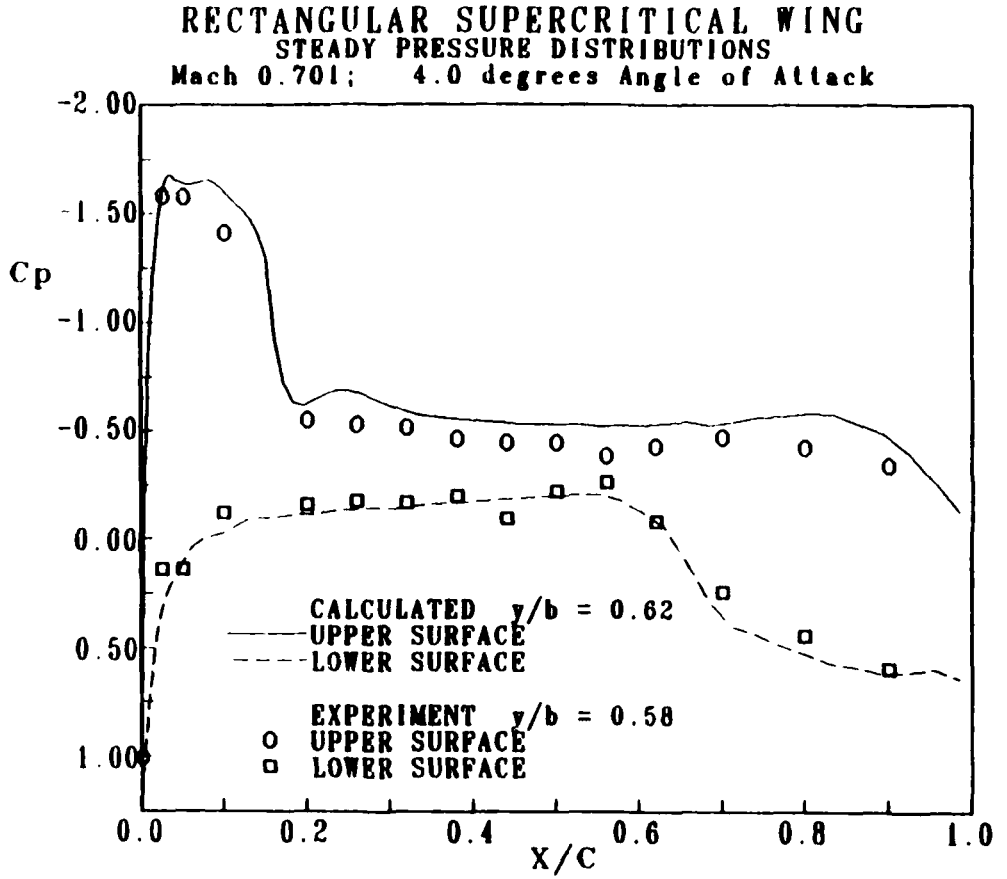

(b) 60% Semispan

Figure (5-2) continued

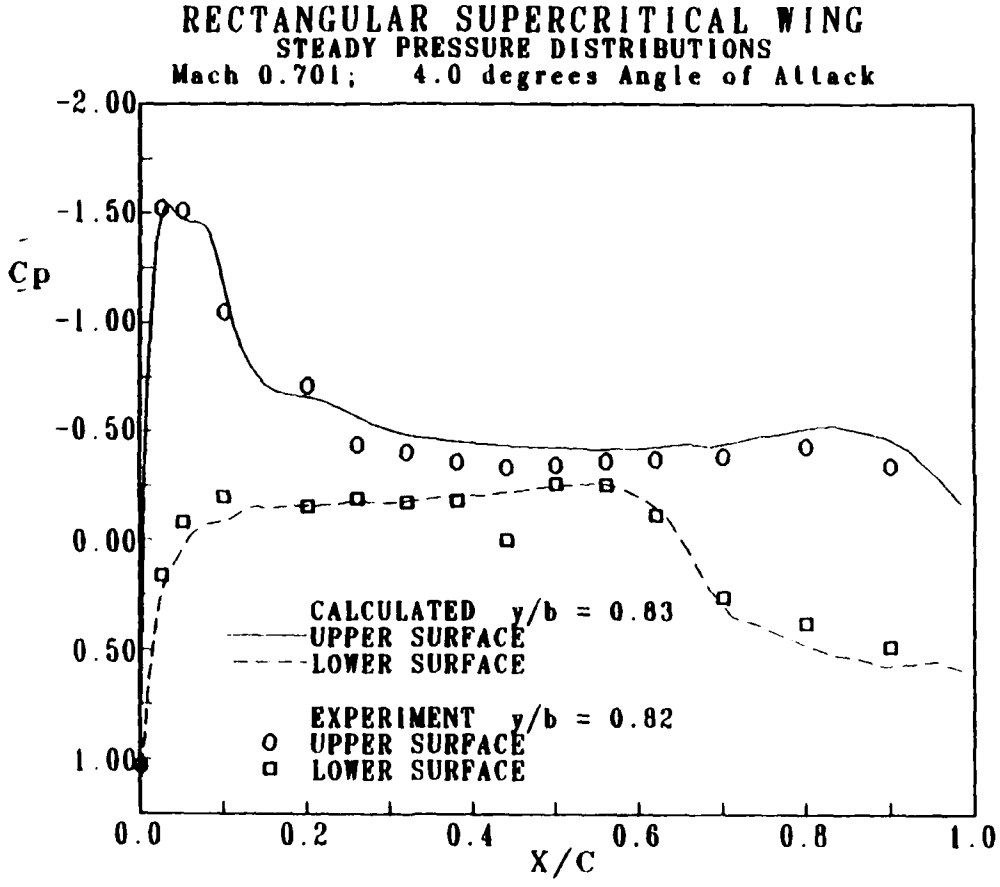

(c) 80% Semispan

Figure (5-2) continued

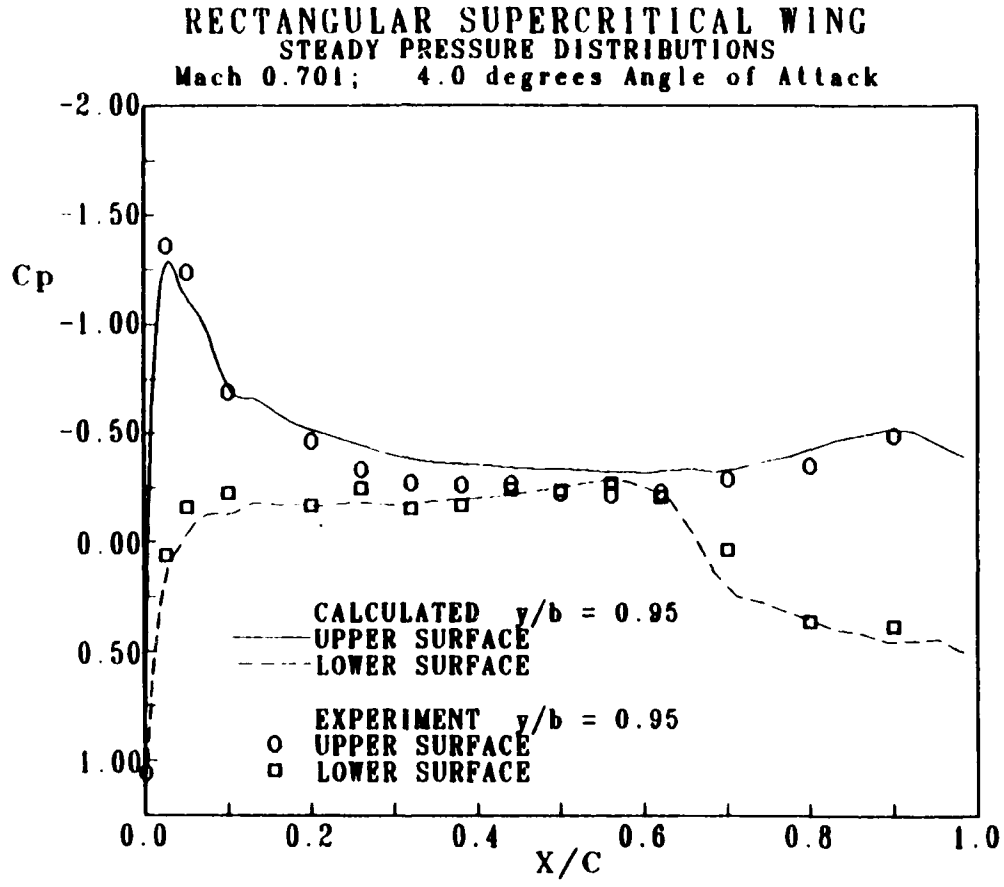

(d) 95% Semispan

Figure (5-2) continued

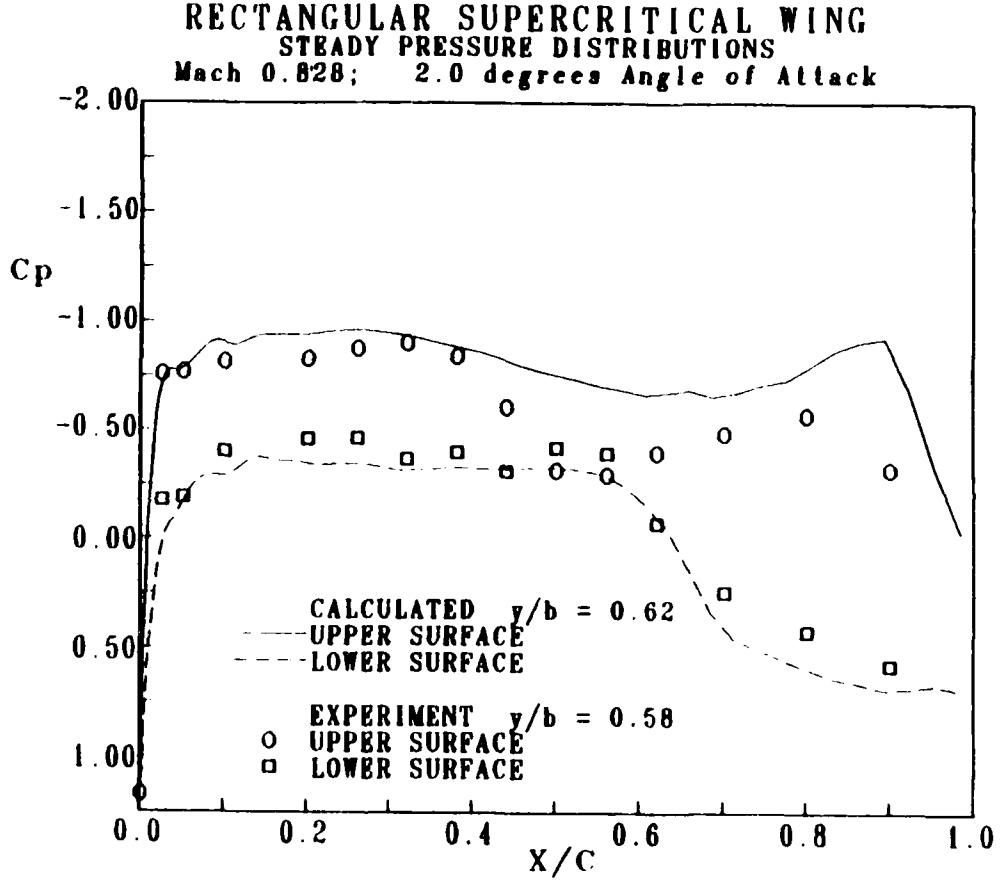

Figure (5-3) Steady Rectangular Wing Pressure Coefficients at 60% Semispan and Mach 0.83

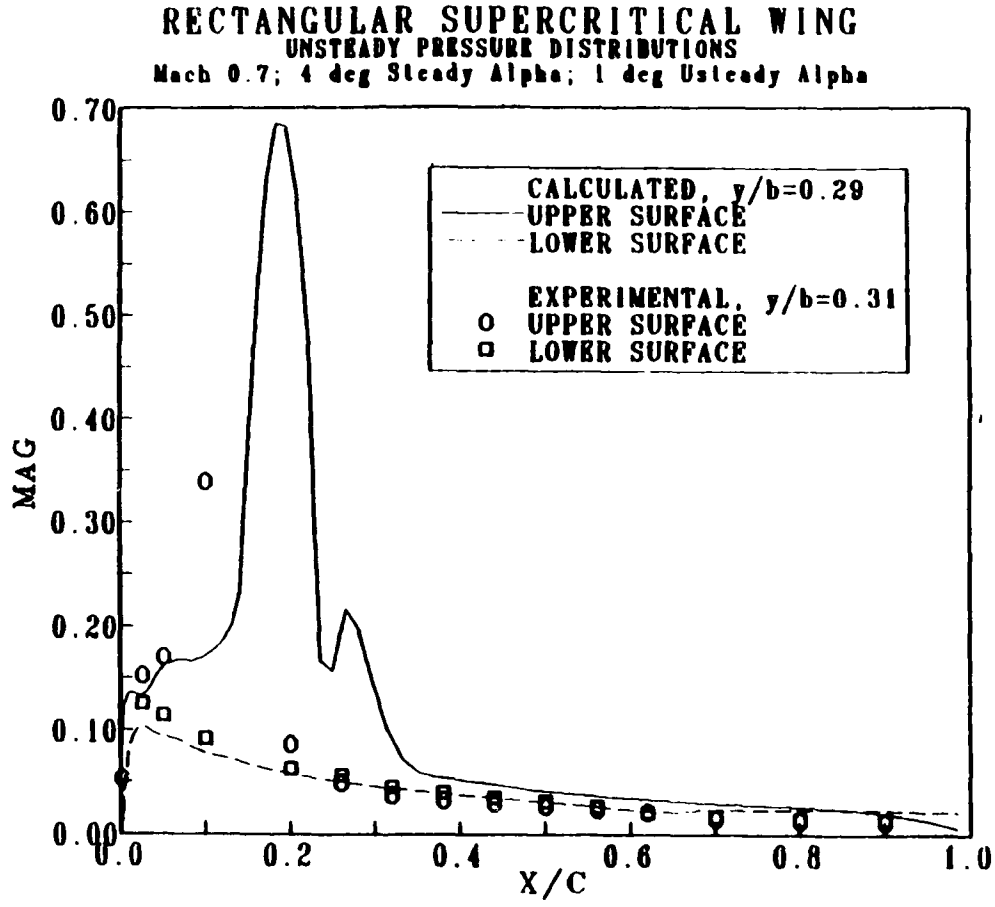

(a) Magnitude at 30% Semispan

Figure (5-4) Magnitude and Phase of Unsteady Rectangular Wing Pressure Coefficients, k = 0.358

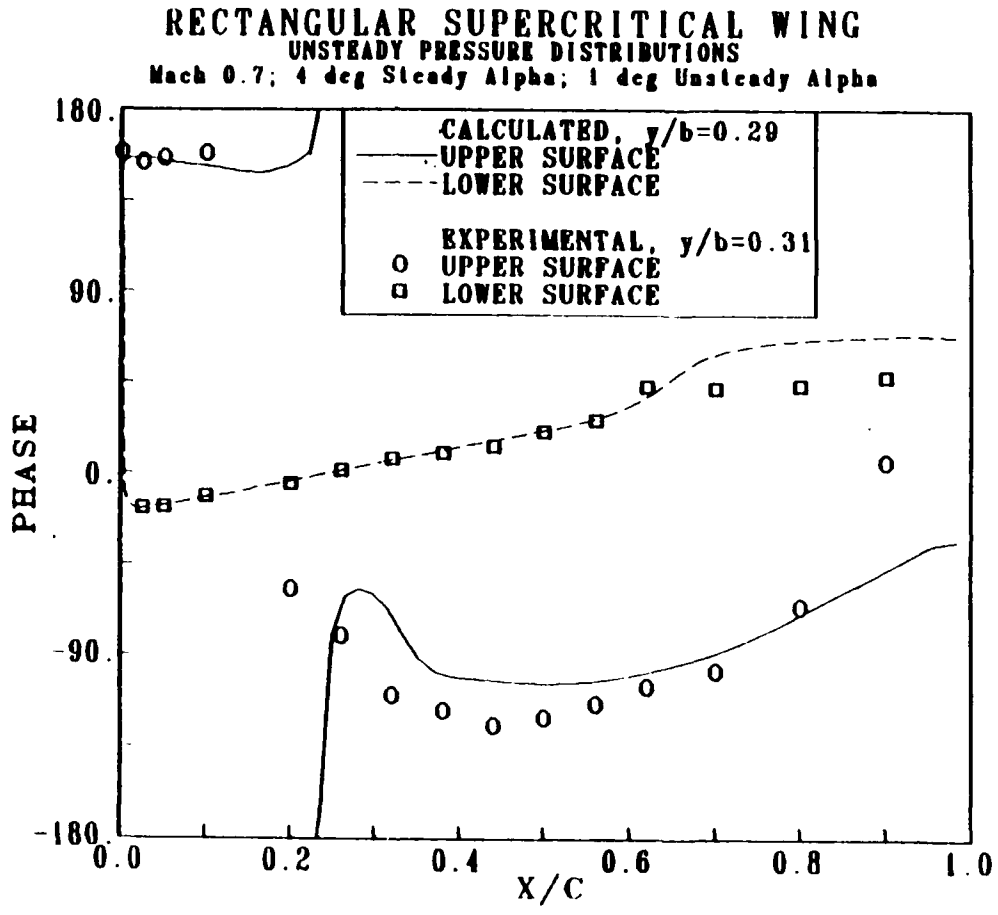

(b) Phase at 30% Semispan

Figure (5-4) continued

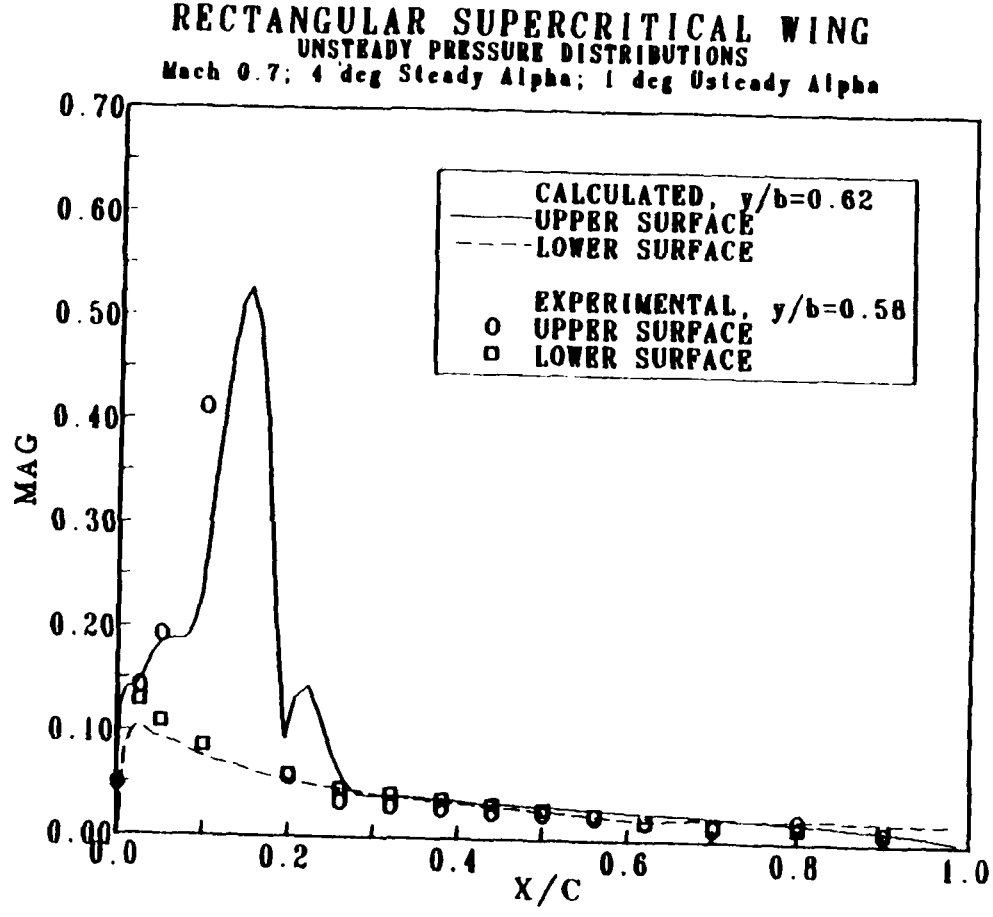

(c) Magnitude at 60% Semispan

Figure (5-4) continued

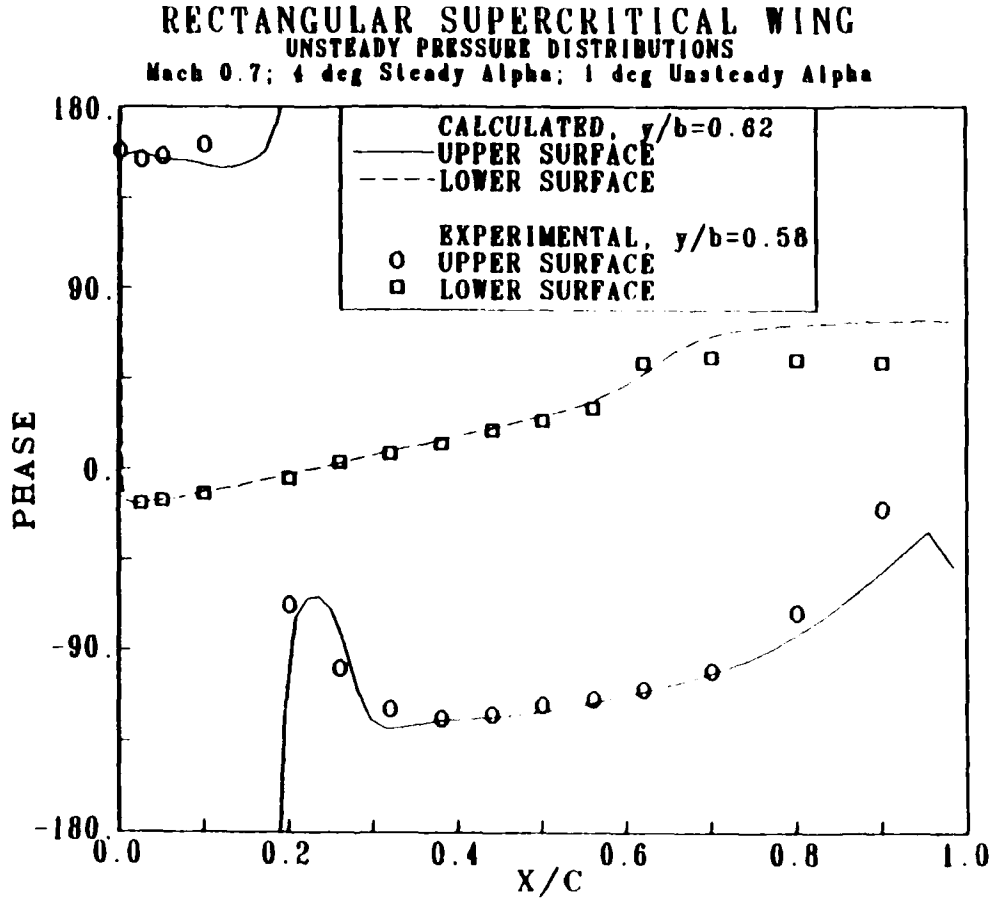

(d) Phase at 60% Semispan

Figure (5-4) continued

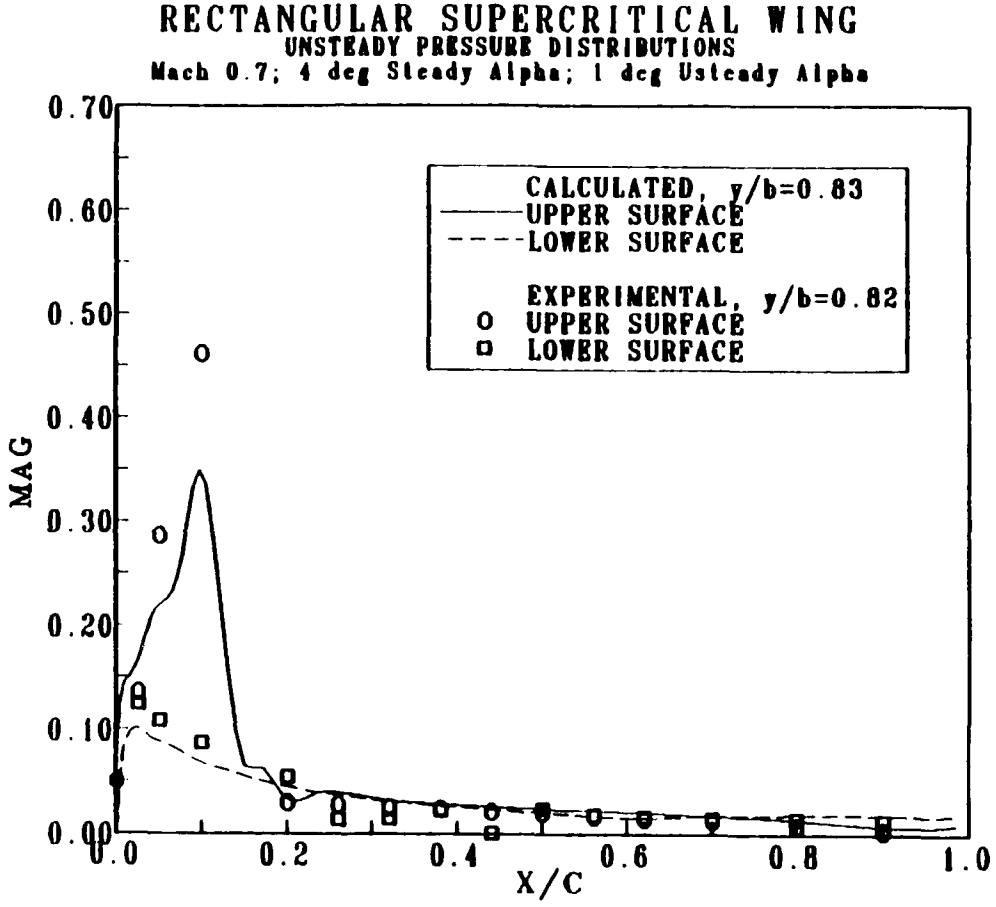

(e) Magnitude at 80% Semispan

Figure (5-4) continued

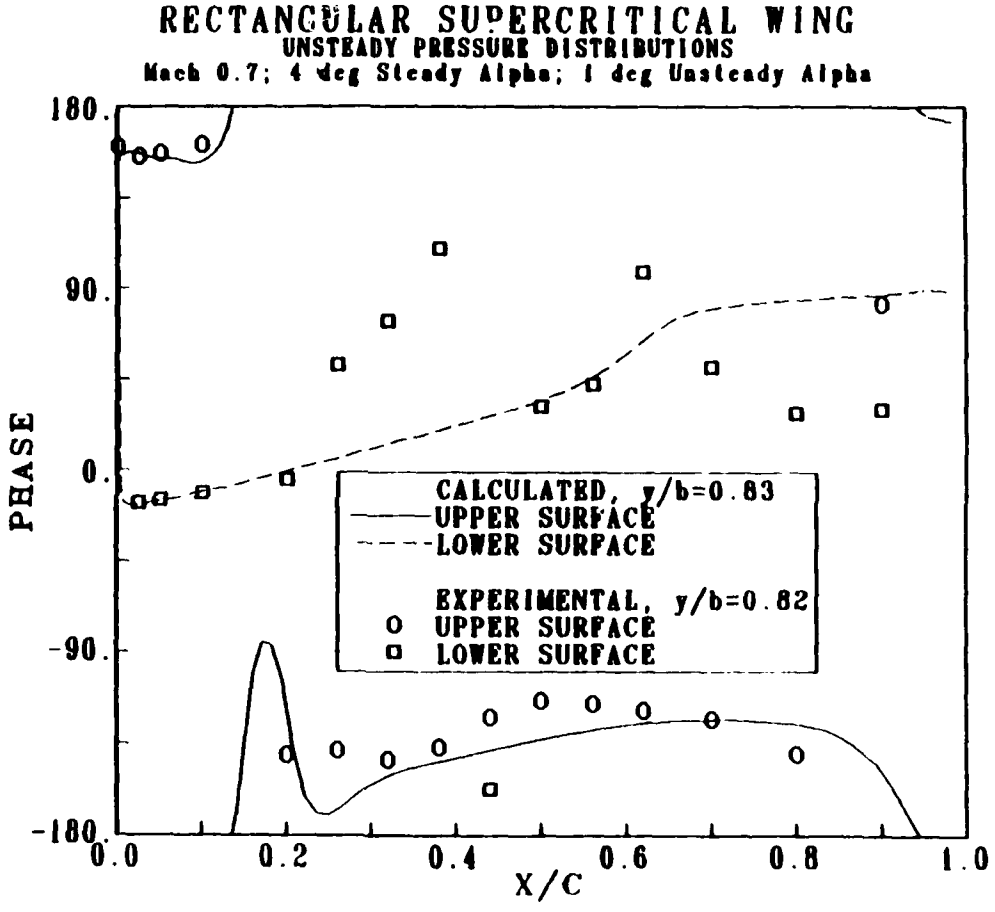

(f) Phase at 80% Semispan

Figure (5-4) continued

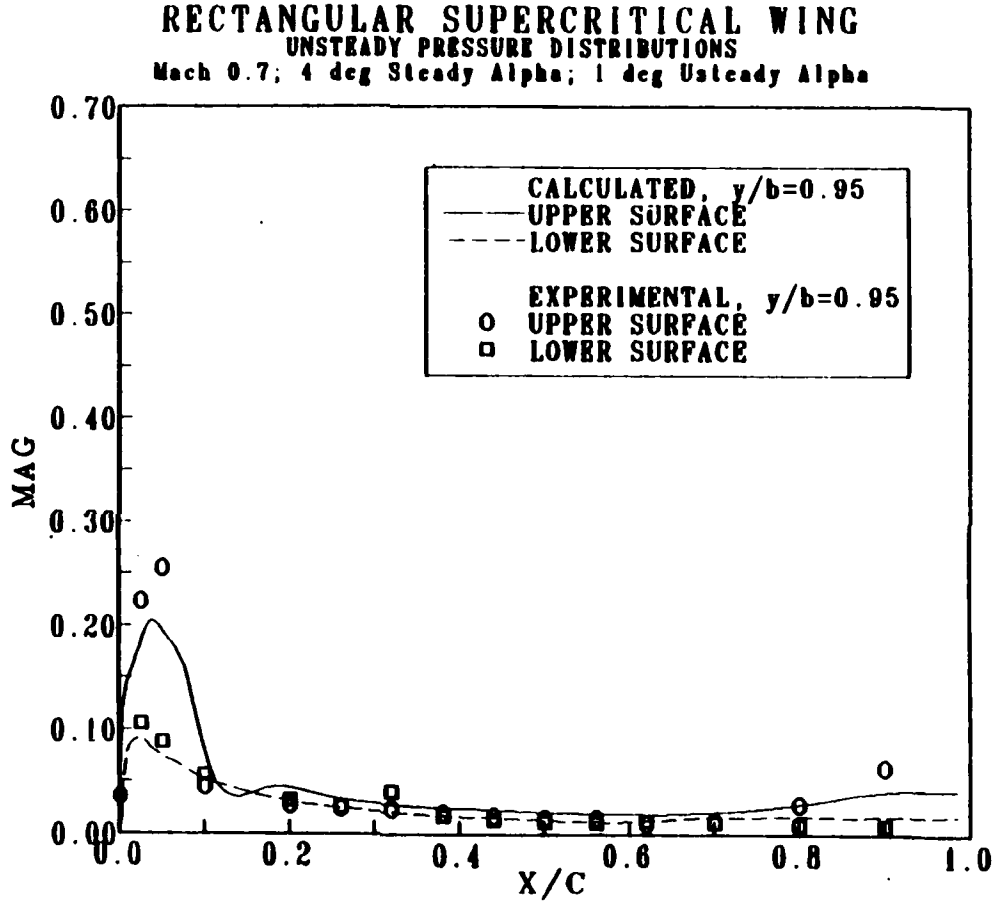

(g) Magnitude at 95% Semispan

Figure (5-4) continued

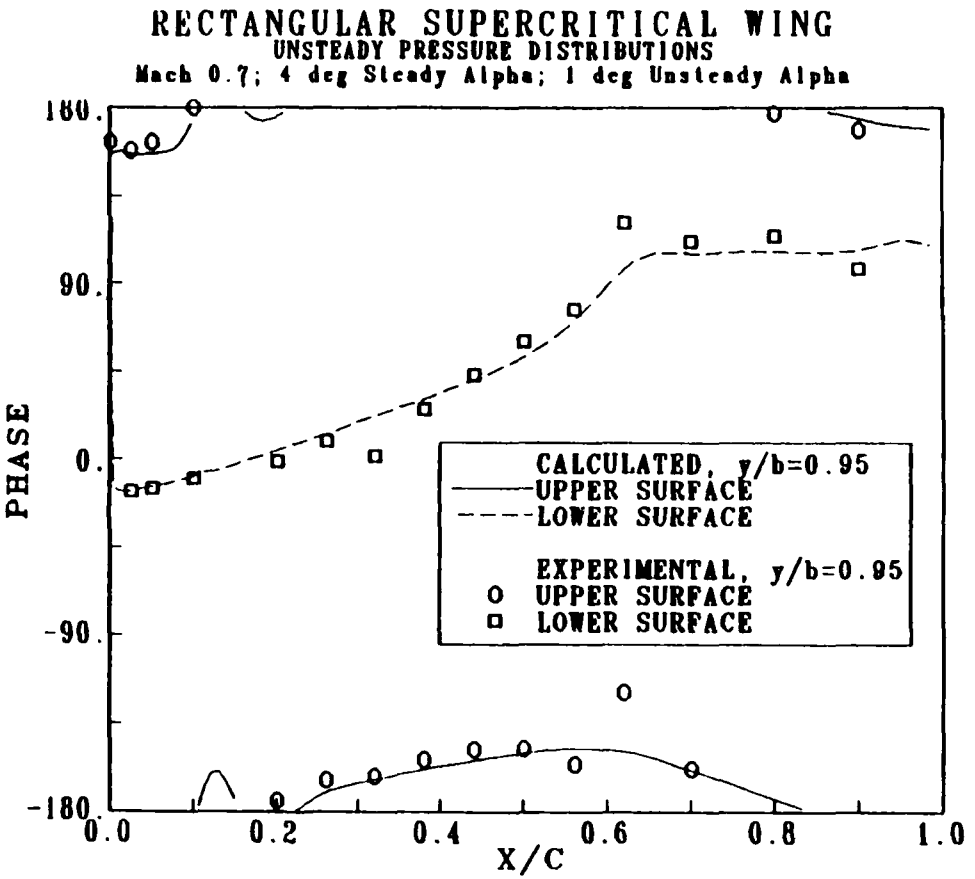

(h) Phase at 95% Semispan

Figure (5-4) continued

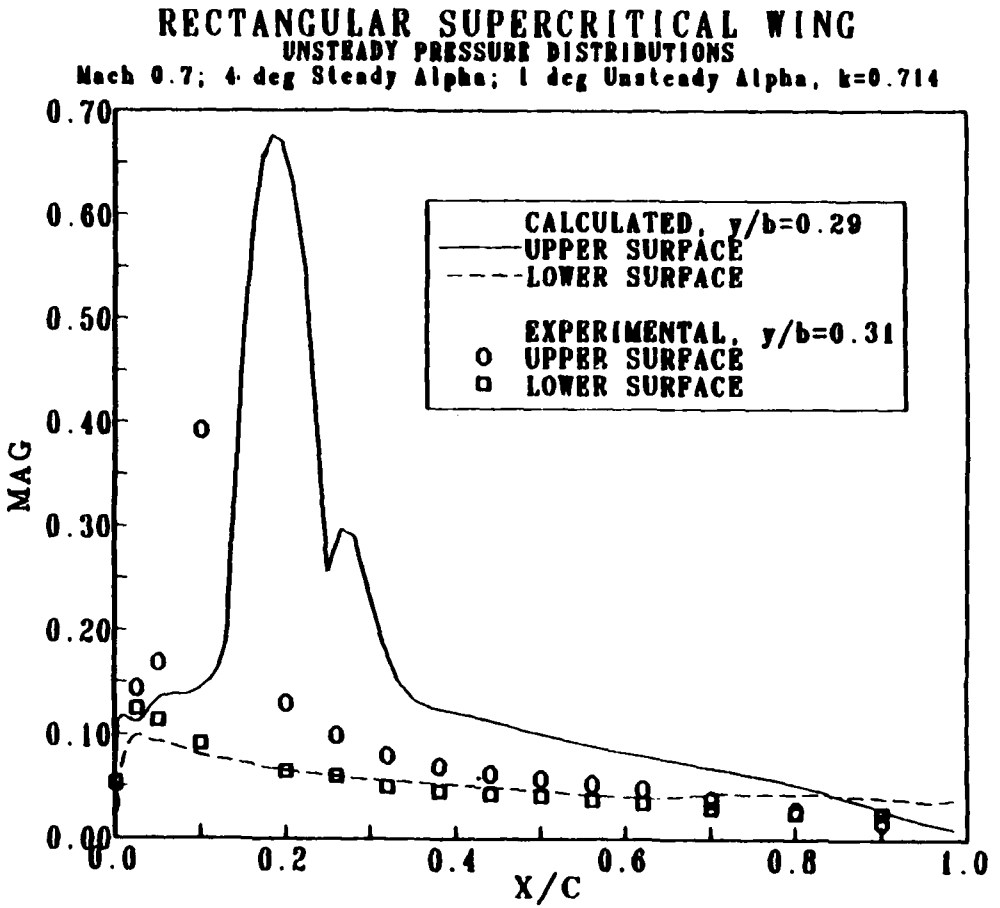

(a) Magnitude at 30% Semispan

Figure (5-5) Magnitude and Phase of Unsteady Rectangular Wing Pressure Coefficients, k = 0.714

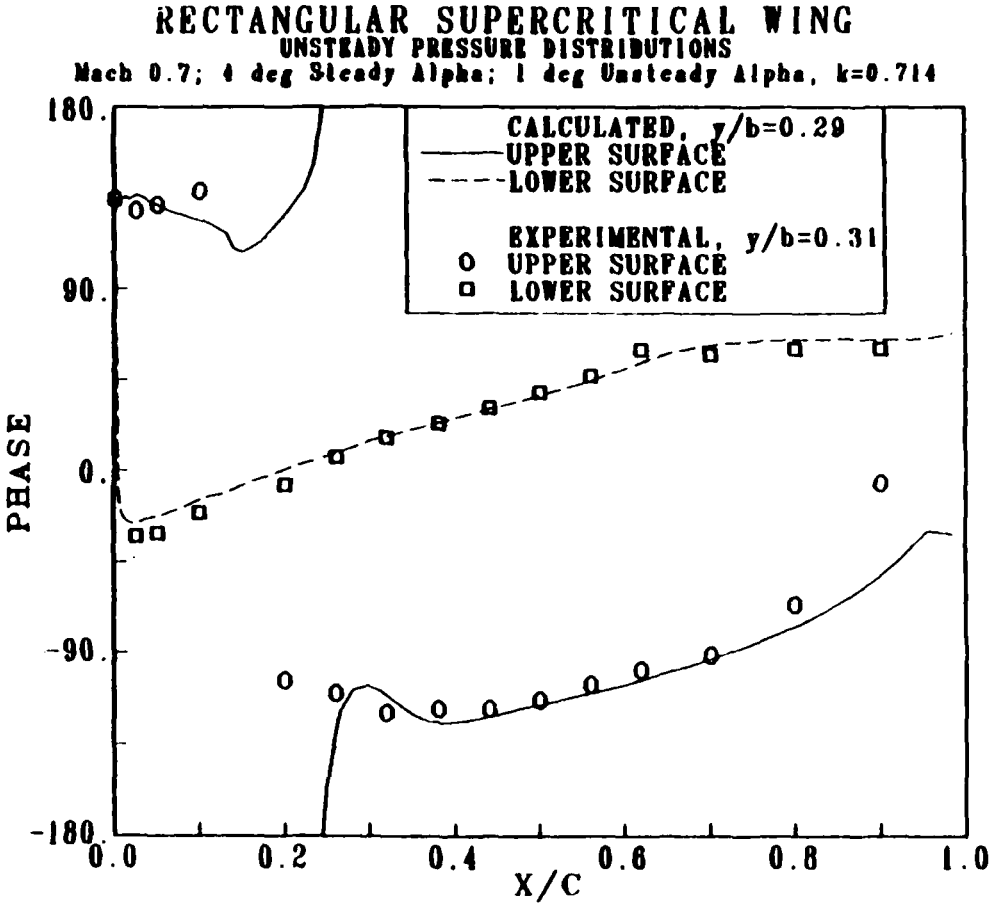

(b) Phase at 30% Semispan

Figure (5-5) continued

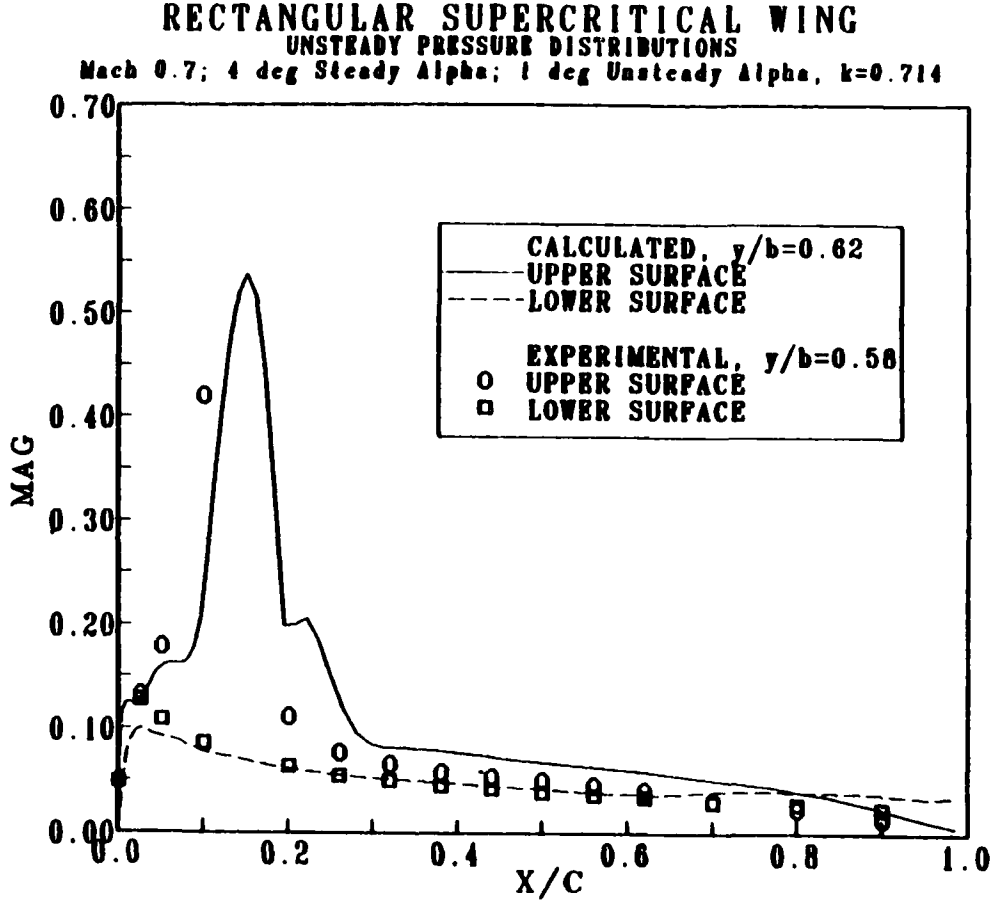

(c) Magnitude at 60% Semispan

Figure (5-5) continued

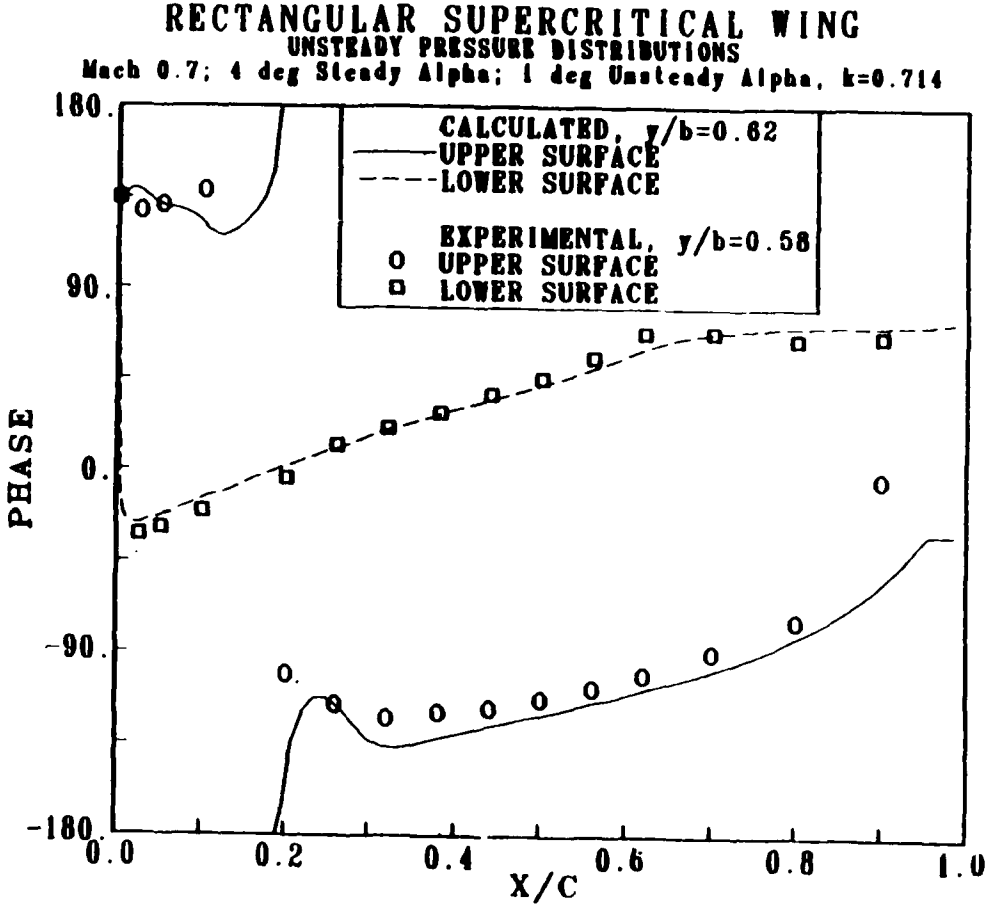

(d) Phase at 60% Semispan

Figure (5-5) continued

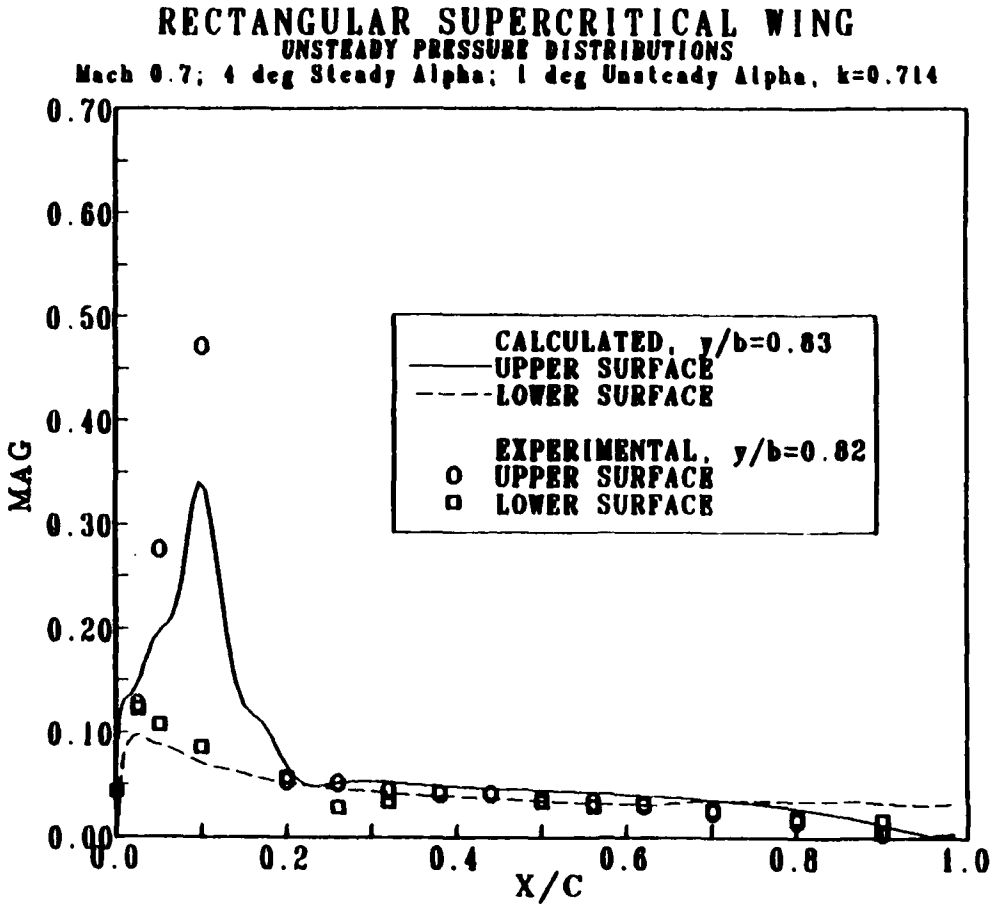

(e) Magnitude at 80% Semispan

Figure (5-5) continued

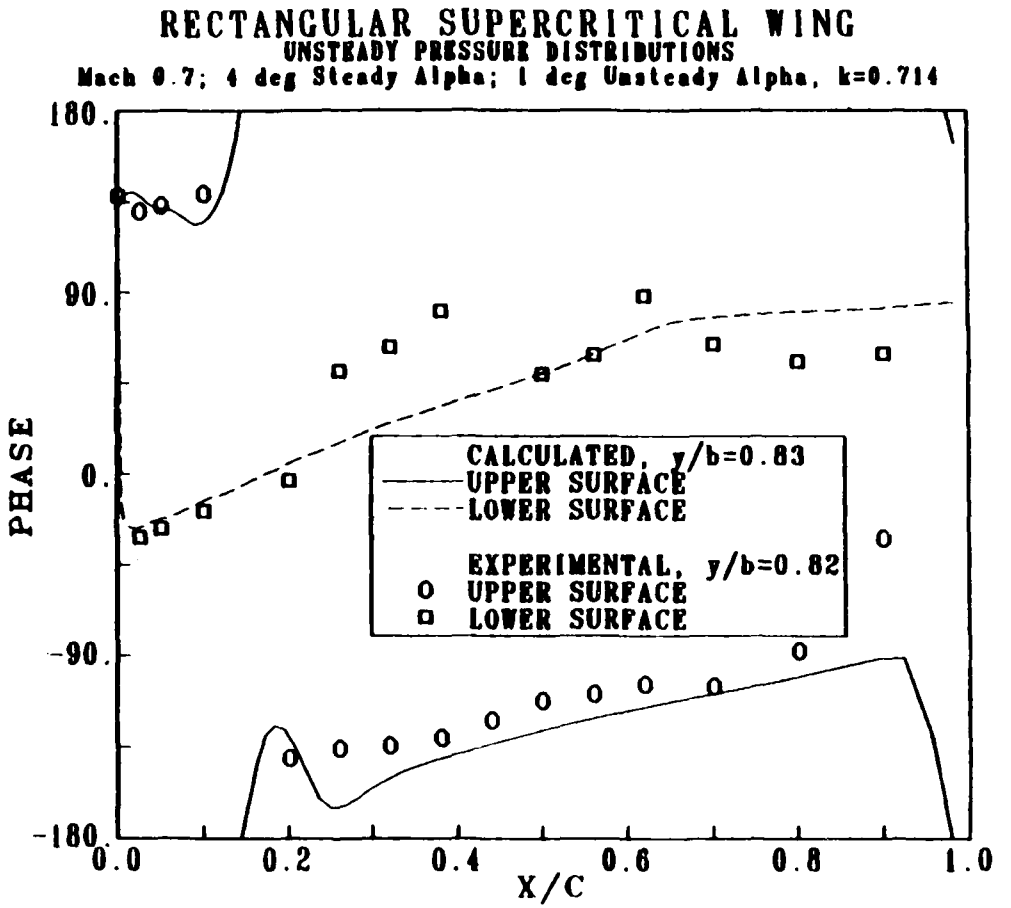

(f) Phase at 80% Semispan

Figure (5-5) continued

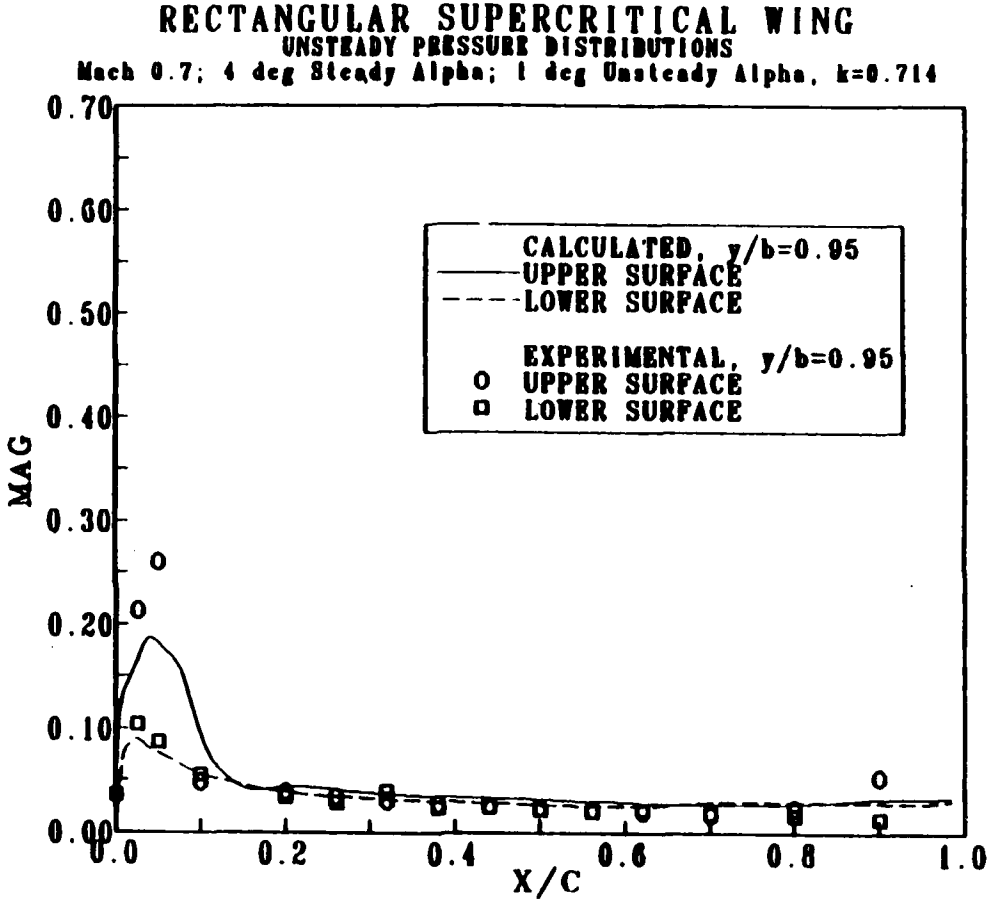

(g) Magnitude at 95% Semispan

Figure (5-5) continued

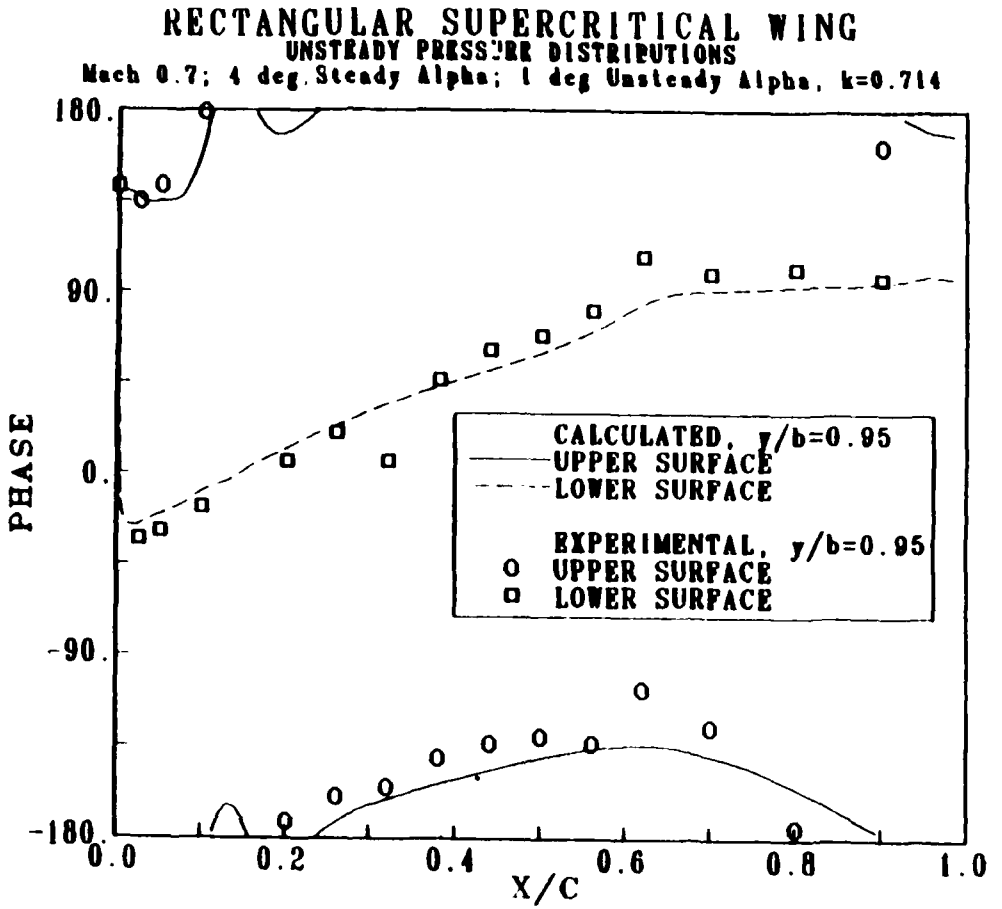

(h) Phase at 95% Semispan

Figure (5-5) continued

(The reverse of this page is blank)

APPENDIX A

TIME-DEPENDENT CURVILINEAR COORDINATES

Rewriting the nondimensional form of Equation (2-1) using the transformed coordinates given by Equation (2-3) and the chain rule yields

$$\begin{aligned} &\frac{\partial q}{\partial \tau}\tau_t + \frac{\partial q}{\partial \xi}\xi_t + \frac{\partial q}{\partial \eta}\eta_t + \frac{\partial q}{\partial \zeta}\zeta_t \\ &+ \frac{\partial f}{\partial \xi}\xi_x + \frac{\partial f}{\partial \eta}\eta_x + \frac{\partial f}{\partial \zeta}\zeta_x \\ &+ \frac{\partial g}{\partial \xi}\xi_y + \frac{\partial g}{\partial \eta}\eta_y + \frac{\partial g}{\partial \zeta}\zeta_y \\ &+ \frac{\partial h}{\partial \xi}\xi_z + \frac{\partial h}{\partial \eta}\eta_z + \frac{\partial h}{\partial \zeta}\zeta_z = 0 \end{aligned} \tag{A-1}$$

Let $J' = \dfrac{\partial(x,y,z,t)}{\partial(\xi,\eta,\zeta,\tau)}$ and $J = \dfrac{\partial(x,y,z)}{\partial(\xi,\eta,\zeta)}$

Then

$$J' = t_\tau J \tag{A-2}$$

where

$$J = \det \begin{bmatrix} x_\xi & y_\xi & z_\xi \\ x_\eta & y_\eta & z_\eta \\ x_\zeta & y_\zeta & z_\zeta \end{bmatrix} \tag{A-3}$$

Multiply Equation (A-1) by J' and regroup terms to arrive at

$$\frac{\partial}{\partial\tau}(J'\tau_t q) + \frac{\partial}{\partial\xi}(J'\xi_t q + J'\xi_x f + J'\xi_y g + J'\xi_z h) + \frac{\partial}{\partial\eta}(J'\eta_t q + J'\eta_x f + J'\eta_y g + J'\eta_z h) + \frac{\partial}{\partial\zeta}(J'\zeta_t q + J'\zeta_x f + J'\zeta_y g + J'\zeta_z h) \tag{A-4}$$

$$= q\left[\frac{\partial(J'\tau_t)}{\partial\tau} + \frac{\partial(J'\xi_t)}{\partial\xi} + \frac{\partial(J'\eta_t)}{\partial\eta} + \frac{\partial(J'\zeta_t)}{\partial\zeta}\right] + f\left[\frac{\partial(J'\xi_x)}{\partial\xi} + \frac{\partial(J'\eta_x)}{\partial\eta} + \frac{\partial(J'\zeta_x)}{\partial\zeta}\right] + g\left[\frac{\partial(J'\xi_y)}{\partial\xi} + \frac{\partial(J'\eta_y)}{\partial\eta} + \frac{\partial(J'\zeta_y)}{\partial\zeta}\right] + h\left[\frac{\partial(J'\xi_z)}{\partial\xi} + \frac{\partial(J'\eta_z)}{\partial\eta} + \frac{\partial(J'\zeta_z)}{\partial\zeta}\right]$$

The coefficient of q on the right hand side of the equation can be evaluated by considering the rate of change of a fixed volume, V_0, in Cartesian coordinates,

$$\frac{d}{dt}\iiint_{V_0} dxdydz = 0. \tag{A-5}$$

Transforming this integral into the time varying curvilinear coordinates ξ, η, ζ yields

$$\frac{d}{dt}\iiint_{V'(t)} d\xi d\eta d\zeta = 0. \tag{A-6}$$

where V' must depend on t in order for the unsteady coordinate representation to refer to the fixed volume V_0 in Cartesian space and J is given by Equation (A-3). Using Leibnitz' rule to take the time derivative of the integral results in

$$\iiint_{V'(t)} \frac{\partial J}{\partial t}\, d\xi d\eta d\zeta + \iint_{S'(t)} J\vec{C} \cdot \vec{n} dS = 0, \tag{A-7}$$

where $\vec{C} = (\xi_t, \eta_t, \zeta_t)$

and $\vec{n}$ is the unit normal in (ξ,η,ζ) space to the surface element dS of volume $V'(t)$. Application of Gauss' Theorem to the second integral yields

$$\iiint_{V'(t)} \left[\frac{\partial J}{\partial t} + \frac{\partial(J\xi_t)}{\partial \xi} + \frac{\partial(J\eta_t)}{\partial \eta} + \frac{\partial(J\zeta_t)}{\partial \zeta}\right] d\xi d\eta d\zeta = 0. \tag{A-8}$$

Since the original volume, V_0, is arbitrary, Equation (A-8) must hold for all $V'(t)$. This implies that the integrand must be identically zero, yielding

$$\frac{\partial J}{\partial t} + \frac{\partial(J\xi_t)}{\partial \xi} + \frac{\partial(J\eta_t)}{\partial \eta} + \frac{\partial(J\zeta_t)}{\partial \zeta} = 0. \tag{A-9}$$

The first term in Equation (A-9) can be rewritten as

$$\frac{\partial J}{\partial t} = \frac{\partial J}{\partial \tau}\, \tau_t \tag{A-10}$$

because τ is a function of t only. Multiplying through by t_τ in Equation (A-9) and using Equation (A-2) and Equation (A-10) yields

$$\frac{\partial(J'\tau_t)}{\partial \tau} + \frac{\partial(J'\xi_t)}{\partial \xi} + \frac{\partial(J'\eta_t)}{\partial \eta} + \frac{\partial(J'\zeta_t)}{\partial \zeta} = 0. \tag{A-11}$$

Therefore, the coefficient of q in Equation (A-4) is identically zero. Because Equation (A-9), or equivalently, Equation (A-11), express conservation of volume, they are referred to as statements of the geometric conservation law.

Evaluation of the coefficients of f, g, and h on the right hand side of Equation (A-4) requires writing the quantities $J'\xi_x$, $J'\eta_x$, $J'\zeta_x$, etc. in terms of x_ξ, x_η, x_ζ, y_ξ, etc. To do this, first use the chain rule to express partial derivatives with respect to the curvilinear coordinates in terms of partial derivatives with respect to the Cartesian coordinates as

$$\begin{bmatrix} \frac{\partial}{\partial\tau} \\ \frac{\partial}{\partial\xi} \\ \frac{\partial}{\partial\eta} \\ \frac{\partial}{\partial\zeta} \end{bmatrix} = \begin{bmatrix} t_\tau & x_\tau & y_\tau & z_\tau \\ 0 & x_\xi & y_\xi & z_\xi \\ 0 & x_\eta & y_\eta & z_\eta \\ 0 & x_\zeta & y_\zeta & z_\zeta \end{bmatrix} \begin{bmatrix} \frac{\partial}{\partial t} \\ \frac{\partial}{\partial x} \\ \frac{\partial}{\partial y} \\ \frac{\partial}{\partial z} \end{bmatrix} \qquad \text{(A-12)}$$

Inverting Equation (A-12) yields

$$\begin{bmatrix} \frac{\partial}{\partial t} \\ \frac{\partial}{\partial x} \\ \frac{\partial}{\partial y} \\ \frac{\partial}{\partial z} \end{bmatrix} = \frac{1}{Jt_\tau} \begin{bmatrix} J & a_{12} & a_{13} & a_{14} \\ 0 & t_\tau(y_\eta z_\zeta - y_\zeta z_\eta) & -t_\tau(y_\xi z_\zeta - y_\zeta z_\xi) & t_\tau(y_\xi z_\eta - y_\eta z_\xi) \\ 0 & -t_\tau(x_\eta z_\zeta - x_\zeta z_\eta) & t_\tau(x_\xi z_\zeta - x_\zeta z_\xi) & -t_\tau(x_\xi z_\eta - x_\eta z_\xi) \\ 0 & t_\tau(x_\eta y_\zeta - x_\zeta y_\eta) & -t_\tau(x_\xi y_\zeta - x_\zeta y_\xi) & t_\tau(x_\xi y_\eta - x_\eta y_\xi) \end{bmatrix} \begin{bmatrix} \frac{\partial}{\partial\tau} \\ \frac{\partial}{\partial\xi} \\ \frac{\partial}{\partial\eta} \\ \frac{\partial}{\partial\zeta} \end{bmatrix} \qquad \text{(A-13)}$$

where $a_{12} = -[x_\tau(y_\eta z_\zeta - y_\zeta z_\eta) - y_\tau(x_\eta z_\zeta - x_\zeta z_\eta) + z_\tau(x_\eta y_\zeta - x_\zeta y_\eta)]$,

$a_{12} = x_\tau(y_\xi z_\zeta - y_\zeta z_\xi) - y_\tau(x_\xi z_\zeta - x_\zeta z_\xi) + z_\tau(x_\xi y_\zeta - x_\zeta y_\xi)$,

$a_{13} = -[x_\tau(y_\xi z_\eta - y_\eta z_\xi) - y_\tau(x_\xi z_\eta - x_\eta z_\xi) + z_\tau(x_\eta y_\xi - x_\xi y_\eta)]$.

Comparing Equation (A-13) with the chain rule expression for the partial derivatives with respect to the Cartesian coordinates in terms of partial derivatives with respect to the curvilinear coordinates,

$$\begin{bmatrix} \frac{\partial}{\partial t} \\ \frac{\partial}{\partial x} \\ \frac{\partial}{\partial y} \\ \frac{\partial}{\partial z} \end{bmatrix} = \begin{bmatrix} \tau_t & \xi_t & \eta_t & \zeta_t \\ \tau_x & \xi_x & \eta_x & \zeta_x \\ \tau_y & \xi_y & \eta_y & \zeta_y \\ \tau_z & \xi_z & \eta_z & \zeta_z \end{bmatrix} \begin{bmatrix} \frac{\partial}{\partial \tau} \\ \frac{\partial}{\partial \xi} \\ \frac{\partial}{\partial \eta} \\ \frac{\partial}{\partial \zeta} \end{bmatrix} \tag{A-14}$$

gives the values of the metrics.

Specifically, the metrics are

$$\tau_t = \frac{1}{t_\tau} \tag{A-15a}$$

$$\tau_x = \tau_y = \tau_z = 0 \tag{A-15b}$$

$$\xi_x = J^{-1}(y_\eta z_\zeta - y_\zeta z_\eta) \tag{A-15c}$$

$$\xi_y = J^{-1}(x_\zeta z_\eta - x_\eta z_\zeta) \tag{A-15d}$$

$$\xi_z = J^{-1}(x_\eta y_\zeta - x_\zeta y_\eta) \tag{A-15e}$$

$$\eta_x = J^{-1}(y_\zeta z_\xi - y_\xi z_\zeta) \tag{A-15f}$$

$$\eta_y = J^{-1}(x_\xi z_\zeta - x_\zeta z_\xi) \tag{A-15g}$$

$$\eta_z = J^{-1}(x_\zeta y_\xi - x_\xi y_\zeta) \tag{A-15h}$$

$$\zeta_x = J^{-1}(y_\xi z_\eta - y_\eta z_\xi) \tag{A-15i}$$

$$\zeta_y = J^{-1}(x_\eta z_\xi - x_\xi z_\eta) \tag{A-15j}$$

$$\zeta_z = J^{-1}(x_\xi y_\eta - x_\eta y_\xi) \tag{A-15k}$$

$$\xi_t = -\tau_t(\xi_x x_\tau + \xi_y y_\tau + \xi_z z_\tau) \tag{A-15ℓ}$$

$$\eta_t = -\tau_t(\eta_x x_\tau + \eta_y y_\tau + \eta_z z_\tau) \tag{A-15m}$$

$$\zeta_t = -\tau_t(\zeta_x x_\tau + \zeta_y y_\tau + \zeta_z z_\tau). \tag{A-15n}$$

The coefficients of f, g, and h in Equation (A-4) can now be evaluated. Using Equation (A-15), the coefficient of f can be written as

$$t_\tau\left[\frac{\partial}{\partial\xi}(y_\eta z_\zeta - y_\zeta z_\eta) + \frac{\partial}{\partial\eta}(y_\zeta z_\xi - y_\xi z_\zeta) + \frac{\partial}{\partial\zeta}(y_\xi z_\eta - y_\eta z_\xi)\right]. \tag{A-16}$$

This is of the form

$$t_\tau\ \nabla \cdot (\nabla y \times \nabla z), \tag{A-17}$$

where the vector operator ∇ is taken to be

$$\nabla \equiv \left(\frac{\partial}{\partial\xi}, \frac{\partial}{\partial\eta}, \frac{\partial}{\partial\zeta}\right) \tag{A-18}$$

and the $\cdot$ and $\times$ represent vector dot and cross products, respectively. Using a well-known vector identity, Expression (A-17) can be rewritten as

$$t_\tau[\nabla z \cdot (\nabla \times \nabla y) - \nabla y \cdot (\nabla \times \nabla z)] \equiv 0. \tag{A-19}$$

The expression is identically equal to zero because the curl of the gradient is always zero.

Similarly, the coefficient of g on the right hand side of Equation (A-4) can be written as

$$t_\tau \nabla \cdot (\nabla z \times \nabla x) \equiv 0, \tag{A-20}$$

and the coefficient of h can be written as

$$t_\tau \nabla \cdot (\nabla x \times \nabla y) \equiv 0. \tag{A-21}$$

Using the metric identities given by Equations (A-11), (A-19), (A-20), and (A-21) in Equation (A-4) yeilds

$$\frac{\partial Q}{\partial \tau} + \frac{\partial F}{\partial \xi} + \frac{\partial G}{\partial \eta} + \frac{\partial H}{\partial \zeta} = 0 \tag{A-22}$$

where $Q = Jq$

$$F = Jt_\tau(\xi_t q + \xi_x f + \xi_y g + \xi_z h)$$

$$G = Jt_\tau(\eta_t q + \eta_x f + \eta_y g + \eta_z h)$$

$$H = Jt_\tau(\zeta_t q + \zeta_x f + \zeta_y g + \zeta_z h).$$

APPENDIX B

JACOBIANS OF THE SPLIT FLUX VECTORS

The Jacobians of the split flux vectors with respect to the dependent variables are derived in this appendix in a form suitable for numerical calculation. The split flux vectors referred to in Equation (3-7) are defined for the one-dimensional case in Equation (3-31). For the three-dimensional case the general flux vector is

$$K^L = \sum_{\ell=1,4,5} \frac{1}{2}(\lambda_k^\ell(Q^L) + |\lambda_k^\ell(Q^L)|)K_\ell(Q^L) \qquad \text{(B-1a)}$$

$$K^R = \sum_{\ell=1,4,5} \frac{1}{2}(\lambda_k^\ell(Q^R) - |\lambda_k^\ell(Q^R)|)K_\ell(Q^R) \qquad \text{(B-1b)}$$

where the symbol K should be replaced by F, G, or H when k is ξ, η, or ζ, respectively, and Q^L and Q^R are obtained by dependent variable extrapolation along the k coordinate from more negative coordinate values and more positive coordinate values, respectively. The eigenvalues, λ_k^1, λ_k^4, and λ_k^5 are given by Equation (3-4), and the split flux vectors, K_1, K_4, and K_5 are given by Equation (3-6). Equation (B-1) illustrates that K^L and K^R are the sum of from zero to three components, depending on the signs of the eigenvalues.

The Jacobian of each of the possible components,

$$\bar{K}_\ell = \frac{\partial(\lambda_k^\ell K_\ell)}{\partial Q}, \quad \ell = 1,4,5, \qquad \text{(B-2)}$$

will be derived.

Expanding the derivative in Equation (B-2) yields

$$\bar{K}_\ell = K_\ell \frac{\partial \lambda_k^\ell}{\partial Q} + \lambda_k^\ell \frac{\partial K_\ell}{\partial Q}. \qquad \text{(B-3)}$$

The elements of the dependent variable vector are given by

$$Q_1 = J\rho \tag{B-4a}$$

$$Q_2 = J\rho u \tag{B-4b}$$

$$Q_3 = J\rho v \tag{B-4c}$$

$$Q_4 = J\rho w \tag{B-4d}$$

$$Q_5 = Je \tag{B-4e}$$

From Equation (3-4), the eigenvalues are

$$\lambda_k^1 = t_\tau \beta_k \tag{B-5a}$$

$$\lambda_k^4 = t_\tau(\beta_k + c|\nabla k|) = t_\tau(\bar{\theta}_k + c)|\nabla k| + t_\tau k_t \tag{B-5b}$$

$$\lambda^5 = t_\tau(\beta_k - c|\nabla k|) = t_\tau(\bar{\theta}_k - c)|\nabla k| + t_\tau k_t \tag{B-5c}$$

where

$$\beta_k = k_x u + k_y v + k_z w + k_t \tag{B-6}$$

$$|\nabla k| = (k_x^2 + k_y^2 + k_z^2)^{1/2} \tag{B-7}$$

$$\theta_k = k_x u + k_y v + k_z w \tag{B-8a}$$

$$\bar{\theta}_k = \frac{\theta_k}{|\nabla k|} \tag{B-8b}$$

The local speed of sound, c, is

$$c = \left(\frac{\gamma p}{\rho}\right)^{1/2} \tag{B-9}$$

where

$$p = (\gamma - 1)e - \frac{\rho(\gamma-1)}{2}(u^2 + v^2 + w^2). \tag{B-10}$$

Expressing β_k, $\bar{\theta}_k$, c, and p in terms of the dependent variables yields

$$\beta_k = \frac{k_x Q_2 + k_y Q_3 + k_z Q_4}{Q_1} + k_t \tag{B-11}$$

$$\bar{\theta}_k = \frac{k_x Q_2 + k_y Q_3 + k_z Q_4}{Q_1 |\nabla k|} \tag{B-12}$$

$$c = \left[\gamma(\gamma - 1)\frac{Q_5}{Q_1} - \frac{\gamma(\gamma-1)}{2}\frac{Q_2^2 + Q_3^2 + Q_4^2}{Q_1^2}\right]^{1/2} \tag{B-13}$$

$$p = J^{-1}\left[(\gamma-1)Q_5 - \frac{(\gamma-1)}{2}\frac{Q_2^2 + Q_3^2 + Q_4^2}{Q_1}\right] \tag{B-14}$$

Note that

$$\frac{\partial \beta_k}{\partial Q_j} = \frac{\partial \theta_k}{\partial Q_j} = |\nabla k| \frac{\partial \bar{\theta}_k}{\partial Q_j}, \qquad j = 1,2,3,4,5. \tag{B-15}$$

Using Equations (B-5), (B-11), (B-12), (B-13), and (B-15), the derivatives of the eigenvalues with respect to the dependent variables can be written as

$$\frac{\partial \lambda_k^1}{\partial Q} = t_\tau\left[-\frac{\theta_k}{Q_1}, \frac{k_x}{Q_1}, \frac{k_y}{Q_1}, \frac{k_z}{Q_1}, 0\right] \tag{B-16}$$

$$\frac{\partial \lambda_k^4}{\partial Q} = t_\tau |\nabla k|\left[\frac{\partial}{\partial Q_1}(\bar{\theta}_k + c), \frac{\partial}{\partial Q_2}(\bar{\theta}_k + c), \frac{\partial}{\partial Q_3}(\bar{\theta}_k + c), \frac{\partial}{\partial Q_4}(\bar{\theta}_k + c), \frac{\partial c}{\partial Q_5}\right] \tag{B-17}$$

$$\frac{\partial \lambda_k^5}{\partial Q} = t_\tau |\nabla k|\left[\frac{\partial}{\partial Q_1}(\bar{\theta}_k - c), \frac{\partial}{\partial Q_2}(\bar{\theta}_k - c), \frac{\partial}{\partial Q_3}(\bar{\theta}_k - c), \frac{\partial}{\partial Q_4}(\bar{\theta}_k - c), -\frac{\partial c}{\partial Q_5}\right] \tag{B-18}$$

The derivatives of $\bar{\theta}_k$ are given by

$$\frac{\partial \bar{\theta}_k}{\partial Q_1} = -\frac{\bar{\theta}_k}{Q_1} \tag{B-19a}$$

$$\frac{\partial \bar{\theta}_k}{\partial Q_2} = \frac{\bar{k}_x}{Q_1} \tag{B-19b}$$

$$\frac{\partial \bar{\theta}_k}{\partial Q_3} = \frac{\bar{k}_y}{Q_1} \tag{B-19c}$$

$$\frac{\partial \bar{\theta}_k}{\partial Q_4} = \frac{\bar{k}_z}{Q_1} \tag{B-19d}$$

$$\frac{\partial \bar{\theta}_k}{\partial Q_5} = 0, \tag{B-19e}$$

where

$$\bar{k}_x = \frac{k_x}{|\nabla k|}$$

$$\bar{k}_y = \frac{k_y}{|\nabla k|}$$

$$\bar{k}_z = \frac{k_z}{|\nabla k|}$$

The derivatives of c are most easily evaluated by rewriting c as cQ_1/Q_1. Using Equation (B-13), the derivatives of cQ_1, are

$$\frac{\partial (cQ_1)}{\partial Q_1} = \frac{\gamma(\gamma-1)Q_5}{2cQ_1} \tag{B-20a}$$

$$\frac{\partial (cQ_1)}{\partial Q_2} = -\frac{\gamma(\gamma-1)Q_2}{2cQ_1} \tag{B-20b}$$

$$\frac{\partial (cQ_1)}{\partial Q_3} = -\frac{\gamma(\gamma-1)Q_3}{2cQ_1} \tag{B-20c}$$

$$\frac{\partial (cQ_1)}{\partial Q_4} = -\frac{\gamma(\gamma-1)Q_4}{2cQ_1} \tag{B-20d}$$

$$\frac{\partial (cQ_1)}{\partial Q_5} = \frac{\gamma(\gamma-1)Q_1}{2cQ_1} = \frac{\gamma(\gamma-1)}{2c}. \tag{B-20e}$$

The derivatives of c are

$$\frac{\partial c}{\partial Q_1} = Q_1^{-1} \left(\frac{\partial (cQ_1)}{\partial Q_1} - c \right) \tag{B-21a}$$

$$\frac{\partial c}{\partial Q_2} = Q_1^{-1} \frac{\partial (cQ_1)}{\partial Q_2} \tag{B-21b}$$

$$\frac{\partial c}{\partial Q_3} = Q_1^{-1} \frac{\partial (cQ_1)}{\partial Q_3} \tag{B-21c}$$

$$\frac{\partial c}{\partial Q_4} = Q_1^{-1} \frac{\partial (cQ_1)}{\partial Q_4} \tag{B-21d}$$

$$\frac{\partial c}{\partial Q_5} = Q_1^{-1} \frac{\partial (cQ_1)}{\partial Q_5}. \tag{B-21e}$$

The derivatives of pJ with respect to the dependent variables will be needed below. Using Equation (B-14), these values are

$$\frac{\partial (pJ)}{\partial Q_1} = \frac{\gamma - 1}{2} \frac{Q_2^2 + Q_3^2 + Q_4^2}{Q_1^2} \tag{B-22a}$$

$$\frac{\partial (pJ)}{\partial Q_2} = - (\gamma - 1) \frac{Q_2}{Q_1} \tag{B-22b}$$

$$\frac{\partial (pJ)}{\partial Q_3} = - (\gamma - 1) \frac{Q_3}{Q_1} \tag{B-22c}$$

$$\frac{\partial (pJ)}{\partial Q_4} = - (\gamma - 1) \frac{Q_4}{Q_1} \tag{B-22d}$$

$$\frac{\partial (pJ)}{\partial Q_5} = \gamma - 1. \tag{B-22e}$$

K_1, K_4, and K_5 written in terms of the dependent variables are

$$K_1 = \frac{\gamma-1}{\gamma}\begin{bmatrix} Q_1 \\ Q_2 \\ Q_3 \\ Q_4 \\ \dfrac{Q_2^2 + Q_3^2 + Q_4^2}{2Q_1} \end{bmatrix} \qquad \text{(B-23a)}$$

$$K_4 = \frac{1}{2\gamma}\begin{bmatrix} Q_1 \\ Q_2 + cQ_1\bar{k}_x \\ Q_3 + cQ_1\bar{k}_y \\ Q_4 + cQ_1\bar{k}_z \\ Q_5 + pJ + cQ_1\bar{\theta}_k \end{bmatrix} \qquad \text{(B-23b)}$$

$$K_5 = \frac{1}{2\gamma}\begin{bmatrix} Q_1 \\ Q_2 - cQ_1\bar{k}_x \\ Q_3 - cQ_1\bar{k}_y \\ Q_4 - cQ_1\bar{k}_z \\ Q_5 + pJ - cQ_1\bar{\theta}_k \end{bmatrix} \qquad \text{(B-23c)}$$

The derivatives of the split flux vectors with respect to the dependent variables are

$$\frac{\partial K_1}{\partial Q} = \frac{\gamma-1}{\gamma}\begin{bmatrix} 1 & 0 & 0 & 0 & 0 \\ 0 & 1 & 0 & 0 & 0 \\ 0 & 0 & 1 & 0 & 0 \\ 0 & 0 & 0 & 1 & 0 \\ -\frac{1}{2}\phi & \frac{Q_2}{Q_1} & \frac{Q_3}{Q_1} & \frac{Q_4}{Q_1} & 0 \end{bmatrix} \qquad \text{(B-24)}$$

where $\phi = \dfrac{Q_2^2 + Q_3^2 + Q_4^2}{Q_1^2}$

$$\frac{\partial K_4}{\partial Q} = \frac{1}{2\gamma}\begin{bmatrix} 1 & 0 & 0 & 0 & 0 \\ \bar{k}_x \dfrac{\partial(cQ_1)}{\partial Q_1} & 1+\bar{k}_x \dfrac{\partial(cQ_1)}{\partial Q_2} & \bar{k}_x \dfrac{\partial(cQ_1)}{\partial Q_3} & \bar{k}_x \dfrac{\partial(cQ_1)}{\partial Q_4} & \bar{k}_x \dfrac{\partial(cQ_1)}{\partial Q_5} \\ \bar{k}_y \dfrac{\partial(cQ_1)}{\partial Q_1} & \bar{k}_y \dfrac{\partial(cQ_1)}{\partial Q_2} & 1+\bar{k}_y \dfrac{\partial(cQ_1)}{\partial Q_3} & \bar{k}_y \dfrac{\partial(cQ_1)}{\partial Q_4} & \bar{k}_y \dfrac{\partial(cQ_1)}{\partial Q_5} \\ \bar{k}_z \dfrac{\partial(cQ_1)}{\partial Q_1} & \bar{k}_z \dfrac{\partial(cQ_1)}{\partial Q_2} & \bar{k}_z \dfrac{\partial(cQ_1)}{\partial Q_3} & 1+\bar{k}_z \dfrac{\partial(cQ_1)}{\partial Q_4} & \bar{k}_z \dfrac{\partial(cQ_1)}{\partial Q_5} \\ a_{51}^4 & a_{52}^4 & a_{53}^4 & a_{54}^4 & 1+a_{55}^4 \end{bmatrix} \qquad \text{(B-25)}$$

where

$$a_{5j}^4 = \frac{\partial(pJ)}{\partial Q_j} + \bar{\theta}_k \frac{\partial(cQ_1)}{\partial Q_j} + cQ_1 \frac{\partial \bar{\beta}_k}{\partial Q_j}, \qquad j = 1,2,3,4,5$$

$$\bar{\beta}_k = \frac{\beta_k}{|\nabla k|}$$

and

$$\frac{\partial K_5}{\partial Q} = \frac{1}{2Y}\begin{bmatrix} 1 & 0 & 0 & 0 & 0 \\ -\bar{k}_x \frac{\partial(cQ_1)}{\partial Q_1} & 1-\bar{k}_x \frac{\partial(cQ_1)}{\partial Q_2} & -\bar{k}_x \frac{\partial(cQ_1)}{\partial Q_3} & -\bar{k}_x \frac{\partial(cQ_1)}{\partial Q_4} & -\bar{k}_x \frac{\partial(cQ_1)}{\partial Q_5} \\ -\bar{k}_y \frac{\partial(cQ_1)}{\partial Q_1} & -\bar{k}_y \frac{\partial(cQ_1)}{\partial Q_2} & 1-\bar{k}_y \frac{\partial(cQ_1)}{\partial Q_3} & -\bar{k}_y \frac{\partial(cQ_1)}{\partial Q_4} & -\bar{k}_y \frac{\partial(cQ_1)}{\partial Q_5} \\ -\bar{k}_z \frac{\partial(cQ_1)}{\partial Q_1} & -\bar{k}_z \frac{\partial(cQ_1)}{\partial Q_2} & -\bar{k}_z \frac{\partial(cQ_1)}{\partial Q_3} & 1-\bar{k}_z \frac{\partial(cQ_1)}{\partial Q_4} & -\bar{k}_z \frac{\partial(cQ_1)}{\partial Q_5} \\ a_{51}^5 & a_{52}^5 & a_{53}^5 & a_{54}^5 & 1+a_{55}^5 \end{bmatrix} \tag{B-26}$$

where

$$a_{5j}^5 = \frac{\partial(pJ)}{\partial Q_j} - \bar{\theta}_k \frac{\partial(cQ_1)}{\partial Q_j} - cQ_1 \frac{\partial \bar{\theta}_k}{\partial Q_j}, \quad j = 1,2,3,4,5.$$

Let $(\bar{K}_\ell)_{ij}$ denote the element in row i and column j of the Jacobian $\bar{K}_\ell$, and let $(K_\ell)_i$ denote element i of the split flux vector K_ℓ. Equation (B-3) can be rewritten as

$$(\bar{K}_\ell)_{ij} = (K_\ell)_i \frac{\partial \lambda_k^\ell}{\partial Q_j} + \lambda_k^\ell \left(\frac{\partial (K_\ell)_i}{\partial Q_j}\right), \tag{B-27}$$

for $i = 1,2,3,4,5$,
$j = 1,2,3,4,5$,
$\ell = 1,4,5$.

Explicitly writing all the elements of $\bar{K}_1$ yields

$$(\bar{K}_1)_{11} = \frac{\gamma-1}{\gamma} t_\tau k_t \tag{B-28a}$$

$$(\bar{K}_1)_{12} = \frac{\gamma-1}{\gamma} t_\tau k_x \qquad \text{(B-28b)}$$

$$(\bar{K}_1)_{13} = \frac{\gamma-1}{\gamma} t_\tau k_y \qquad \text{(B-28c)}$$

$$(\bar{K}_1)_{14} = \frac{\gamma-1}{\gamma} t_\tau k_z \qquad \text{(B-28d)}$$

$$(\bar{K}_1)_{15} = 0 \qquad \text{(B-28e)}$$

$$(\bar{K}_1)_{21} = -\frac{\gamma-1}{\gamma} t_\tau \frac{Q_2}{Q_1} \theta_k \qquad \text{(B-29a)}$$

$$(\bar{K}_1)_{22} = \frac{\gamma-1}{\gamma} t_\tau \left(\frac{Q_2}{Q_1} k_x + \beta_k\right) \qquad \text{(B-29b)}$$

$$(\bar{K}_1)_{23} = \frac{\gamma-1}{\gamma} t_\tau \frac{Q_2}{Q_1} k_y \qquad \text{(B-29c)}$$

$$(\bar{K}_1)_{24} = \frac{\gamma-1}{\gamma} t_\tau \frac{Q_2}{Q_1} k_z \qquad \text{(B-29d)}$$

$$(\bar{K}_1)_{25} = 0 \qquad \text{(B-29e)}$$

$$(\bar{K}_1)_{31} = -\frac{\gamma-1}{\gamma} t_\tau \frac{Q_3}{Q_1} \theta_k \qquad \text{(B-30a)}$$

$$(\bar{K}_1)_{32} = \frac{\gamma-1}{\gamma} t_\tau \frac{Q_3}{Q_1} k_x \qquad \text{(B-30b)}$$

$$(\bar{K}_1)_{33} = \frac{\gamma-1}{\gamma} t_\tau \left(\frac{Q_3}{Q_1} k_y + \beta_k\right) \qquad \text{(B-30c)}$$

$$(\bar{K}_1)_{34} = \frac{\gamma-1}{\gamma} t_\tau \frac{Q_3}{Q_1} k_z \qquad \text{(B-30d)}$$

$$(\bar{K}_1)_{35} = 0 \qquad \text{(B-30e)}$$

$$(\bar{K}_1)_{41} = -\frac{\gamma-1}{\gamma} t_\tau \frac{Q_4}{Q_1} \theta_k \qquad \text{(B-31a)}$$

$$(\bar{K}_1)_{42} = \frac{\gamma-1}{\gamma} t_\tau \frac{Q_4}{Q_1} k_x \tag{B-31b}$$

$$(\bar{K}_1)_{43} = \frac{\gamma-1}{\gamma} t_\tau \frac{Q_4}{Q_1} k_y \tag{B-31c}$$

$$(\bar{K}_1)_{44} = \frac{\gamma-1}{\gamma} t_\tau \left(\frac{Q_4}{Q_1} k_z + \beta_k\right) \tag{B-31d}$$

$$(\bar{K}_1)_{45} = 0 \tag{B-31e}$$

$$(\bar{K}_1)_{51} = -\frac{\gamma-1}{\gamma} t_\tau \frac{\phi}{2} (\theta_k + \beta_k) \tag{B-32a}$$

$$(\bar{K}_1)_{52} = \frac{\gamma-1}{\gamma} t_\tau \left[\frac{\phi}{2} k_x + \frac{Q_2}{Q_1} \beta_k\right] \tag{B-32b}$$

$$(\bar{K}_1)_{53} = \frac{\gamma-1}{\gamma} t_\tau \left[\frac{\phi}{2} k_y + \frac{Q_3}{Q_1} \beta_k\right] \tag{B-32c}$$

$$(\bar{K}_1)_{54} = \frac{\gamma-1}{\gamma} t_\tau \left[\frac{\phi}{2} k_z + \frac{Q_4}{Q_1} \beta_k\right] \tag{B-32d}$$

$$(\bar{K}_1)_{55} = 0. \tag{B-32e}$$

Writing out all 25 elements of $\bar{K}_4$,

$$(\bar{K}_4)_{11} = \frac{1}{2\gamma} \left[Q_1 \frac{\partial \lambda_k^4}{\partial Q_1} + \lambda_k^4\right] \tag{B-33a}$$

$$(\bar{K}_4)_{12} = \frac{1}{2\gamma} Q_1 \frac{\partial \lambda_k^4}{\partial Q_2} \tag{B-33b}$$

$$(\bar{K}_4)_{13} = \frac{1}{2\gamma} Q_1 \frac{\partial \lambda_k^4}{\partial Q_3} \tag{B-33c}$$

$$(\bar{K}_4)_{14} = \frac{1}{2\gamma} Q_1 \frac{\partial \lambda_k^4}{\partial Q_4} \tag{B-33d}$$

$$(\bar{K}_4)_{15} = \frac{1}{2\gamma} Q_1 \frac{\partial \lambda_k^4}{\partial Q_5} \tag{B-33e}$$

$$(\bar{K}_4)_{21} = \frac{1}{2\gamma}\left[(Q_2 + cQ_1\bar{k}_x)\frac{\partial\lambda_k^4}{\partial Q_1} + \lambda_k^4\,\bar{k}_x\frac{\partial(cQ_1)}{\partial Q_1}\right] \tag{B-34a}$$

$$(\bar{K}_4)_{22} = \frac{1}{2\gamma}\left[(Q_2 + cQ_1\bar{k}_x)\frac{\partial\lambda_k^4}{\partial Q_2} + \lambda_k^4\,(1 + \bar{k}_x\frac{\partial(cQ_1)}{\partial Q_2})\right] \tag{B-34b}$$

$$(\bar{K}_4)_{23} = \frac{1}{2\gamma}\left[(Q_2 + cQ_1\bar{k}_x)\frac{\partial\lambda_k^4}{\partial Q_3} + \lambda_k^4\,\bar{k}_x\frac{\partial(cQ_1)}{\partial Q_3}\right] \tag{B-34c}$$

$$(\bar{K}_4)_{24} = \frac{1}{2\gamma}\left[(Q_2 + cQ_1\bar{k}_x)\frac{\partial\lambda_k^4}{\partial Q_4} + \lambda_k^4\,\bar{k}_x\frac{\partial(cQ_1)}{\partial Q_4}\right] \tag{B-34d}$$

$$(\bar{K}_4)_{25} = \frac{1}{2\gamma}\left[(Q_2 + cQ_1\bar{k}_x)\frac{\partial\lambda_k^4}{\partial Q_5} + \lambda_k^4\,\bar{k}_x\frac{\partial(cQ_1)}{\partial Q_5}\right] \tag{B-34e}$$

$$(\bar{K}_4)_{31} = \frac{1}{2\gamma}\left[(Q_3 + cQ_1\bar{k}_y)\frac{\partial\lambda_k^4}{\partial Q_1} + \lambda_k^4\,\bar{k}_y\frac{\partial(cQ_1)}{\partial Q_1}\right] \tag{B-35a}$$

$$(\bar{K}_4)_{32} = \frac{1}{2\gamma}\left[(Q_3 + cQ_1\bar{k}_y)\frac{\partial\lambda_k^4}{\partial Q_2} + \lambda_k^4\,\bar{k}_y\frac{\partial(cQ_1)}{\partial Q_2}\right] \tag{B-35b}$$

$$(\bar{K}_4)_{33} = \frac{1}{2\gamma}\left[(Q_3 + cQ_1\bar{k}_y)\frac{\partial\lambda_k^4}{\partial Q_3} + \lambda_k^4\,(1 + \bar{k}_y\frac{\partial(cQ_1)}{\partial Q_3})\right] \tag{B-35c}$$

$$(\bar{K}_4)_{34} = \frac{1}{2\gamma}\left[(Q_3 + cQ_1\bar{k}_y)\frac{\partial\lambda_k^4}{\partial Q_4} + \lambda_k^4\,\bar{k}_y\frac{\partial(cQ_1)}{\partial Q_4}\right] \tag{B-35d}$$

$$(\bar{K}_4)_{35} = \frac{1}{2\gamma}\left[(Q_3 + cQ_1\bar{k}_y)\frac{\partial\lambda_k^4}{\partial Q_5} + \lambda_k^4\,\bar{k}_y\frac{\partial(cQ_1)}{\partial Q_5}\right] \tag{B-35e}$$

$$(\bar{K}_4)_{41} = \frac{1}{2\gamma}\left[(Q_4 + cQ_1\bar{k}_z)\frac{\partial\lambda_k^4}{\partial Q_1} + \lambda_k^4\,\bar{k}_z\frac{\partial(cQ_1)}{\partial Q_1}\right] \tag{B-36a}$$

$$(\bar{K}_4)_{42} = \frac{1}{2\gamma}\left[(Q_4 + cQ_1\bar{k}_z)\frac{\partial\lambda_k^4}{\partial Q_2} + \lambda_k^4\,\bar{k}_z\frac{\partial(cQ_1)}{\partial Q_2}\right] \tag{B-36b}$$

$$(\bar{K}_4)_{43} = \frac{1}{2\gamma}\left[(Q_4 + cQ_1\bar{k}_z)\frac{\partial\lambda_k^4}{\partial Q_3} + \lambda_k^4\,\bar{k}_z\frac{\partial(cQ_1)}{\partial Q_3}\right] \tag{B-36c}$$

$$(\bar{K}_4)_{44} = \frac{1}{2Y}\left[(Q_4 + cQ_1\bar{k}_z)\frac{\partial\lambda_k^4}{\partial Q_4} + \lambda_k^4\left(1 + \bar{k}_z\frac{\partial(cQ_1)}{\partial Q_4}\right)\right] \quad \text{(B-36d)}$$

$$(\bar{K}_4)_{45} = \frac{1}{2Y}\left[(Q_4 + cQ_1\bar{k}_z)\frac{\partial\lambda_k^4}{\partial Q_5} + \lambda_k^4\,\bar{k}_z\frac{\partial(cQ_1)}{\partial Q_5}\right] \quad \text{(B-36e)}$$

$$(\bar{K}_4)_{51} = \frac{1}{2Y}\left[(Q_5 + pJ + cQ_1\bar{\theta}_k)\frac{\partial\lambda_k^4}{\partial Q_1} + \lambda_k^4\left(\frac{\partial(pJ)}{\partial Q_1} + \bar{\theta}_k\frac{\partial(cQ_1)}{\partial Q_1} + cQ_1\frac{\partial\bar{\theta}_k}{\partial Q_1}\right)\right] \quad \text{(B-37a)}$$

$$(\bar{K}_4)_{52} = \frac{1}{2Y}\left[(Q_5 + pJ + cQ_1\bar{\theta}_k)\frac{\partial\lambda_k^4}{\partial Q_2} + \lambda_k^4\left(\frac{\partial(pJ)}{\partial Q_2} + \bar{\theta}_k\frac{\partial(cQ_1)}{\partial Q_2} + cQ_1\frac{\partial\bar{\theta}_u}{\partial Q_2}\right)\right] \quad \text{(B-37b)}$$

$$(\bar{K}_4)_{53} = \frac{1}{2Y}\left[(Q_5 + pJ + cQ_1\bar{\theta}_k)\frac{\partial\lambda_k^4}{\partial Q_3} + \lambda_k^4\left(\frac{\partial(pJ)}{\partial Q_3} + \bar{\theta}_k\frac{\partial(cQ_1)}{\partial Q_3} + cQ_1\frac{\partial\bar{\theta}_k}{\partial Q_3}\right)\right] \quad \text{(B-37c)}$$

$$(\bar{K}_4)_{54} = \frac{1}{2Y}\left[(Q_5 + pJ + cQ_1\bar{\theta}_k)\frac{\partial\lambda_k^4}{\partial Q_4} + \lambda_k^4\left(\frac{\partial(pJ)}{\partial Q_4} + \bar{\theta}_k\frac{\partial(cQ_1)}{\partial Q_4} + cQ_1\frac{\partial\bar{\theta}_k}{\partial Q_4}\right)\right] \quad \text{(B-37d)}$$

$$(\bar{K}_4)_{55} = \frac{1}{2Y}\left[(Q_5 + pJ + cQ_1\bar{\theta}_k)\frac{\partial\lambda_k^4}{\partial Q_5} + \lambda_k^4\left(\frac{\partial(pJ)}{\partial Q_5} + \bar{\theta}_k\frac{\partial(cQ_1)}{\partial Q_5} + 1\right)\right]. \quad \text{(B-37e)}$$

The elements of $\bar{K}_5$ are

$$(\bar{K}_5)_{11} = \frac{1}{2Y}\left[Q_1\frac{\partial\lambda_k^5}{\partial Q_1} + \lambda_k^5\right] \quad \text{(B-38a)}$$

$$(\bar{K}_5)_{12} = \frac{1}{2Y}\,Q_1\frac{\partial\lambda_k^5}{\partial Q_2} \quad \text{(B-38b)}$$

$$(\bar{K}_5)_{13} = \frac{1}{2Y}\,Q_1\frac{\partial\lambda_k^5}{\partial Q_3} \quad \text{(B-38c)}$$

$$(\bar{K}_5)_{14} = \frac{1}{2Y}\,Q_1\frac{\partial\lambda_k^5}{\partial Q_4} \quad \text{(B-38d)}$$

$$(\bar{K}_5)_{15} = \frac{1}{2\gamma} Q_1 \frac{\partial \lambda_k^5}{\partial Q_5} \tag{B-38e}$$

$$(\bar{K}_5)_{21} = \frac{1}{2\gamma}[(Q_2 - cQ_1\bar{k}_x)\frac{\partial \lambda_k^5}{\partial Q_1} - \lambda_k^5 \bar{k}_x \frac{\partial (cQ_1)}{\partial Q_1}] \tag{B-39a}$$

$$(\bar{K}_5)_{22} = \frac{1}{2\gamma}[(Q_2 - cQ_1\bar{k}_x)\frac{\partial \lambda_k^5}{\partial Q_2} + \lambda_k^5(1 - \bar{k}_x \frac{\partial (cQ_1)}{\partial Q_2})] \tag{B-39b}$$

$$(\bar{K}_5)_{23} = \frac{1}{2\gamma}[(Q_2 - cQ_1\bar{k}_x)\frac{\partial \lambda_k^5}{\partial Q_3} - \lambda_k^5 \bar{k}_x \frac{\partial (cQ_1)}{\partial Q_3}] \tag{B-39c}$$

$$(\bar{K}_5)_{24} = \frac{1}{2\gamma}[(Q_2 - cQ_1\bar{k}_x)\frac{\partial \lambda_k^5}{\partial Q_4} - \lambda_k^5 \bar{k}_x \frac{\partial (cQ_1)}{\partial Q_4}] \tag{B-39d}$$

$$(\bar{K}_5)_{25} = \frac{1}{2\gamma}[(Q_2 - cQ_1\bar{k}_x)\frac{\partial \lambda_k^5}{\partial Q_5} - \lambda_k^5 \bar{k}_x \frac{\partial (cQ_1)}{\partial Q_5}] \tag{B-39e}$$

$$(\bar{K}_5)_{31} = \frac{1}{2\gamma}[(Q_3 - cQ_1\bar{k}_y)\frac{\partial \lambda_k^5}{\partial Q_1} - \lambda_k^5 \bar{k}_y \frac{\partial (cQ_1)}{\partial Q_1}] \tag{B-40a}$$

$$(\bar{K}_5)_{32} = \frac{1}{2\gamma}[(Q_3 - cQ_1\bar{k}_y)\frac{\partial \lambda_k^5}{\partial Q_2} - \lambda_k^5 \bar{k}_y \frac{\partial (cQ_1)}{\partial Q_2}] \tag{B-40b}$$

$$(\bar{K}_5)_{33} = \frac{1}{2\gamma}[(Q_3 - cQ_1\bar{k}_y)\frac{\partial \lambda_k^5}{\partial Q_3} + \lambda_k^5(1 - \bar{k}_y \frac{\partial (cQ_1)}{\partial Q_3})] \tag{B-40c}$$

$$(\bar{K}_5)_{34} = \frac{1}{2\gamma}[(Q_3 - cQ_1\bar{k}_y)\frac{\partial \lambda_k^5}{\partial Q_4} - \lambda_k^5 \bar{k}_y \frac{\partial (cQ_1)}{\partial Q_4}] \tag{B-40d}$$

$$(\bar{K}_5)_{35} = \frac{1}{2\gamma}[(Q_3 - cQ_1\bar{k}_y)\frac{\partial \lambda_k^5}{\partial Q_5} - \lambda_k^5 \bar{k}_y \frac{\partial (cQ_1)}{\partial Q_5}] \tag{B-40e}$$

$$(\bar{K}_5)_{41} = \frac{1}{2\gamma}[(Q_4 - cQ_1\bar{k}_z)\frac{\partial \lambda_k^5}{\partial Q_1} - \lambda_k^5 \bar{k}_z \frac{\partial (cQ_1)}{\partial Q_1}] \tag{B-41a}$$

$$(\bar{K}_5)_{42} = \frac{1}{2\gamma}[(Q_4 - cQ_1\bar{k}_z)\frac{\partial \lambda_k^5}{\partial Q_2} - \lambda_k^5 \bar{k}_z \frac{\partial (cQ_1)}{\partial Q_2}] \tag{B-41b}$$

$$(\bar{K}_5)_{43} = \frac{1}{2Y}\left[(Q_4 - cQ_1\bar{\kappa}_z)\frac{\partial\lambda_k^5}{\partial Q_3} - \lambda_k^5\bar{\kappa}_z\frac{\partial(cQ_1)}{\partial Q_3}\right] \tag{B-41c}$$

$$(\bar{K}_5)_{44} = \frac{1}{2Y}\left[(Q_4 - cQ_1\bar{\kappa}_z)\frac{\partial\lambda_k^5}{\partial Q_4} + \lambda_k^5\left(1 - \bar{\kappa}_z\frac{\partial(cQ_1)}{\partial Q_4}\right)\right] \tag{B-41d}$$

$$(\bar{K}_5)_{45} = \frac{1}{2Y}\left[(Q_4 - cQ_1\bar{\kappa}_z)\frac{\partial\lambda_k^5}{\partial Q_5} - \lambda_k^5\bar{\kappa}_z\frac{\partial(cQ_1)}{\partial Q_5}\right] \tag{B-41e}$$

$$(\bar{K}_5)_{51} = \frac{1}{2Y}\left[(Q_5 + pJ - cQ_1\bar{\theta}_k)\frac{\partial\lambda_k^5}{\partial Q_1} + \lambda_k^5\left(\frac{\partial(pJ)}{\partial Q_1} - \bar{\theta}_k\frac{\partial(cQ_1)}{\partial Q_1} - cQ_1\frac{\partial\bar{\theta}_k}{\partial Q_1}\right)\right] \tag{B-42a}$$

$$(\bar{K}_5)_{52} = \frac{1}{2Y}\left[(Q_5 + pJ - cQ_1\bar{\theta}_k)\frac{\partial\lambda_k^5}{\partial Q_2} + \lambda_k^5\left(\frac{\partial(pJ)}{\partial Q_2} - \bar{\theta}_k\frac{\partial(cQ_1)}{\partial Q_2} - cQ_1\frac{\partial\bar{\theta}_k}{\partial Q_2}\right)\right] \tag{B-42b}$$

$$(\bar{K}_5)_{53} = \frac{1}{2Y}\left[(Q_5 + pJ - cQ_1\bar{\theta}_k)\frac{\partial\lambda_k^5}{\partial Q_3} + \lambda_k^5\left(\frac{\partial(pJ)}{\partial Q_3} - \bar{\theta}_k\frac{\partial(cQ_1)}{\partial Q_3} - cQ_1\frac{\partial\bar{\theta}_k}{\partial Q_3}\right)\right] \tag{B-42c}$$

$$(\bar{K}_5)_{54} = \frac{1}{2Y}\left[(Q_5 + pJ - cQ_1\bar{\theta}_k)\frac{\partial\lambda_k^5}{\partial Q_4} + \lambda_k^5\left(\frac{\partial(pJ)}{\partial Q_4} - \bar{\theta}_k\frac{\partial(cQ_1)}{\partial Q_4} - cQ_1\frac{\partial\bar{\theta}_k}{\partial Q_4}\right)\right] \tag{B-42d}$$

$$(\bar{K}_5)_{55} = \frac{1}{2Y}\left[(Q_5 + pJ - cQ_1\bar{\theta}_k)\frac{\partial\lambda_k^5}{\partial Q_5} + \lambda_k^5\left(1 + \frac{\partial(pJ)}{\partial Q_5} - \bar{\theta}_k\frac{\partial(cQ_1)}{\partial Q_5} - cQ_1\frac{\partial\bar{\theta}_k}{\partial Q_5}\right)\right] \tag{B-42e}$$

When forming the Jacobian of K^L or K^R in Equation (B-1), the derivatives of only those components with a non-zero coefficient are used.

(The reverse of this page is blank)

REFERENCES

1. Sankar, L.N., Malone, J.B., and Schuster, D., "Full Potential and Euler Solutions for the Unsteady Transonic Flow Past a Fighter Wing," AIAA 85-4061, October 1985.

2. Salmond, J., "Calculation of Harmonic Aerodynamic Forces on Aerofoils and Wings from the Euler Equations," from Transonic Unsteady Aerodynamics and Its Aeroelastic Applications, AGARD CP-374, January 1985.

3. Magnus, R., and Yoshihara, H., "Unsteady Transonic Flows over an Airfoil," AIAA Journal, Vol. 13, No. 12, pp., 1622-1628, December 1975.

4. Steger, J.L., and Bailey, H.E., "Calculation of Transonic Aileron Buzz," AIAA Journal, Vol. 18, No. 3, pp. 249-255, March 1980.

5. Chyu, W.J., and Davis, S.S., "Numerical Studies of Unsteady Transonic Flow Over an Oscillating Airfoil," from Transonic Unsteady Aerodynamics and Its Aeroelastic Applications, AGARD CP-374, January 1985.

6. Janus, J.M., "The Development of a Three-Dimensional Split Flux Vector Euler Solver with Dynamic Grid Applications," M.S. Thesis, Mississippi State University, August 1984.

7. Smith, G.E., Whitlow, W., Jr., and Hassan, H.A., "Unsteady Transonic Flows Past Airfoils Using the Euler Equations," AIAA-86-1764, June 1986.

8. Belk, D.M., Janus, J.M., and Whitfield, D.L., "Three-Dimensional Unsteady Euler Equations Solutions on Dynamic Grids," Air Force Armament Laboratory Report, AFATL-TR-86-21, April 1986.

9. Whitfield, D.L., "Implicit Upwind Finite Volume Scheme for the Three-Dimensional Euler Equations," Mississippi State University Report MSSU-EIRS-ASE-85-1, September 1985.

10. Beam, R.M., and Warming, R.F., "An Implicit Finite-Difference Algorithm for Hyperbolic Systems in Conservation-Law Form," Journal of Computational Physics, Vol. 22, pp. 87-110, 1976.

11. Briley, W.R., and McDonald, H., "On the Structure and Use of Linearized Block Implicit Schemes," Journal of Computational Physics, Vol. 34, pp. 54-73, 1980.

12. Beam, R.M., and Warming, R.F., "An Implicit Factored Scheme for the Compressible Navier-Stokes Equations," AIAA Journal, Vol. 16, No. 4, pp. 393-402, April 1978.

13. Thomas, P.D., and Lombard, C.K., "Geometric Conservation Law and Its Application to Flow Computations on Moving Grids," AIAA Journal, Vol. 17, No. 10, pp. 1030-1037, October 1979.

14. Steger, J.L., and Warming, R.F., "Flux Vector Splitting of the Inviscid Gasdynamic Equations with Application to Finite-Difference Methods," Journal of Computational Physics, Vol. 40, No. 2, pp. 263-293, April 1981.

15. Anderson, W.K., Thomas, J.L., and Whitfield, D.L., "Multigrid Acceleration of the Flux Split Euler Equations," AIAA Paper 86-0274, January 1986.

16. Janus, J.M., Private Communication.

17. Whitfield, D.L., and Janus, J.M., "Three-Dimensional Unsteady Euler Equations Solution Using Flux Vector Splitting," AIAA Paper 84-1552, June 1984.

18. Landon, R.H., "NACA 0012. Oscillatory and Transient Pitching," Compendium of Unsteady Aerodynamic Measurements, AGARD-R-702, August 1982.

19. Dougherty, F.C., Benek, J.A., and Steger, J.L., "On Application of Chimera Grid Schemes to Store Separation," NASA TM 88193, October 1985.

20. Benek, J.A., Buning, P.G., and Steger, J.L., "A 3-D Chimera Grid Embedding Technique," AIAA Paper No. 85-1523-CP, July 1985.

21. Rai, M.M., "An Implicit, Conservative, Zonal-Boundary Scheme for Euler Equation Calculations," NASA CR 3865, February 1985.

22. Thompson, J.F., Abstract submitted to 1987 Aerospace Sciences Meeting.

23. Lasinski, T.A., Andrews, A.E., Sorenson, R.L., Chaussee, D.S., Pulliam, T.H., Kutler, P., "Computation of the Steady Viscous Flow Over a Tri-Element 'Augmenter Wing' Airfoil," AIAA-82-0021, January 1982.

24. Hessenius, K.A., and Pulliam, T.H., "A Zonal Approach to Solution of the Euler Equations," AIAA-82-0969, June 1982.

25. Weatherill, N.P., and Forsey, C.R., "Grid Generation and Flow Calculations for Complex Aircraft Geometries Using a Multi-Block Scheme," AIAA-84-1665, June 1984.

26. Miki, K. and Takagi, T., "A Domain Decomposition and Overlapping Method for the Generation of Three-Dimensional Boundary-Fitted Coordinate Systems," Journal of Computational Physics, Vol. 53, p. 319, 1984.

27. Thoman, D.C., and Szewczyk, A.A., "Time-Dependent Viscous Flow over a Circular Cylinder," The Physics of Fluids Supplement II, p. 76, 1969.

28. Norton, R.J.G., Thompkins, W.T. Jr., and Haimes, R., "Implicit Finite-Difference Schemes with Non-Simply-Connected Grids: A Novel Approach," AIAA-84-0003, January 1984.

29. Ricketts, R.H., Sandford, M.C., Watson, J.J., and Seidel, D.A., "Subsonic and Transonic Unsteady- and Steady-Pressure Measurements on a Rectangular Supercritical Wing Oscillated in Pitch," NASA TM-85765, August 1984.

INITIAL DISTRIBUTION

ASD/ENSZ	1	AFATL/DOIL	2
OO-ALC/MMWRB	1	AFATL/CC	1
AFIS/INTA	1	AFATL/CCN	1
ASD/ENES	1	AFOSR/NA	1
HQ TAC/DRA	1		
HQ PACAF/DOQQ	1		
HQ TAC/INAT	1		
ASD/XRX	1		
HQ PACAF/OA	1		
INTELLIGENCE CTR PACIFIC/PT-3	1		
USA BRL/AMXBR-OD-ST	1		
HQ AFSC/DLW	1		
AFATL/FX	1		
AFATL/MN	1		
AFATL/MNW	2		
AFATL/XP	1		
AFATL/SA	1		
AD/XR	1		
ASD/XR	2		
AFWAL/FIM	2		
AFWL/NTSAC	1		
USA MSL CMD/AMSMI-RD-CS-R	2		
NSWC/TECH LIB	1		
NWC/CODE 343	1		
NASA AMES RESEARCH CTR	1		
NASA LANGLEY RESEARCH CTR/TECH LIB	1		
NASA LANGLEY RESEARCH CTR/407	1		
THE RAND CORP/AFELM	1		
AVCO SYSTEMS TEXTRON/RES LIB	1		
AVCO-EVERETT RESEARCH LAB/TECH DEPT	1		
FAIRCHILD IND/TECH INFO CTR	1		
GEN DYNAMICS/RESEARCH LIB	1		
GEN DYNAMICS/FT WORTH DIV	1		
HONEYWELL INC/DSD LIB	1		
HUGHES AIRCRAFT/MSL SYS GP	1		
LOCKHEED MSL & SPACE/TECH LIB	1		
LOCKHEED MSL & SPACE/WSI CTR	1		
MARTIN MARIETTA CORP/INFO CTR	1		
MCDONNELL DOUGLAS CO/TECH LIB	1		
ROCKWELL I'NAL/TECH INFO CTR	1		
LTV AEROSPACE & DEFENSE CO/LIB	1		
SCIENCE APPLICATIONS I'NAL CORP	1		
AFATL/FXA	10		
DTIC-DDAC	2		
AUL/LSE	1		
FTD/SDNF	1		
HQ USAFE/INATW	1		
AFWAL/FIES/SURVIAC	1		
AFSCA/SAMI	1		

END

12-86

DTIC